JAERI-M
85-074

JAPANESE CONTRIBUTIONS TO IAEA INTOR WORKSHOP, PHASE TWO A, PART 2

CHAPTER III : IMPURITY CONTROL (PHYSICS)

July 1985

Noboru FUJISAWA, Masayoshi SUGIHARA, Seiji SAITO[*1]
Shigehisa HITOKI[*2], Hiromasa IIDA, Takaichi KAWAMURA[*3]
Masaki MAENO, Yoshio MURAKAMI, Yohta NAKAI,
Michiya SHIMADA, Toshizo SHIRAI, Kazuho SONE,
Hidero SUGAI[*4] and Hiroyuki TAWARA[*3]

日本原子力研究所
Japan Atomic Energy Research Institute

JAERI-M レポートは，日本原子力研究所が不定期に公刊している研究報告書です。
入手の問合わせは，日本原子力研究所技術情報部情報資料課（〒319—11 茨城県那珂郡東海村）あて，お申しこしください。なお，このほかに財団法人原子力弘済会資料センター（〒319-11 茨城県那珂郡東海村日本原子力研究所内）で複写による実費頒布をおこなっております。

JAERI-M reports are issued irregularly.
Inquiries about availability of the reports should be addressed to Information Division, Department of Technical Information, Japan Atomic Energy Research Institute, Tokai-mura, Naka-gun, Ibaraki-ken 319-11, Japan.

編集兼発行　日本原子力研究所
印　　刷　山田軽印刷所

JAERI-M 85-074

Japanese Contributions to IAEA INTOR Workshop, Phase Two A, Part 2 Chapter III : Impurity Control (Physics)

Noboru FUJISAWA, Masayoshi SUGIHARA, Seiji SAITO[*1], Shigehisa HITOKI[*2], Hiromasa IIDA, Takaichi KAWAMURA[*3], Masaki MAENO[+1], Yoshio MURAKAMI[+2], Yohta NAKAI[+3], Michiya SHIMADA, Toshizo SHIRAI[+3], Kazuho SONE[+2], Hidero SUGAI[*4] and Hiroyuki TAWARA[*3]

Department of Large Tokamak Research, Naka Fusion Research Establishment, JAERI

(Received May 31, 1985)

This report corresponds to the first half of Chapter III of Japanese contribution report to IAEA INTOR Workshop, Phase Two A, Part 2. Data base assessments are made for divertor, limiter, ergodic limiter, RF pumpout, fuelling, atomic and molecular processes, surface interaction, and vessel preparation. Divertor and limiter modelling and their validation are discussed, and impurity control performance for INTOR is evaluated with the predictive modelling.

Keywords: INTOR, Impurity Control, Divertor, Limiter, Ergodic Limiter, RF Pumpout, A&M Process, Surface Interaction, Vacuum Vessel Preparation, Modelling, Tokamak, Assessment

---

+1 Department of JT-60 Facility
+2 Department of Thermonuclear Fusion Research
+3 Nuclear Data Center, JAERI
*1 Energy Research Lab., Hitachi Ltd.
*2 Fusion Center, Mitsubishi Co.
*3 Institute of Plasma Physics, Nagoya University
*4 Department of Electric Engineering, Nagoya University

IAEA INTORワークショップ，フェーズⅡA，パート2 報告書

第Ⅲ章：不純物制御（物理）

日本原子力研究所那珂研究所臨界プラズマ研究部

藤沢　登・杉原　正芳・斉藤　誠次[*1]
一木　繁久[*2]・飯田　浩正・川村　孝式[*3]
前野　勝樹[+1]・村上　義夫[+2]・中井　洋太[+3]
嶋田　道也・白井　稔三[+3]・曽根　和穂[+2]
菅井　秀郎[*4]・俵　博之[*3]

（1985年5月31日受理）

この報告書はIAEA主催のINTORワークショップ，フェーズⅡA，パート2の日本の報告書の第Ⅲ章（前半）に相当するものである。ダイバータ，リミタ，エルゴディック・リミタ，高周波ポンプアウト，粒子補給，原子分子過程，壁表面との相互作用，真空容器の処理などに関するデータベースの評価を行なった。ダイバータ，リミタのモデリングとその有効性について検討し，このモデルによりINTORの不純物制御性能について評価した。

＋1　JT－60試験部
＋2　核融合研究部
＋3　原研　核データセンター
＊1　㈱日立
＊2　㈱三菱核融合センター
＊3　名古屋大学　プラズマ研究所
＊4　名古屋大学　工学部

Contents

目　　次

1. Physics

1.1 Introduction to physics

An INTOR core plasma produces high-energy alpha particles with their heating power, 124MW, and its heat and particles flow out of a plasma core through conduction and convection with their finite confinement times. The essential objective of impurity control is to remove such large heat and particle fluxes without deteriorating plasma confinement performance. Heat and particle fluxes finally reach a first wall and a collector plate through a scrape-off plasma around the main plasma and interact with them. Critical issues for impurity control physics are, then, related strongly to the scrape-off layer property. Impurity control needs for INTOR are briefly summarized here.

(1) Parameters of scrape-off plasmas

One third of the alpha heating power, around 40MW, is assumed to be radiated to the first wall in an INTOR operating scenario. The rest of it, about 80MW, therefore is transfered through a main plasma edge to the scrape-off plasma, and heats it up. What parameters the scrape-off plasma gets is basically essential for impurity control. This is partly because the scrape-off plasma directly interacts with a collector plate through a sheath, where ions accelerated by a sheath potential collide on the plate and sputter its material and incident particles are also reemitted from the plate with certain energy, and partly because the energy of charge exchange neutral particles incident upon the first wall is also closely related to the scrape-off plasma parameters. Selection of materials for the first wall and collector plate therefore strongly depends on the scrape-off plasma parameters. The width of the scrape-off plasma layer is also a crucial parameter, because it is deeply connected with heat and particle flux densities on the plate. When the width happens to be so narrow, temperatures of the layer would become high and it results in an unmanageable large heat flux density for the plate.

The key parameters of the scrape-off layer, such as densities, temperatures and a layer width, are strongly subject to heat and particle fluxes from the main plasma, particle and heat diffusivities of the layer, behaviors of neutal particles from the collector plate and first wall, and impurities. The reliable evaluation of those parameters, indispensable for a design study, evidently needs adequate data bases from experimental and theoretical research and developments.

(2) Behaviors of impurities

The most essential way for impurity control is to avoid impurities from being released from the collector plate and first wall. It is however actually impossible to completely cut out the impurity release. Then, it becomes crucial for impurity control to shield impurities from going into the main plasma and to keep it as clean as possible. The behaviors of impurities including helium particles produced from D-T reactions in the main plasmas are really important and also influencial on the plasma confinement performance. Some part of impurities from the first wall and collector plate could unavoidably penetrate into the main plasma,

especially high-Z impurities have great influences on the confinement performance. Therefore, the behaviors of impurities in the main and scrape-off plasmas should be understood in an enough depth.

If effects of impurities on the confinement performance fortunately would turn out to be so little and impurities would not accumulate in the center part of the main plasma region, their radiations could be used positively in a way to reduce the scrape-off temperature and to decrease the heat load onto the collector plate.

The long confinement time of helium ions is dangerous for a long burn, because of its tendencies to dilute D-T reactions and increase plasma beta values. The steady exhaust of the helium ashes also needs adequate understanding of the helium ash behavior in the main and scrape-off plasmas.

(3) Helium ash exhaust

The helium ash should be removed continuously at the same rate, about 2×10^{20}/s, as an alpha production rate to achieve the long burn operation of 100-200s with a helium concentration of less than a few percent (e.g. less than 5%) in the plasma. The pumping requirement should of course be as small as possible to mitigate needs on research and development for a evacuating system. Moreover, if possible, a selective evacuation of the helium ash, which means to pump out mainly helium gases, should be paid some heeds to reduce requirements on a tritium processing system.

(4) Basic data for surface and moleculer/atomic collisions

A data base for atomic and molecular collision processes is indispensable for adequate understanding of the scrape-off plasma. Incident energy of impurity ions, which mainly determines sputtering yield of materials, is closely related to a charge state of impurities. Radiation losses from impurities, which are useful in cooling down temperatures of scrape-off plasmas, are also dependent on behaviors of impurities. Futhermore, scrape-off plasma temperatures near the collector plate seem to be strongly coupled with moleculer and atomic processes of hydrogen particles.

It is evident that the data base for plasma-surface interaction is necessary for impurity control studies. Quantities of released impurities from the collector plate and first wall hinge upon their sputtering yields. Recycling D-T particles, which have significant influences on plasma parameters near the collector plate, are substancially subject to their reflection energy and coefficient.

In an INTOR operation scenario, the alpha heating power is 124MW. It therefore is necessary for impurity control in INTOR to remove a heat flow of around 100MW and a helium particle flow of 2×10^{20}/s.

There is a considerable difference in a heat flow to be removed between INTOR and JT-60. The tokamaks such as JFT-2M and Doublet III, under operation, have their maximum heating powers of about 10MW, and the large tokamak, JT-60, is scheduled to be heated with a power of 30MW in a few years.

The heating power for INTOR, therefore, is considerably beyond those tokamaks and then impurity controlability for INTOR can not practically be demonstrated in a few years and it is on an extrapolation from the large tokamak. Another difference is a pulse length. INTOR is speculated to have its pulse length of 100-200s, while the maximum time is 10s for JT-60, which has also no plan for D-T experiments. The long confinement time of around 10s of helium particles could be harmful to the helium ash exhaust from the main plasma. Hence, in this context, complete capability of helium ash exhaust will not be demonstrated in JT-60, when the particle confinement time will become considerable. Consequently, impurity controlability in INTOR must be evaluated on the basis of present data bases including near future. In other words, success of impurity control in INTOR is essentially dependent on to what extent the data obtained are understood.

Various methods of impurity control for tokamaks have been proposed and discussed so far, and some methods have been actually used in experiments. Unfortunately, there seems to be no way, which could surely survive to future tokamak reactors. Two impurity control methods, limiter and divertor, are widely adopted in present-day tokamaks and they have succeeded in producing high temperature plasmas to some extent. They have however many serious problems even to be solved.

Progresses in divertor experiments are in fact marvelous in the last few years, and a new operation regime has been developed, which is suitable to impurity control. The high-density, low-temperature divertor plasmas near the collector plate are realized successfully under strong heating operations in Doublet III. The new regime of a divertor operation has many advantages for impurity control, i.e. reduction in material erosion due to decreased temperatures, reducing heat load to the collector plate due to enhanced radiation losses, and reduced pumping requirement due to compressed neutral gases. Furthermore, diverted discharges show a good plasma confinement performance. Those results provide useful data bases for impurity control for INTOR.

The limiter has made a steady progress lately. Most present experiments accommodate low-Z material limiters and have got high temperature plasmas with large heating power of NBI and/or RF. However, degraded confinement performance has been observed with increasing heating power and severe critical problems to be solved are found in its future extention, while the limiter has some benefits in an engineering area. Recent experiments with the limiter in Doublet III improve the plasma confinement by means of a pellet injection. It seems to give useful data bases for impurity control by a pumped limiter.

Some progress have been made in innovative schemes, an ergogic limiter and an RF pumpout. They have been conducted only in analytical areas, and experiments in small machines are going to be performed in a few years.

Impurity control physics for INTOR is on an extrapolation from the present large tokamaks, as mentioned previously, and a step from the large tokamaks to INTOR is never small. What is the most favorable impurity control for INTOR therefore must be partly judged by analyses codes for impurity control. Those codes therefore should be credible, which therefore can reproduce the present and near future experiments. Results from the codes will be usedfor a design guideline, so the codes must include various physics

ranging from the main plasma to the surface. To get reliable informations from the codes, then, they should be checked by experiments with wide parameter ranges. In this context, experimental results with detail measurements are indispensable for code calibrations. Unfortunately, the experimental data base for impurity control is still insufficient, although the remarkable progress have been made lately. More efforts are needed in both of experimental and theoretical works.

Many tokamaks ranging from large- to small-scale are listed in the following table. Their objectives widely spread out.

Table Tokamak Devices in Japan

evice	Institution	R (m)	a/b (m)	B (T)	I_p (I_pd)[a] (MA)	Heating (MW) NBI	LHRF	ICRF	ECR	Objectives	Operation
JFT-2	JAERI	0.9	0.25	1.8	0.16	2	0.8	1		Multipurpose (keV plasma)	1972–1982
DIVA/JFT-2a	JAERI	0.6	0.14/0.1	2	0.07			0.3		Divertor, impurity control, low q	1974–1979
JFT-2M	JAERI	1.31	0.35/0.53	1.43	0.3 (0.55)	2	0.8	5.5	0.2	Heating, RF CD[b]/SU,[c] elongation, high beta	1983–
Doublet-III	GAT/JAERI	1.43	0.45/0.7	2.4	1	10			2	High beta, elongated plasma, divertor, low q	1979–
Doublet-III-D	GAT/JAERI	1.67	0.67/1.34	2.2	(2.5)	14			2	High beta, large elongated plasma, divertor	1985–
JIPP-T-II	IPP, Nagoya Univ.	0.91	0.17	3	0.17	0.2	0.32	2	0.064	Stellerator vs tokamak, heating	1976–1982
JIPP-TII-U	IPP, Nagoya Univ.	0.91	0.23	3	(0.3)		0.32	2	0.064	Heating, RF CD/SU	1983–
JT-60	JAERI	3.0	0.95	4.5	(2.7)	20	24	5		Multipurpose (break-even plasma)	1985–
TRIAM-1	RIAM, Kyushu Univ.	0.25	0.04	4	0.047					High field, turbulent heating	1978–
TRIAM-1M	RIAM, Kyushu Univ.	0.8	0.12/0.18	8	(0.5)					High field, Nb_3Sn coil, turbulent heating	1985–
R-Tokamak	IPP, Nagoya Univ.	2.09	0.76/1.18	3	(3)	15		> 5[d]		D-T-reacting plasma (Q ~ 0.3), heating	Approx 1989–
WT-II	Kyoto Univ.	0.4	0.09	1.4	0.03		0.1		0.05	RF CD/SU	1980–
WT-III	Kyoto Univ.	0.6	0.17	1.5	(0.15)		0.3		0.2	RF CD/SU	1985–
TORIUT-4	Univ. of Tokyo	0.3	0.12	0.4	0.02					Plasma control, low q	1980–
TNT-A	Univ. of Tokyo	0.4	0.09/0.13	0.4	0.012			0.2		Elongated plasma, heating	1975–
Hybtok-I	Nagoya Univ.	0.3	0.1	0.6	0.02		0.03			RF CD	1975–
CSTN-II	Nagoya Univ.	0.4	0.09	0.15	0.003		0.03			RF CD	1981–
FER	JAERI	5.5	1.1/1.67	5.7	(5.3)	30		30[e]		Multipurpose (ignited plasma), technology	Approx 1995–

[a] Design value of I_p.
[b] Current Drive.
[c] Start-up.
[d] At torus.
[e] Net.

This table is from J. Fusion Energy, Vol.3, No.5/6(Special Issues on Nuclear Fusion R&D Actiity in Japan)

1.2 Divertor

1.2.1 Experimental data base for the high recycling divertor

The previous data base assessment on the impurity control physics was performed as a critical item to be assessed in the Zero Phase of the INTOR Workshop conducted mainly in 1979. The adequate impurity control, including helium exhaust, was appreciated to play a key role for attaining a reactor-relevant core plasma compatible with the INTOR objectives.

The long burn operation of INTOR demands enough understandings on the transport of helium ions in main and scrape-off plasmas and on a pumping requirement for helium ashes. A permissible level of impurities in the main plasma was evaluated and it resulted in less contaminated plasmas with proper impurity control, which of course needed deep understandings on characteristics of the scrape-off plasma interacting directly with a collector plate and a first wall. In addition to them, engineering evaluations on a collector plate and a first wall, being under severe conditions, were found to be necessary.

Various concepts on the impurity control were widely assessed in the Zero Phase Workshop. Among them, the divertor concepts were evaluated to have great potential, especially the poloidal divertor was assessed to be the most promising for the INTOR impurity control concept. It was however agreed that the poloidal divertor did not always lead to a commercial reactor, and that other concepts needed further studies. It was also appreciated in the Zero Phase to evaluate requirements on a fuel feed and necessity on basic data for analyses of the impurity control, e.g. atomic and molecular collission data and surface data.

About five years have been elapsed since the data base assessment of the Zero Phase. During those years, many new tokamaks went into operation and provided new useful informations, and understandings on impurity control has made great progresses. In a divertor concept, a quite new operating regime, i.e. the high-density, low-temperature divertor plasma, was discovered. The limiter concept with particle exhaust was also developed. Furthermore, other innovative impurity control concepts make progress steadily and basic data are also accumulated and evaluated. For updating the INTOR conceptual design in Phase Two A, then, reassessment of the data base on impurity control is necessary and beneficial for the future research and development programs.

1.2.1.1 Credibility of high recycling divertor

For the impurity control in next generation tokamaks like INTOR the following two points are essential, if impurities are not positively taken advantage of, e.g. cooling a plasma boundary by appropriate impurities. Firstly, impurities released from a first wall and a collector plate, interacting directly with scrape-off plasmas, should be as low as possible. The second is to avoid the deterioration of confinement performance of main plasmas by impeding unavoidably released impurities from flowing into the main plasma confinement region.

In the past divertor experiments such as DIVA, effective screening of impurities intentionally injected within a divertor chamber was observed and considerable clean plasmas were obtained by means of a divertor operation.

The simple empirical scaling law for scrape-off parameters was also proposed, where the density along a magnetic field line in the scrape-off layer to the collector plate was to be almost constant. No past data shows a high-density divertor plasma operation. The temperature of the scrape-off layer, therefore, was estimated to be significantly high in the next generation tokamaks with a heating power of around 100MW evaluating from the old simple empirical scaling law for the scrape-off plasmas.

The high-density and low-temperature divertor plasmas were observed in Doublet III experiments with a single-null poloidal configuration as shown in Fig.1.2.1-1 for the first time [NAGAMI:1,2]. Their parameters are in a quite new regime different from the past divertor plasmas, and they have several interesting features beneficial to impurity control by the divertor concept [SHIMADA:6].

(1) The density in the divertor region increases nonlinearly with a density increase of the main plasma [NAGAMI:2]. The density near the collector plate increases to the order of $10^{20}m^{-3}$ (Fig.1.2.1-2) [SENGOKU:1,2].

(2) The high-density near the collector plate reduces the divertor plasma temperature there below 10eV (Fig.1.2.1-3) [SENGOKU:2].

(3) Radiation losses from the divertor region also increase with changes in the density and temperature (Fig.1.2.1-4) [SHIMADA:6, MAENO:1, MIYA:1]. They reduce the input power to the collector plate.

(3) Along with the changes in the divertor plasma parameters, neutral hydrogen gas pressures were also observed to be remarkably enhanced (Fig.1.2.1-5) [SHIMADA: 1].

(4) Changing magnetic configurations from limiter to divertor operation, considerable impurity reduction in the main plasmas were attained by the divertor operation [NAGAMI:2, SHIMADA:6]. Especially, the reduction in metal impurities is observed to be remarkable(FIg.1.2.1-6).

(5) Even in NBI heated discharges, similar phenomena to Joule heating were obtained [SENGOKU:2, SHIMADA:9, YOKOMIZO:1].

(6) The high-density divertor operation is compatible with the so-called H-mode discharges with good confinement time.

The high-density, low-temperature divertor plasma is caused by highly recycling particles in the divertor chamber, and the high recycling divertor concept have great advantages for impurity control. The low plasma temperature near the collector plate could results in significant reduction in an amount of released impurity from it. The high density plasma, moreover, could really be effective in avoiding penetration of released impurities from the plate. The strong radiation in the divertor chamber could also certainly ease difficulties in the heat removal of the collector plate. The pumping requirement for helium ash could also be reduced by the neutral gas compression around the divertor plasma.

From those favorable experimental results, it may be concluded that the high recycling divertor concept has some more credible features for impurity control than the conventional divertor and other impurity control concepts at

present.

1.2.1.2 Credibility of high recycling in open geometry

The magnetic configuration of the single-null poloidal divertor realized in the Doublet III experiments is significantly different from the conventional divertor, as shown in Fig.1.2.1-1. The divertor has no narrow throat between the divertor region and the main plasma, and hence has no specific divertor room separated from the main plasma chamber, and then it is called as an open-type divertor. The open divertor configuration of INTOR results from exterior poloidal coils to toroidal coils. The divertor configuration of the Doublet III device is quite similar to the single-null poloidal divertor of the present INTOR design, and results of controlability for impurities on the Doublet III experiments are significantly useful for INTOR operation.

A key point of the high recycling operation in the open divertor concept is whether most of neutral particles reemitted from the collector plate can be ionized in the divertor chamber and not return to the main plasma region and cause an amplification of a particle flow to the collector plate. Hence, it seems crucial to narrow the gap between the scrape-off edge and the divertor wall at the divertor throat, because in a case of a wide gap neutral particles can easily pass without ionization and charge exchange reactions. The vacuum chamber of the Doublet III device fortunately has a dent on the outboard wall at the midplane, as shown in Fig.1.2.1-1, which seems to prevent neutral particles from going to the main plasma and is considered to play an important role in obtaining the high recycling divertor. On the inboard side, magnetic field lines run almost parallel to the inboard wall and the gap between the wall and the scrape-off plasma edge becomes significantly narrow. Those facts are thought to lead to that the neutral particles can not go far away from the collector plate [NAGAMI:2, SHIMADA:4].

No data is reported so far from Doublet III on what configuration is effective to the high recycling divertor and on what is the allowable width for the gap. The Doublet III experimental results, however, suggest at least that the open-type divertor concept could have big potential for impurity controlability as mentioned previously, if neutral particles released from the collector plate are sufficiently impeded by making the gap narrow between the scrape-off plasma edge and the wall.

1.2.1.3 Plasma edge conditions in the "H-mode"

Discharges, a confinement time of which does not degrade with increasing a heating power and almost same as in Joule heating (H-mode), seem to be strongly associated with the divertor operation so far. The H-mode discharges can be attained with operating a divertor in the Doublet III experiments [NAGAMI:5,6]. All divertor configurations do not always lead to the H-mode discharges in the Doublet III. Some fine adjustments of the magnetic configuration is necessary for obtaining the H-mode, especially at the divertor region. It seems crucial for the H-mode operation that neutral particles should be confined in the divertor chamber and their effects should be minimized on the scrape-off layer around the main plasma as shown in Fig.1.2.1-7.

The H-mode obtained in the Doublet III discharges is somewhat different

from ASDEX, i.e. no clear-cut changes from the H-mode to the L-mode (degraded confinement diccharges) has not been observed so far. Confinement time broadly spreads in a range from the H-mode to the L-mode. Superficial differences between the H- and L-modes have been observed mainly in the scrape-off plasmas in Doublet III. The H-mode discharges have fairly low recycling in the scrape-off layer around the main plasma, and an substantial increase of its temperature and a slight decrease in its density have been measured there [KOBAYASHI:1]. No sufficient understanding on a relation between the H-mode and the divertor operation has not been established yet. At least, no H-mode discharge has been obtained with a limiter operation with gas puffing, and the Doublet III experiments evidently suggest importance of a control of the scrape-off plasmas around the main plasma by the divertor operation.

1.2.1.4 Impurity transport

Changing from a limiter operation to a divertor, impurities in the main plasma are decreased and their radiations also drop. In the high recycling divertor operation, metal impurities significantly decrease in Doublet III, as shown in Fig.1.2.1-6[NAGAMI:3]. The fact may be explained by that the metal impurities are released mainly from the collector plate and that they are reduced with decreased plasma temperatures near the collector plate and moreover released impurities could be forced to return back by effects of pre-sheath electric field and frictional forces of particle flows to the plate. On the contrary, light impurities such as oxygen and carbon decrease moderately even in the high recycling divertor operation. This may be understood in a way that most of light impurities are originated from the first wall and that screening effects for them have not clear differences between the limiter and divertor discharges.

The impurity transport in the divertor region was intensively investigated in DIVA, the conventional divertor, which was already assessed in the Zero Phase. Scarce informations on the impurity transport, however, have been obtained so far in the Doublet III high recycling divertor. Urgent studies in this area are strongly needed.

1.2.1.5 Power balance

The high recycling divertor obtained in the Doublet III experiments can be partly characterized with their high radiation losses from the divertor chamber. In Joule heating experiments, about a half of the input power is radiated in the divertor chamber for the high recycling divertor operation, as shown in Fig.1.2.1-4 [SHIMADA:6, NAGAMI:4]. NBI heated discharges are also observed to radiate a considerable part of the heating power in the high-density, low-temperature divertor operation. Those radiation losses of course reduce the heat load to the collector plate significantly [YOKOMIZO:1, SHIMADA:8].

Understanding on the main cause of the high radiation loss is a key factor for reduction of a heat load to the collector plate and no definite answer has been got yet. Radiation losses by hydrogen and light impurities are considered to be plausible candidates to explain the Doublet III experiments [SHIMADA:6].

1.2.1.6 Gas pumping from divertor

For helium exhaust in reactor relevant plasmas, essential are the confinement time of helium ions in the main plasma, transport of helium in the scrape-off layer, and behaviours of helium gas in the divertor chamber. In the Doublet III experiments, neutral gas fuel is observed to be compressed remarkably in the divertor chamber as shown in Fig.1.2.1-5. Helium gas pressure is also observed to increase just as the same way as fuel gas, when a small amount of helium gas is injected during a discharge. It means that most helium particles also recycle in the divertor chamber just like hydrogen particles [SHIMADA:2].

There is no information on behaviours of helium ions in the main plasma. Metal impurity ions, however, were measured and some analyses have been developed lately [HIRAYAMA:1,2]. It discloses that metal ions can be explained by the almost same transport as hydrogen ions.

1.2.1.7 Scrape-off and divertor plasma transport

Plasma transport in both a scrape-off layer and a followed divertor chamber play a key role in what parameters the scrape-off layer gets and how the released impurities behave. In particular, in the high recycling divertor a flow velocity of the scrape-off layer around the main plasma is observed to be considerably slow [SENGOKU:2]. The screening effect of the scrape-off plasma for impurities released from the first wall could become weak in such a case, and contamination of the main plasma is considered to be unavoidable.

In the high recycling divertor in Doublet III, the quantity of impurities is significantly reduced compared with discharges with a low-density divertor and the limiter, as mentioned above. Those facts indicate that the impurity transport in the high-density divertor plasma may not at least drastically change from other density regimes, i.e. it may be estimated that no severe impurity clogging, impeding impurities in the scrape-off layer from flowing into the divertor chamber, could occur in the high recycling divertor plasma. In any way no detail information has not been obtained yet in the Doublet III experiments. Further intensive studies are required on the scrape-off and divertor transport.

References for subsection 1.2.1

[HIRAYAMA:1]
HIRAYAMA, T., TAKIZUKA, M., NAGAMI, M., KONOSHIMA, S., ABE, M., KAMEARI, A., KODAMA, K., SENGOKU, S., WASHIZU, M., YAMAMOTO, T., BURRELL, K., BROOKS, N., and GROEBNER, R.,: "Numerical Transport Studies of Injected Titanium into Doublet III Beam Heated Discharges" GA-A17406 (1984).
[HIRAYAMA:2]
HIRAYAMA, T., TAKIZUKA, T., SHIMADA, M., NAGAMI, M., KONOAHIMA, S., ABE, M., KAMEARI, A., KITSUNEZAKI, A., KODAMA, K., SESNGOKU, S., WASHIZU, M., YAMAMOTO, T., BURRELL, K., ZAWDSKI, G., BROOKS, N., and GROEBNER, R.,: "Trace Impurity Transport in Doublet III Beam heated Plasma: Comparison of Numerical Simulations with Decay Time of Titanium Line Emission in L- and H-Mode Discharges", to be published in J. Nuclear Materials.
[IOKI:1]
IOKI, K., SHIMADA, M., NAGAMI, M., MAENO, M., IZUMI, S., YOKOMIZO, H., YOSHIDA, H., SHINYA, K., BROOKS, N., SERAYDAIAN, R., TAYLOR, T., McMAHON, T., and KITSUNEZAKI, A.: "Reduction of Heat Flux on Divertor Plates by Remote Radiative Cooling in Doublet III", Nuclear Engineering and Design 73 (1982) 45.
[KOBAYASHI:1]
KOBAYASHI, T., SHIMADA, M., SENGOKU, S., MIYA, N., KASAI, M., AIKAWA, A., KONOSHIMA, S., MATSUDA, T., NAGAMI, M., NINOMIYA, H., YOKOMIZO, H., and KAHN, C.: "Langmuir Plobe Measurements in Beam Heated Divertor Discharges in Doublet III", J. Nuclear Materials, 121(1984)17.
[MAENO:1]
MAENO, M., IOKI, K., IZUMI, S., KITSUNEZAKI, A., NAGAMI, M., SHIMADA, M., YOKOMIZO, H., YOSHIDA, H., and BROOKS, N.: "Reduction of Divertor Heat Load in Doublet III", Nuclear Fusion 21 (1981) 1474.
[MIYA:1]
MIYA, N., SHIMADA, M., KOBAYASHI, T., SENGOKU, S., KASAI, M., AIKAWAW, H., KITSUNEZAKI, A., KONOSHIMA, S., MATSUDA, T., NAGAMI, M., NINOMIYA, H., YOKOMIZO, H.: "Heat Load Reduction to the Divertor Plate by Remote Radiative Cooling in D-III Beam Heated Divertor Discharges", J. Nuclear Materials, 121(1984)126.
[NAGAMI:1]
NAGAMI, M., FUJISAWA, N., IOKI, K., KITSUNEZAKI, A., KONOSHIMA, S., OHARA, Y., SEKI, S., SHIMADA, M., SUGAWARA, T., YOKOMIZO, H., BROOKS, N., GROEBNER, R., and SERAYDARIAN, R.: "A Single Null Poloidal Divertor Experiment in Doublet III", JAERI-M 8983 (1980).
[NAGAMI:2]
NAGAMI, M., SHIMADA, M., YOKOMIZO, H., SEKI, S., KONOSHIMA, S., FUJISAWA, N., OHARA, Y., SUGAWARA, T., BROOKS, N., GROEBNER, R., SERAYDARIAN, R., and KITSUNEZAKI, A.: "Formation of Dee-shaped Plasmas with Single-Null Poloidal Divertor in Doublet III", Nuclear Fusion 20 (1980) 1325.
[NAGAMI:3]
NAGAMI, M., FUJISAWA, N., IOKI, K., KITSUNEZAKI, A., KONOSHIMA, S., OHARA, Y., SEKI, S., SHIMADA, M., SUGAWAWRA, T., YOKOMIZO, H., and the Doublet III GA Groups: "Simplified Poloidal Divertor Experiments in Doublet III", in Plasma Physics and Controlled Nuclear Fusion Research 1980 (Proc. 8th Int. Conf. Brussels, 1980) Vol.II, IAEA, Vienna (1981) 367.
[NAGAMI:4]
NAGAMI, M., SHIMADA, M., IOKI, K., IZUMI, S., MAENO, M., YOKOMIZO, H., SHINYA, K., YOSHIDA, H., BROOKS, N., HSIEH, C., DeGRASSIE, J., and KITSUNEZAKI, A.,: "Remote Radiative Cooling and Helium Ash Exhaustion with

Single-Null Ploidal Divertor in Doublet III", IAEA Technical Committee Meeting on Divertor and Impurity Control (Garching, 1981).
[NAGAMI:5]
NAGAMI, M., KASAI, M., AIKAWA, H., KITSUNEZAKI, A., KOBAYASHI, T., KONOSHIMA, S., MATSUDA, T., MIYA, N., NINOMIYA, H., SHIMADA, M., YOKOMIZO, H., and the Doublet III GA team: "High Temperature and High Density Plasmas in Beam Heated Divertor Discharges in Doublet III", in 11th European Conf. on Controlled Fusion and Plasma Physics (Aachen, 1983) B13.
[NAGAMI:6]
NAGAMI, M., KASAI, M., KITSUNEZAKI, A., KOBAYASHI, T., KONOSHIMA, S., MATSUDA, T., MIYA, N., NINOMIYA, H., SENGOKU, S., SHIMADA, M., YOKOMIZO, H., and the Doublet III GA Groups: "Energy Confinement of Beam Heated Divertor and Limiter Discharges in Doublet III", Nuclear Fusion 24 (1984) 183.

[SENGOKU:1]
SENGOKU, S., SHIMADA, M., KASAI, M., MIYA, N., AIKAWA, H., AZUMI, M., HOSHINO, K., KITSUNEZAKI, A., KOBAYASHI, T., KONOSHIMA, S., MATSUDA, T., NAGAMI, M., NINOMIYA, H., NISHIKAWA, M., TOKUTAKE, T., YAMAUCHI, T., YOKOMIZO, H., BURRELL, K. H., KAHN, C. L.: "Observation of Very Dense and Cold Divertor Plasma in Beam Heated Doublet III Tokamak with Single-Null Poloidal Divertor", JAERI-M 83-008 (1983).
[SENGOKU:2]
SENGOKU, S., SHIMADA, M., MIYA, N., KASAI, M., AIKAWA, H., AZUMI, M., HOSHINO, K., KITSUNEZAKI, A., KOBAYASHI, ., KONOSHIMA, S., MATSUDA, T., MAGAMI, M., NINOMIYA, H., NISHIKAWA, M., TOKUTAKE, T., YAMAUCHI, T., YOKOMIZO, H., BURRELL, K., and KAHN, C.,: "Observation of Very Dense and Cold Divertor Plasma in Beam Heated Doublet III Tokamak with Single-Null Poloidal Divertor", Nuclear Fusion, 24(1984)415.
[SHIMADA:1]
SHIMADA, M., NAGAMI, M., IOKI, K., BROOKS, N., GROEBNER, R.,SERAYDARIAN, R., YOKOMIZO, H., IZUMI, S., SHINYA, K., YOSHIDA, H., and KITSUNEZAKI, A.,: "Helium Compression and Enrichment with Poloidal Divertor", JAERI-M 9470 (1981).
[SHIMADA:2]
SHIMADA, M., NAGAMI, M., IOKI, K., IZUMI, S., MAENO, M., YOKOMIZO, H., SHINYA, K., YOSHIDA, H., and KITSUNEZAKI, A.: "Helium Ash Exhaust with Single-Null Poloidal Divertor in Doublet III", Phy. Rev. Lett. (1981) 796.
[SHIMADA:3]
SHIMADA, M., NAGAMI, M., IOKI, K., IZUMI, S., MAENO, M., YOKOMIZO, H., SHINYA, K., YOSHIDA, H., BROOKS, N., HSIEH, C., KITSUNEZAKI, A., and FUJISAWA, N.: "Heat Load Reduction of Divertor Plate and Formation of Dense and Cold Divertor Plasma by Remote Radiative Cooling in Doublet III and INTOR", JAERI-M 9862 (1881)
[SHIMADA:4]
SHIMADA, M., NAGAMI, M., IOKI, K., IZUMI, S., MAENO, M., MATSUDA, T., NISHIKAWA, M., OHTSUKA, M., SHINYA, K., YOKOMIZO, H., YOSHIDA, H., KITSUNEZAKI, A., BROOKS, N., DeGRASSIE, J., GROEWBNER, R., and HSIEH, C.: "High Density, Single-Null Poloidal Divertor Results in Doublet III", J. Nuclear Matrials 111&112 (1982) 362.
[SHIMADA:5]
SHIMADA, M.: "Studies on Divertor Effects by Means of the Doublet-III High Temperature Plasma Device", JAERI-M 82-195 (1982).
[SHIMADA:6]
SHIMADA, M., NAGAMI, M., IOKI, K., IZUMI, S., MAENO, M., YOKOMIZO, H., SHIMYA, K., YOSHIDA, H., BROOKS, N., HSIEH C., GROEBNER, R., and

KITSUNEZAKI, A.: "Impurity Reduction and Remote Radiative Cooling with Single-Null Poloidal Divertor in Doublet III", Nuclear Fusion 22 (1982) 643.
[SHIMADA:7]
SHIMADA, M., and the JAERI team: "Modelling of Dense and Cold Divertor Plasma in D-III", J. Nuclear Materials, 121(1984)184.
[SHIMADA:8]
SHIMADA, M., SENGOKU, S., KOBAYASHI, T., MIYA, N., KASAI, M., and the JAERI team, KAHN, C., BURRELL, K., and the GA Doublet Group: "Experimental of a Dense and Cold Divertor Plasma in D-III Beam-Heated Divertor Discharges and its Numerical Simulation", in 11th European Conf. on Controlled Fusion and Plasma Physics (Aachen, 1983) C25.
[SHIMADA:9]
SHIMADA, M., SENGOKU, S., MIYA, N., KOBAYASHI, T., WASHIZU, M., KASAI, M., NAAGAMI, M., KONOSHIMA, S., KAMEARI, A., ABE, M., HIRAYAMA, T., KODAMA, K., YAMAMOTO, T., KITSUNEZAKI, A., KAHN, C., FAIRBANKS, E., HSIEH, C., BURRELL, K., and the GA Doublet III Groups: "Divertor Studies in Beam Heated Discharges in D-III", to be published in J. Nuclear Materials.
[YOKOMIZO:1]
YOKOMIZO, H., SHIMADA, M., AIKAWA, H., HOSHINO, K.,
IOKI, K., IZUMI, S., KASAI, M., KITSUNEZAKI, A., KOBAYASHI, T., KONOSHIMA, S., MAENO, M., MATSUDA, T., MIYA, N., NAGAMI, M., NINOMIYA, H., NISHIKAWA, M., OTSUKA, M., SENGOKU, S., SHINYA, K., YAMAUCHI, T., YOSHIDA, H., and the Doublet III GA Groups: "Verticval Stability of Elongated Plasmas and Divertor Experiments in Doublet III", in Plasma Physics and Controlled Nuclear Fusion Research 1982 (Proc. 9th Int. Conf. Baltimore, 1982) Vol.III, IAEA Vienna (1983) 173.

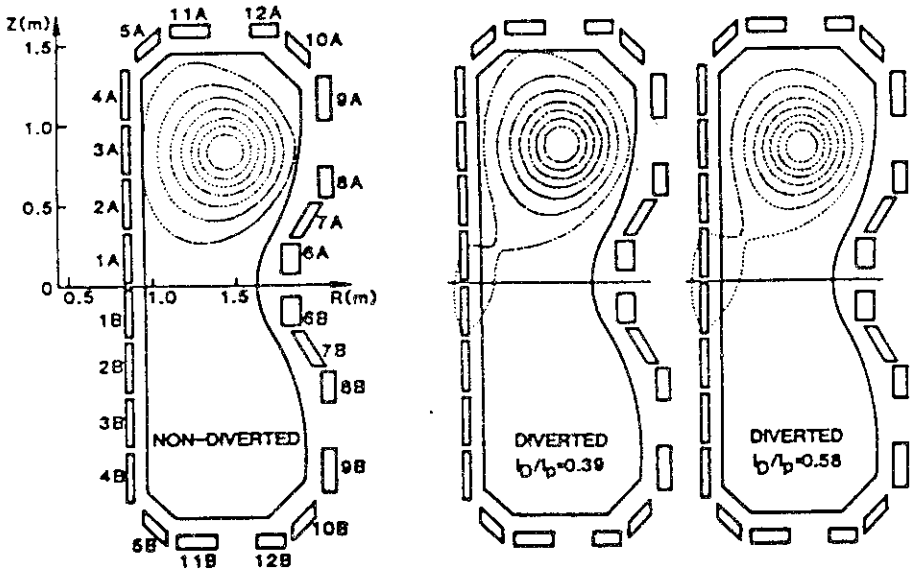

Fig.1.2.1-1 The single-null poloidal divertor equilibria can be obtained as a simple modification of a D-shaped plasma.

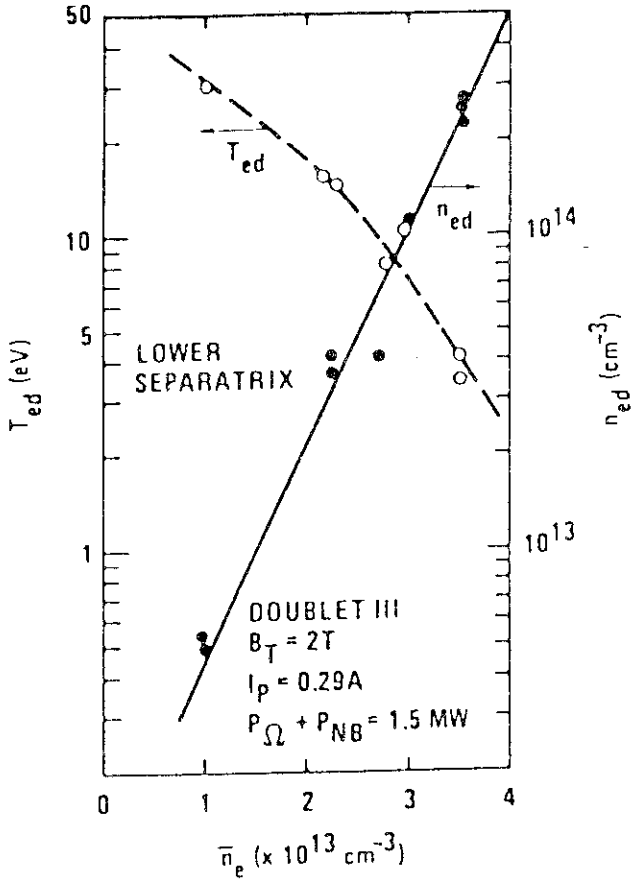

Fig.1.2.1-2 Electron density, n_{ed}, and temperature, T_{ed}, at the peaks of the density profile on the divertor plate as a function of the average density of the main plasma $\bar{n}_e$.

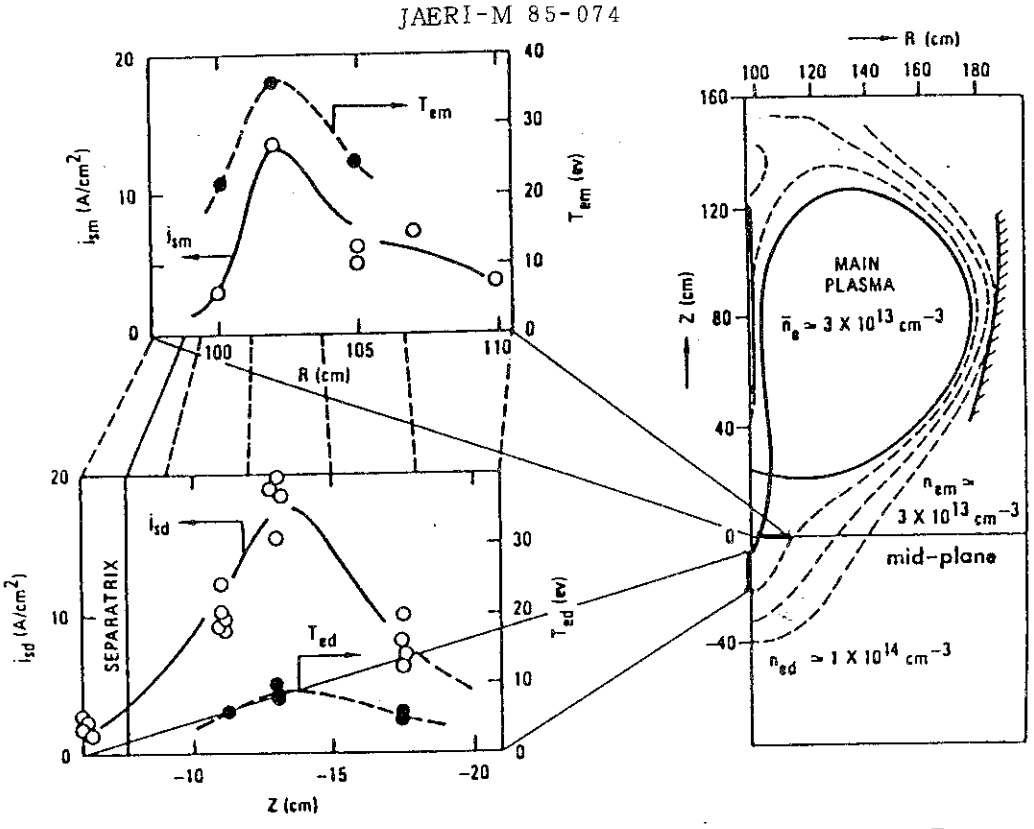

Fig.1.2.1-3 The holizontal profile of the electron temperature, T_{em}, and ion saturation current, j_{sm}, across the lower divertor channel (mid-plane: z=0cm) and corresponding vertical profiles of T_{ed} and n_{ed} on the divertor plate at t=800ms. The connection of the field lines between both profiles is shown with dotted lines.

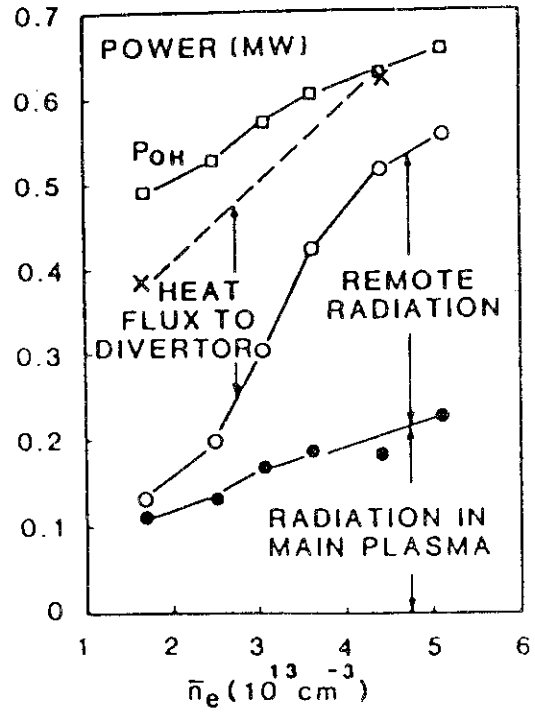

Fig.1.2.1-4 Power balance of diverted discharges of I_p=500kA. Ohmic input power P_{OH}, radiation power in the main plasma P_r, remote radiative cooling power P_{rr} as a function of $\bar{n}_e$. The power to the divertor plates measured by thermocouples is also shown in the figure. The remote radiation reaches 50% of ohmic input at high $\bar{n}_e$.

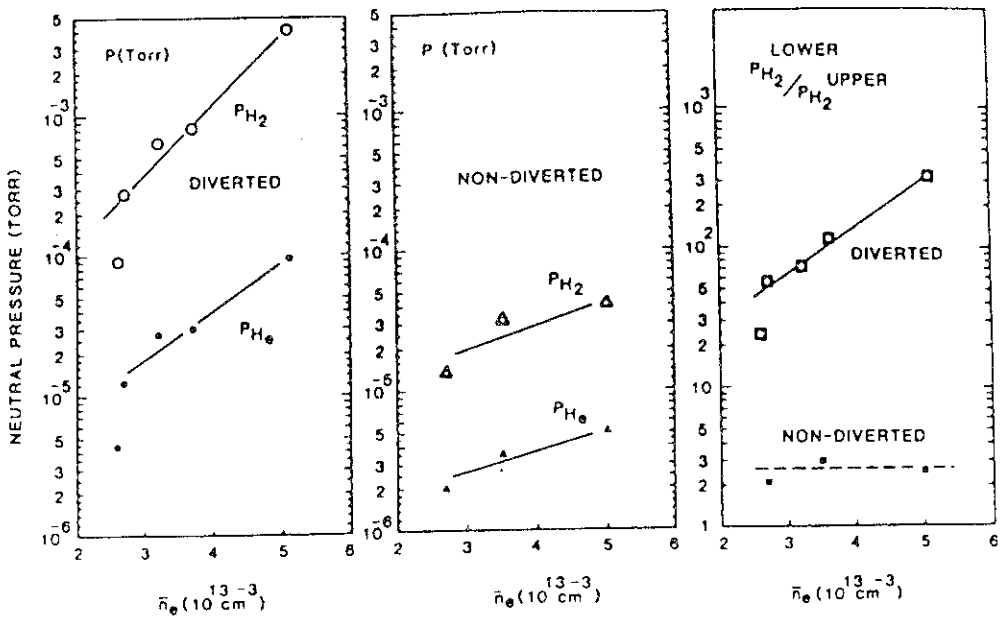

Fig.1.2.1-5 Pressure of molecular hydrogen and helium measured at the lower chamber ports versus electron density with and without the divertor (electron density was measured just before the helium gas input). The ratio of P_{H_2} measured lower chamber port to P_{H_2} near the main plasma is also shown. In a high density divertor discharge, P_{He} reaches 1×10^{-4}Torr with a helium concentration of 1.6% in the main plasma. This result demonstrates the effective ash exhaust function of a divertor.

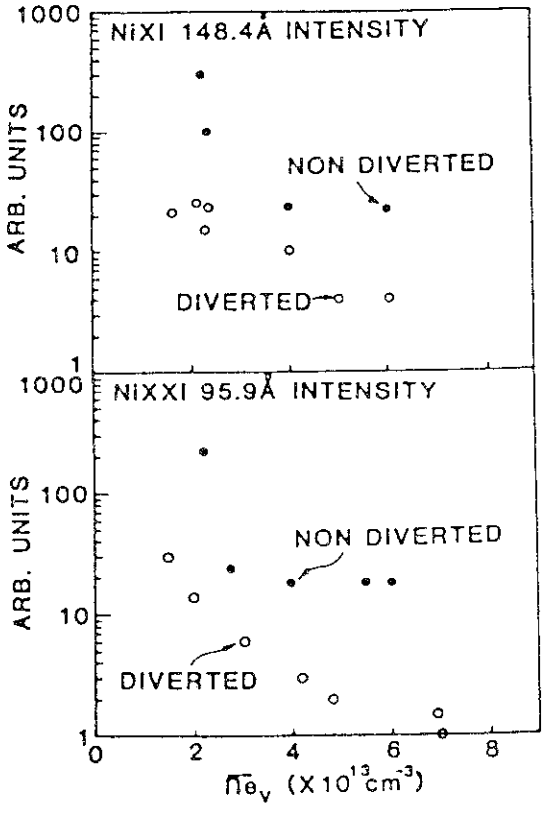

Fig.1.2.1-6 The divertor reduces the influx and sccumlation of metallic impurity by a factor of 5-10.

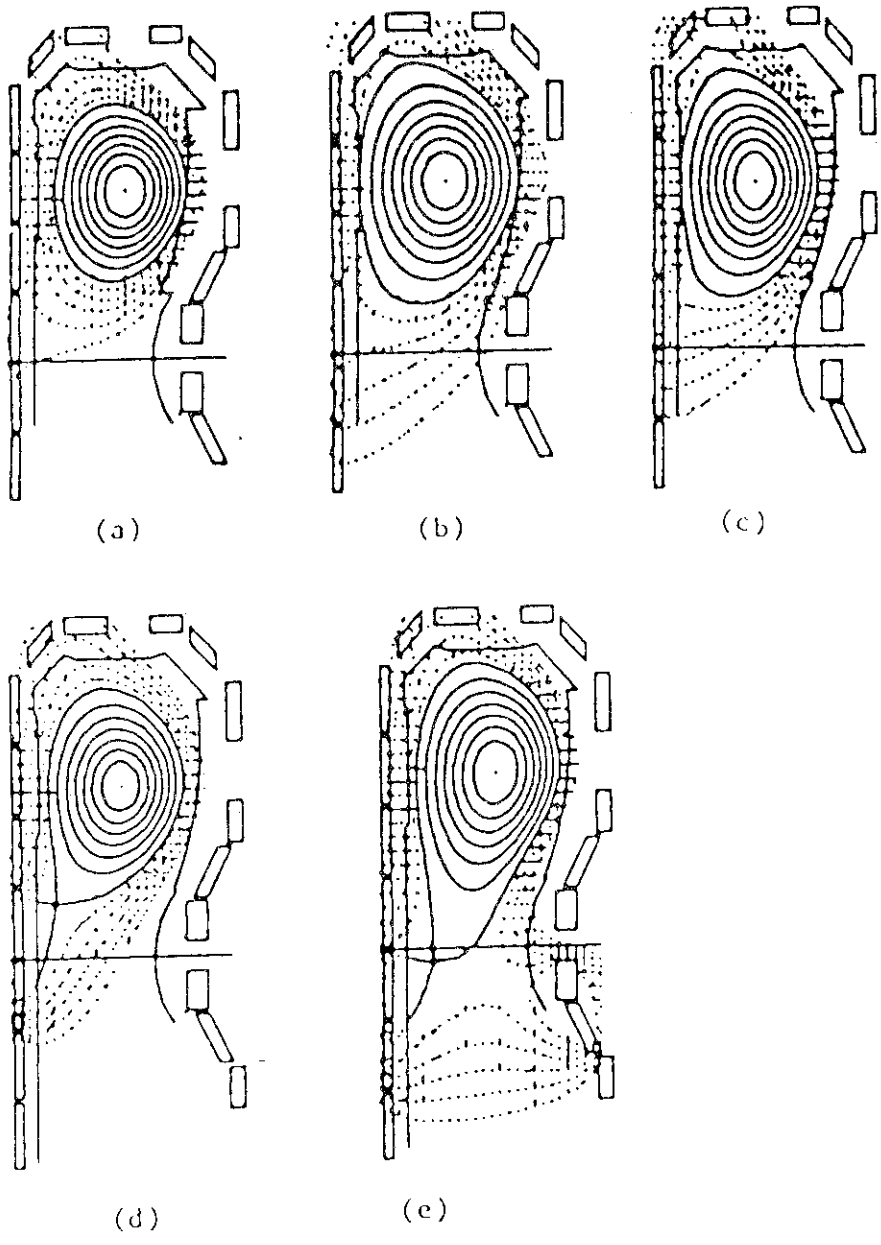

Fig.1.2.1-7 Five typical equilibria. (a)-(c) limiter discharges, (d)-(e) divertor discharges. H-mode is obtained in equilibrium (e).

1.2.2 Divertor modelling and validation

1.2.2.1 Two dimensional modelling of divertor plasma

Poloidal divertor scheme has been adopted as the most reliable control measure for impurities including helium ash through discussions during the past four years on the INTOR workshop [1-3]. Experimental [4-6] and theoretical studies [7-10] have strongly suggested a possibility of cold and dense divertor plasmas that could lead to reduction of sputtering erosion and heat load on the divertor plate and to improvement of the helium pumping efficiency.

In order to discuss the possibility of the cold and dense divertor operation, a two dimensional program for the divertor plasma and neutral particles has been developed. The divertor plasma is strongly influenced by the neutral particles emitted from the divertor plate and traversing the divertor chamber through ionization and charge exchange reactions. Therefore, a self-consistent modelling is necessary for the description of the divertor plasma and neutral particles. The divertor plasma is described by the fluid equations and the neutral particle transport in the divertor chamber is solved by the Monte Carlo simulation. The interactions between the divertor plasma and neutral particles are self-consistently solved by an iterative procedure.

The two dimensional flow of the divertor plasma is described by the particle, momentum and energy conservation equations along the magnetic field line [10] as follows:

$$\frac{\partial}{\partial z} f_{k,z}(x,z) = S_k(x,z) + \frac{\partial}{\partial x}\left(D_\perp \frac{\partial n_k(x,z)}{\partial x}\right) , \quad (k = D,T,He) ,$$

$$\frac{\partial}{\partial z}\left[n_p(x,z)(2U(x,z) + z_p T_e(x,z) + T_i(x,z))\right] = \frac{B_T}{B_p}\left[S_p(x,z) + \frac{\partial}{\partial x}\left\{\frac{2U(x,z)}{V_{/\!/}(x,z)} D_\perp \frac{\partial n_p(x,z)}{\partial x}\right\}\right] ,$$

$$\frac{\partial}{\partial z}\left[f_z(x,z)\left(U(x,z) + \frac{5}{2} T_i(x,z)\right) + q_i(x,z)\right] = - V_z \frac{\partial}{\partial z} P_e(x,z) + P_{ei}(x,z) + S_{Ei}(x,z) + \frac{\partial}{\partial x}\left[\left\{U(x,z) + \frac{3}{2} T_i(x,z)\right\} D_\perp \frac{\partial n_p(x,z)}{\partial x} + K_{i\perp} \frac{\partial T_i(x,z)}{\partial x}\right] ,$$

$$\frac{\partial}{\partial z}\left[\frac{5}{2} f_z(x,z)\, T_e(x,z) + q_e(x,z)\right] = - V_z \frac{\partial}{\partial z} P_e(x,z) - P_{ei}(x,z) + P_r(x,z) + S_{Ee}(x,z) + \frac{\partial}{\partial x}\left[\frac{3}{2} T_e(x,z)\, D_\perp \frac{\partial n_e(x,z)}{\partial x} + K_{e\perp} \frac{\partial T_e(x,z)}{\partial x}\right] ,$$

where the coordinates along and across the divertor throat are denoted by z and x, respectively. The symbol used here are explained as follows:

$f_{K,Z}$(K=D,T and He) : ion fluxes for D, T and He particles in the z-direction,
f_Z : total ion flux in the z-direction,
n_K(K=D,T and He) : ion densities for D, T and He particles,
n_p : total ion density,
n_e : electron density,
$V_{//}$: ion flow velocity along the field line,
V_z : ion flow velocity in the z-direction,
U : $\frac{1}{2} m_p V^2$ (m_p : average ion mass),
T_e : electron temperature,
T_i : ion temperature,
P_e : electron pressure,
q_{ez} : electron conduction heat flux in the z-direction,
q_{iz} : ion conduction heat flux in the z-direction,
P_{ei} : collisional energy transfer between electrons and ions,
S_K, S_P, S_{Ee}, S_{Ei} : plasma source for the ionization and charge exchange of the neutrals,
P_R : radiation loss term,
D : perpendicular diffusion coefficient,
K_e : perpendicular heat conductivity for electrons,
K_i : perpendicular heat conductivity for ions.

Part of the boundary conditions to solve the fluid equations are given at the divertor throat entrance as the incoming particle fluxes $f_{K,Z}(x,o)$, the total heat fluxes $Q_{TOT}(x,o)$ and the ratio of the electron to ion temperature in order to describe the linkage to the main plasma. The rest of the boundary conditions is imposed by the sheath electric field which is formed in front of the divertor plate, Z=L:

$$U(x,L) = \frac{1}{2}\left[Z_p T_e(x,L) + T_i(x,L) \right] ,$$

$$Q_{TOT}(x,L) = \gamma_{TOT} T_e(x,L) f_Z(x,L) ,$$

$$\left.\frac{\partial q_{iz}(x,z)}{\partial z}\right|_{z=L} = 0 .$$

The plasma sources $S_{K,N}$, S_P, S_{Ee} and S_{Ei} are calculated with the use of the Monte Carlo simulation for the neutral particle transport, where the following physical processes are included: ionization and charge exchange of the atoms, dissociation of hydrogen molecules and reflection of atoms at divertor chamber walls [11].

1.2.2.2 Comparisons between the numerical results and experiments

The experimental studies of the divertor plasmas have been made on the several tokamaks as stimulated by the development of tokamak reactors such as INTOR. The experiments have indicated important characteristics as follows:

(a) formation of high density and low temperature plasmas,
(b) strong radiative cooling of the divertor plasmas, and
(c) nonlinear dependence of the divertor plasma density on the main plasma density.

The numerical simulation based on the model presented in the previous section was compared with the Doublet III experiments under 1 MW NBI heating. The main features of the D-III experiments were shown to be successfully reproduced. (See Appendix 1)

1.2.2.3 Simplified divertor model

The numerical simulation gives the dual equilibrium solutions of the divertor plasma in the limited range of the ion flux entering the divertor. The origin of the dual solutions can be explained by a simplified modelling of the neutral particle recycling in the divertor plasma in the following.

The incident ion flux at the divertor throat, $F_\xi(0)$, is amplified to the ion flux at the divertor plate, $F_\xi(L)$. The ion flux amplification defined by $R=F_\xi(L)/F_\xi(0)$ is determined by the trapping efficiency, η, of the neutral particles in the divertor plasma as follows:

$$R = \frac{1}{1-\eta}$$

A gross particle balance in the divertor gives the following relationship.

$$\eta = [1 - g_0 \exp(\frac{L}{\lambda_\xi})] \; [1 - \eta_{esc} \exp(\frac{b}{\lambda_\perp})]$$

The first bracketed term in the last equation is the probability for a neutral particle to be reionized when it moves back to the main plasma region through the divertor plasma. The factor $\exp(-b/\lambda_\perp)$ in the second bracketed term is the probability for a neutral particle to flow out of the divertor plasma across the divertor channel, and η_{esc} is the probability for a neutral particle emerging from the divertor plasma to escape from the divertor chamber. The mean free paths of the neutral particles λ_ξ and $\lambda_\perp$ can be expressed as functions of the ion flux amplification, R. Therefore, the ion flux amplification R can be determined from the last equation. The electron density and temperature in front of the plate can also be expressed as functions of R. The solutions of the last equation can explain the existence of the dual solutions as described in detail in Appendix 2.

References for subsection 1.2.2

[1] INTOR GROUP, International Tokamak Reactor: Phase Zero (Rep. Int. Tokamak Reactor Workshop, Vienna, 1979), International Atomic Energy Agency, Vienna (1980).
[2] INTOR GROUP, International Tokamak Reactor: Phase One (Rep. Int. Tokamak Reactor Workshop Vienna, 1981), International Atomic Energy Agency, Vienna (1982).
[3] INTOR GROUP, International Tokamak Reactor: Phase Two A (Rep. Int. Tokamak Reactor Workshop, Vienna, 1983), International Atomic Energy Agency, Vienna (1983)
[4] M. Shimada, et al., Phys. Rev. Lett. 47, 796 (1981), S. Sengoku, et al., Nucl. Fusion 24, 415 (1984).
[5] Y. Shimomura, et al., IPP III/80 (1982).
[6] R.J. Fonk, et al., J. Nucl. Mater 111 & 112, 343 (1982).
[7] M. Petravic, et al., Phys. Rev. Lett. 48, 326 (1982).
[8] M.F.A. Harrison, et al., Nucl. Technol./Fusion 3, 432 (1982).
[9] M. Petravic et al., Ninth IAEA Conf. Baltimore, 1982, IAEA-CN-41/D-3-2.
[10] S. Saito et al., J. Nucl. Mater. 121, 199 (1984).
[11] S. Saito et al., Nucl. Technol./Fusion 4, 498 (1983).

1.2.3 Predictive modelling of single-null poloidal divertor for the high recycling regime

1.2.3.1 High recycling regime

The characteristics of the divertor plasma would strongly depend on the main plasma state, i.e. on the particle and heat fluxes flowing from the main plasma into the divertor throat entrance. Therefore, the electron density and temperature near the divertor plate are calculated as a function of the incoming ion flux and heat flux, as shown in Figs.1.2.3.2 and 1.2.3.3.

The divertor configuration is simply modified as shown in Fig. 1.2.3.1 where the divertor throat length from the null point of the poloidal field is set to 50 cm. The distributions of the incoming ion flux and heat flux at the divertor throat entrance are assumed to have an exponential distribution where the e-folding distances are 7 cm, since the e-folding distance of the scrape-off plasma, around 3 cm on the main plasma edge, expands, by a factor of about 3, going from the main plasma edge to the divertor throat.

Figure 1.2.3.2 shows the relation between the peak electron density at the divertor plate and the incoming ion fluxes for the case of the incoming heat flux of 6, 24 and 40 MW. It should be noted that the electron density rapidly increases to a level of $10^{14}/cm^3$ with the increased incoming ion flux. As shown in Fig. 1.2.3.3, the corresponding electron temperature decreases to less than 10 eV. In this study, the effective pumping speed for the helium neutrals is set to a rather high value of 2.5×10^5 1/s compared with the pumping speed required for the helium ash removal. Higher pumping speed would result in lower ion flux amplification that leads to the lower electron density and higher electron temperature near the divertor plate. In order to assure the feasibility of the cool and dense divertor operation in INTOR, it is necessary to discuss the divertor operation under the higher pumping speed possible for the INTOR divertor operation. It should be remarked that the cool and dense divertor plasma can be obtained even for the rather low ion flux of 10^{22}/s that corresponds to a very long particle confinement time of 1.7 s for the INTOR standard operation parameters.

The two dimensional distributions of the ion flux in the z-direction and the electron density and temperature are shown in Figs. 1.2.3.4, 5 and 6, respectively, for the case of the incoming ion flux 3×10^{22}/s and the pumping speed 2.5×10^5 1/s. As shown in Fig. 1.2.3.4, the ion flux is amplified, by a factor of about 100, from the divertor throat entrance z=0 cm to the divertor plate z=50 cm. It can be seen from Fig. 1.2.3.5 that the electron density increases from $6\times10^{13}/cm^3$ at the divertorthroat to about $5\times10^{14}/cm^3$ at the divertor plate. The electron density $6\times10^{13}/cm^3$ at the divertor throat could be compatible with the edge density of the main plasma, i.e. the solution of the divertor plasma could be smoothly connected with the main plasma scrape-off layer. The electron temperature varies from about 50 eV at the divertor throat entrance down to less than 10 eV near the divertor plate. These cold plasma layer formed in front of the divertor plate could protect the divertor plate from the sputtering erosion by ions. From these viewpoints, the typical solution shown in Fig. 1.2.3.4, 5 and 6 is selected as the standard parameters for the design of the divertor chamber.

Total loss powers from the divertor plasma increase with the increased ion flux as illustrated in Fig. 1.2.3.7 and reach about 50% of the incoming

heat flux at the particle confinement time of about 1 s. The large total loss power is mainly due to the radiation loss from the recycling hydrogen neutrals. It is obviously found in Fig. 1.2.3.7 that the fraction of the total loss power slightly depends on the incoming heat flux. The fraction of the radiation power depends mainly on the electron temperature. The weak dependence of the loss power fraction can be explained by the fact that the electron temperature depends weakly on the incoming heat flux.

The power balance of the divertor plasma and neutral particles is shown in Fig. 1.2.3.8 for the standard divertor parameters, Q=40 MW and $I=3\times10^{22}$/s. The total incoming heat flux of 40 MW is carried by the electrons, ions, neutral particles and radiations, and finally absorbed on the inside wall of the divertor chamber and on the first wall. The heat load on the divertor plate is found to be reduced by a factor of 2 due to the dissipation of the heat flux by the radiations and neutral particles.

1.2.3.2 Impurity control

We have indicated that there exists a possiblity for a dense and cold divertor plasma near the neutralizer plate by using the detail numerical code in the previous section. More investigations are required before we conclude, since the characteristic feature of divertor plasma may depend on other parameters, for examples, the ratio of the poloidal to toroidal magnetic field B_p/B_T, perpendicular diffusion and thermal conduction coefficients and the widths of incoming ion and heat flux spatial profiles.

The used parameters are classified into four cases.

Case I : $D_\perp = \chi_\perp = 0$, $B_p/B_T = 0.1$

Case II : $D_\perp = \chi_\perp = 0$, $B_p/B_T = 0.15$

Case III: $D_\perp(z) = 10^4$ cm^2/sec, $\chi_\perp(z) = 2D_\perp(z)$, $B_p/B_T = 0.15$

Case IV : $D_\perp(z) = 10^4$ cm^2/sec, $\chi_\perp(z) = 2D_\perp(z)$, $B_p/B_T = 0.1$

Other parameters are the same as designated in all the cases. The hydrogen line radiation is included, but the radiation due to impurities and the multi-step ionization process are not included yet. Two dimensional profiles of electron temperature and density are investigated again but no significant change appears. The electron temperature near the neutralizer plate becomes very low (below 10 eV) and the density very high (order of 10^{14} cm^{-3}). These indicate that one can attain the low temperature and high density plasmas near the plate with the benchmark parameters. Diffusion and thermal conduction processes cause no remarkable differences between Case I and Case III qualitatively. If the ratio B_p/B_T becomes large from 0.1 to 0.15 for Cases I and II, the electron density at the plate decreases and the electron temperature increases. According to a broad range of parameter survey, the e-folding lengthes of the distributions of the incoming ion and or heat fluxes may have more effects rather than the diffusion and the thermal conduction processes in the divertor chamber for the range of $D < 5\times10^3$ cm^2/sec. We cannot find any qualitative difference as concerns the radiation loss and power flow.

Here we examine in detail the characteristic feature of the equilibrium solutions of the divertor plasma by the numerical code. There exists a single equilibrium solution in the low range of the incoming ion flux, where the plasma density is sufficiently low (we call it lower solution). Another solution (upper solution) can be obtained, the value of which jumps at some incoming ion flux as the incoming ion flux becomes large. The latter solution is a high density and low temperature one. These features are clearly explained elsewhere [1] together with the simple analytic model developed in §1.2.2.3. The low temperature below 10 eV is confirmed by both the numerical code and the simple divertor plasma model.

Neverthless, a quantitative problem, i.e. whether more than 10 eV or less than 10 eV, is left. The difference in the temperature was estimated to be caused from difference in a width of incoming power flow into the divertor region. A broad profile assumed could lead to the low temperature plasma, less than 10 eV, near the divertor plate. To check the above guess, a divertor with a narrow width of a incoming power flux is investigated by a model based on 2D plasma transport and Monte-Carlo transport of neutrals within a divertor. A divertor geometry used is a rectangular chamber, as shown in Fig. 1.2.3.9. The peak values of density and temperature near the neutralizer plate are shown in Figs. 1.2.3.10 and 11, which also include the previous results with the broad profile. The low temperature below 10 eV is obtained.

The reason of the difference in temperatures (more than 10 eV or less than 10 eV) is not clear. Only the narrow power profile can not explain the difference. Some combined effects with it could be important for the peak temperature to go above 10 eV.

1.2.3.3 Pumping of helium

For a steady-state operation of the INTOR, accumulation of the helium ash in the main plasma should be reduced to less than 5% of the plasma density. For this purpose, the helium neutrals must be evacuated through the exhaust systems at the production rate of the helium ions in the main plasma, Γ_α . Therefore, the following relation must be satisfied from the particle balance:

$$\frac{N_\alpha}{N_i} I (1 - f_{bf}) = \Gamma_\alpha \quad ,$$

$$f_{bf} = 1 - \frac{\Gamma_\alpha}{I} \left(\frac{N_\alpha}{N_i}\right)^{-1} \quad ,$$

where f_{bf} is the backflow fraction of the helium which is defined as the ratio of the helium neutral flux returning to the main plasma to the incoming helium ion flux. The above equation yields the helium backflow fraction 0.86 in order to keep the 5% concentration of the helium ash in the main plasma for the case of the INTOR standard parameters and $I=3\times10^{22}$/s.

On the other hand, the relation between the helium backflow fraction f_{bf} and the effective conductance C_{eff} is obtained by the numerical calculation as shown in Fig. 1.2.3.12. The helium backflow fraction 0.86 is found in Fig. 1.2.3.12 to correspond to the effective conductance of about 2×10^4 l/s which

could ease the R and D needs for the exhausting systems.

If the effects of B_p/B_T, $D_\perp$ and $\chi_\perp$ are taken into account, the results become as follows. For Case I, we have already reported the value of 2×10^4 1/sec for the required pumping speed, where the self consistent procedure was taken. There will be no significant difference in the required pumping speed for Case I and III.

1.2.3.4 Optimization of geometry

A possibility of the formation of dense and cold divertor plasma relies on not only the incoming ion and heat fluxes but also the divertor geometry. We have done the parameter survey for various geometries [1]. The essential parameters of geometrical dependence are the throat length L and void width d if the width of the plasma region is the same. We express the geometrical characteristics by the terms, close-standard-open. We have concentrated on the standard geometry (L=50 cm and d=5 cm) so far. We will change L and d. The term, close, is used when the throat length L is long and/or the void width d is narrow. On the other hand, the term, open, is used when L is short and/or d is wide.

We will discuss the formation of dense and cold divertor plasma from two points of views, that is, the plasma temperature near the plate and the required pumping speed. In both close, standard and open geometries, the low temperature solution below 10 eV can be obtained. However the range of incoming ion flux, I, that stable dense and cold solution exists changes depending on the incoming heat flux, Q. As the geometry becomes open and/or the incoming heat flux becomes large, such range becomes higher. When Q=40 MW in open geometry (L=d=25 cm), such range is above 7×10^{22}/s. In the case of Q=24 MW, such range is above 5×10^{22}/s. A single solution is obtained in the whole range as a function of incoming ion flux in the case of Q=6 MW, where $T_e < 10$ eV in the range $I > 3\times10^{22}$/s. When Q=24 MW in the standard geometry (L=50 cm and d=5 cm), such range is above 2×10^{22}/s. As the geometry becomes close, the lower limit that stable dense and cold solution exists decreases. It depends on the particle confinement time in the main plasma what range the incoming ion flux I exists on.

The throat length and the void width are also limited by the required pumping speed. In the standard geometry, the required pumping speed becomes 10^5 1/s from the relation between the neutral helium density at the evacuating duct by the numerical code and the required helium density to exhaust same number of helium particles as being produced. In the open geometry, when I is in the range $2\times10^{22}/s \leqslant I \leqslant 4\times10^{22}$/s, the serious erosion problem of the plate can well be mitigated by achieving the upper solution, whereas the helium ash exhaust may be difficult even by the quite large pumping speed of 5×10^5 1/s.

1.2.3.5 Conclusions

The divertor operating condition for INTOR was investigated based on the two dimensional program, solving consistently the divertor plasma and neutral particles. Simple analytic model is also developed to clarify the dual structure of the solution of the numerical code. The numerical results strongly suggest that the cold plasma layer less than 10 eV could be produced in front of the divertor plate, provided that the particle confinement time of the main plasma is shorter than 1.7 s. The evaluation of the backflow

fraction of the neutrals indicated the low effective pumping speed of about 2×10^4 l/s to keep the 5% concentration of the helium ash in the main plasma. When the void margin is taken into account, however, the required pumping speed should be 10^5 l/s from the relation between the neutral helium density at the evacuating duct by the numerical code and the required helium density to exhaust same number of helium particles as being produced in the main plasma [1]. These low temperature and the required pumping speed conditions indicate that the divertor throat length should be about 50 cm and the void width be 5 ~ 25 cm.

The sputtering erosion of the divertor plate and the other inside wall of the divertor seems not to be serious problem, since the electron temperature could be reduced to less than 10 eV near the divertor plate.

References

[1] M. Sugihara, S. Saito, S. Hitoki and N. Fujisawa, J. Nucl. Mater. 128-129 (1984) 114.

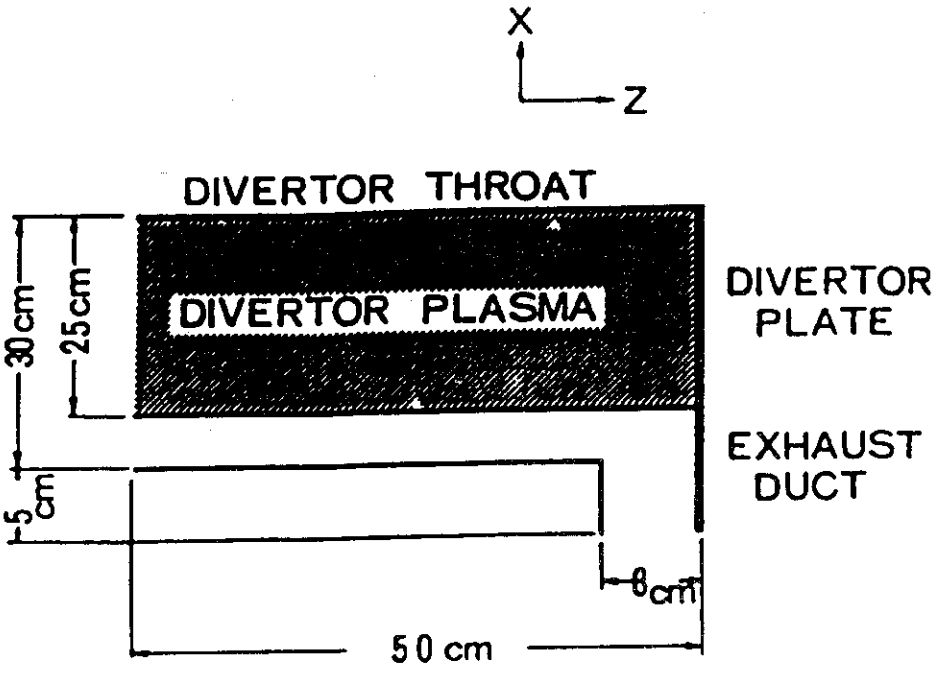

Fig. 1.2.3.1 Model divertor chamber for INTOR.

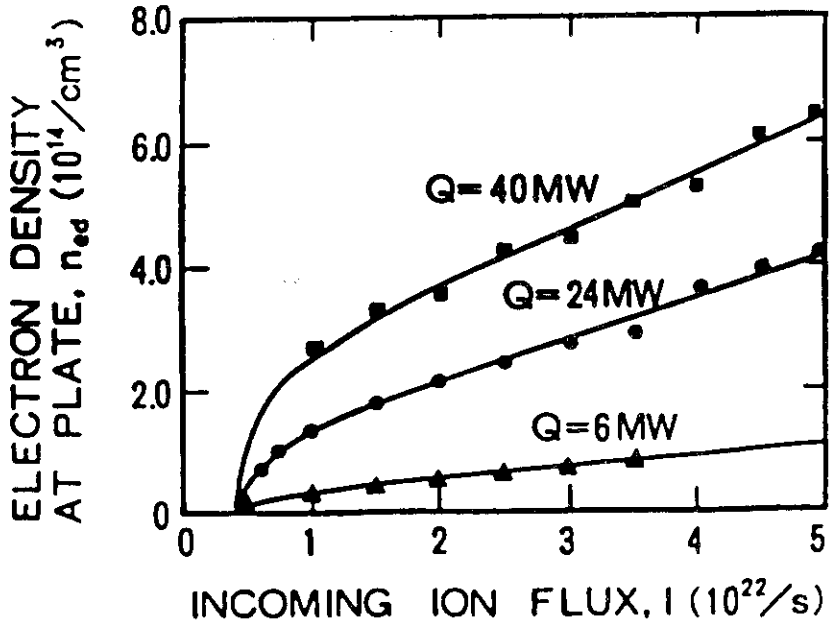

Fig. 1.2.3.2 Calculated peak electron density at the divertor plate as a function of the incoming ion flux. The calculated results are shown for the incoming heat fluxes of 6, 24 and 40 MW.

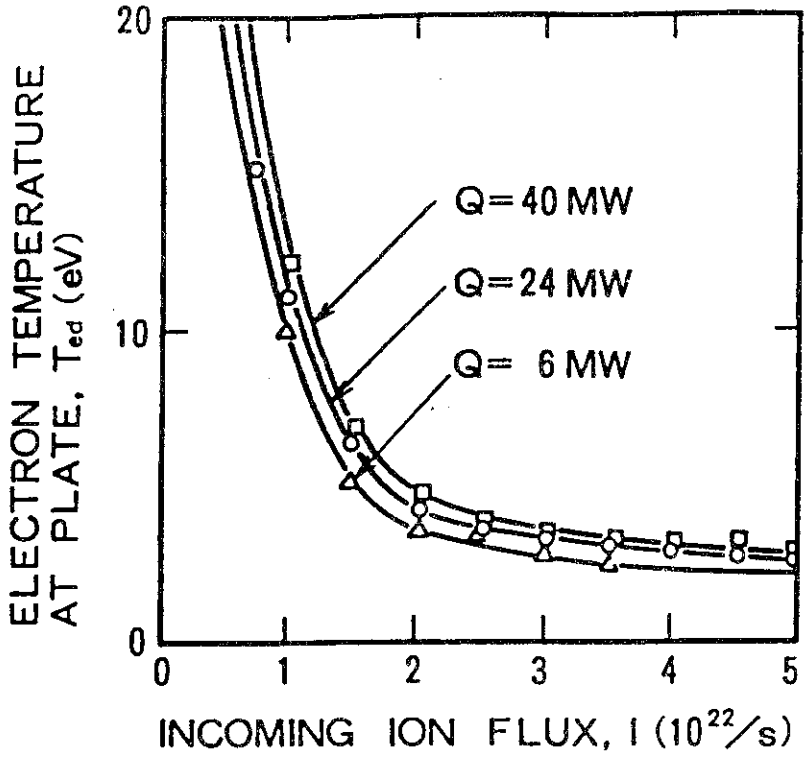

Fig. 1.2.3.3 Calculated peak electron temperature at the divertor plate as a function of the incoming ion flux. The calculated results are shown for the incoming heat fluxes of 6, 24 and 40 MW.

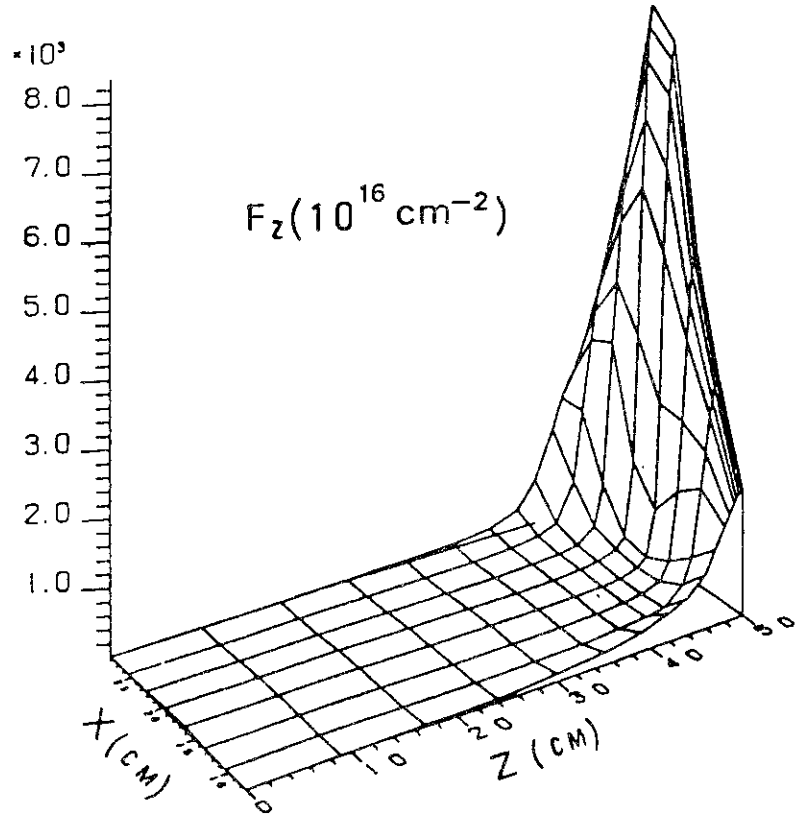

Fig. 1.2.3.4 Two dimensional distribution of the ion flux in the z-direction. (Q=40 MW, I=3x10^{22}/s)

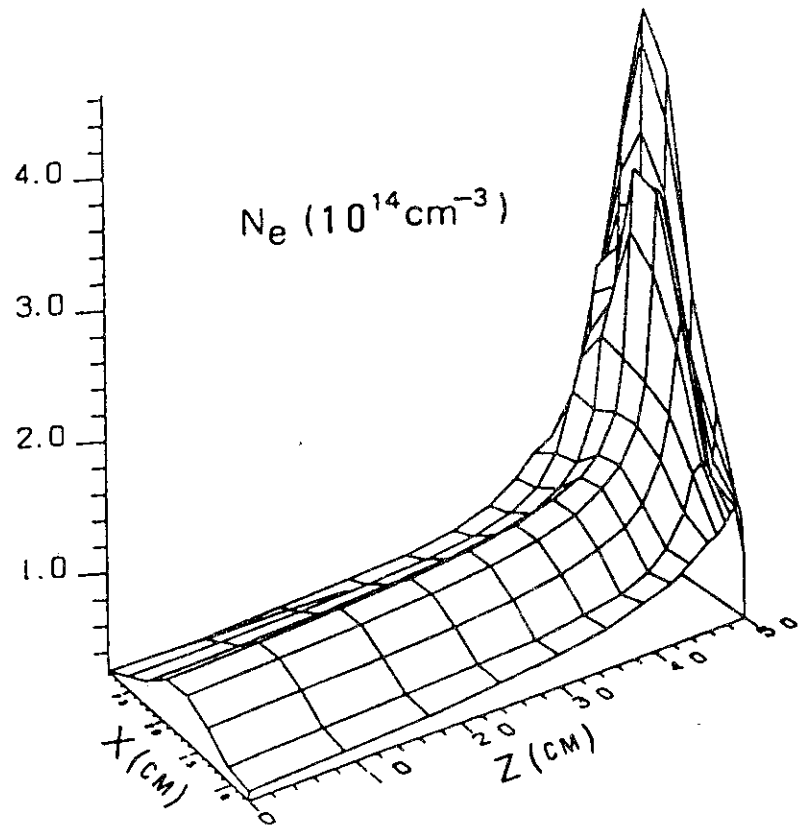

Fig. 1.2.3.5 Two dimensional distribution of the electron density in the divertor plasma. (Q=40 MW, I=3x10^{22}/s)

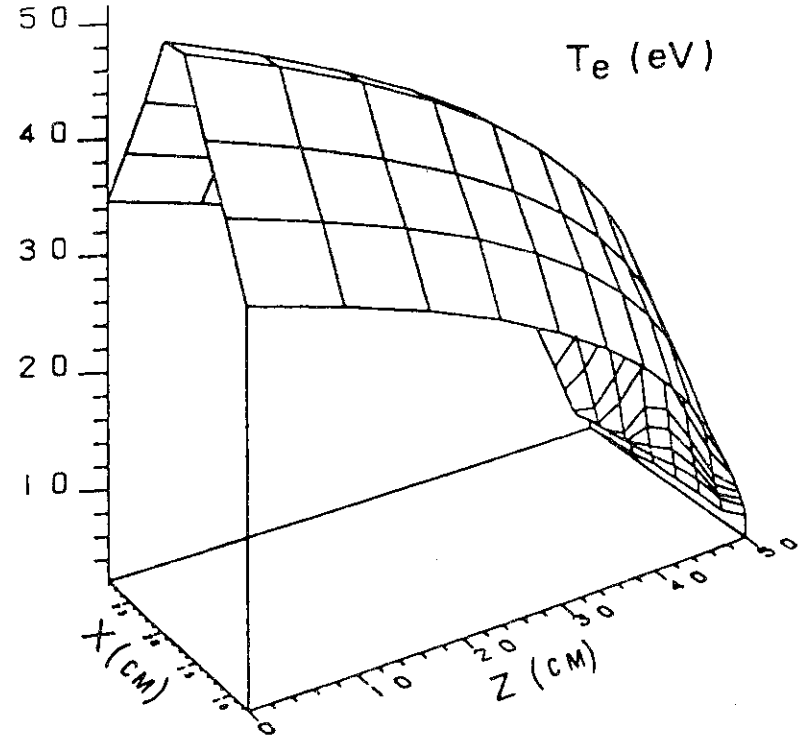

Fig. 1.2.3.6 Two dimensional distribution of the electron temperature in the divertor plasma. (Q=40 MW, I=3x10^{22}/s)

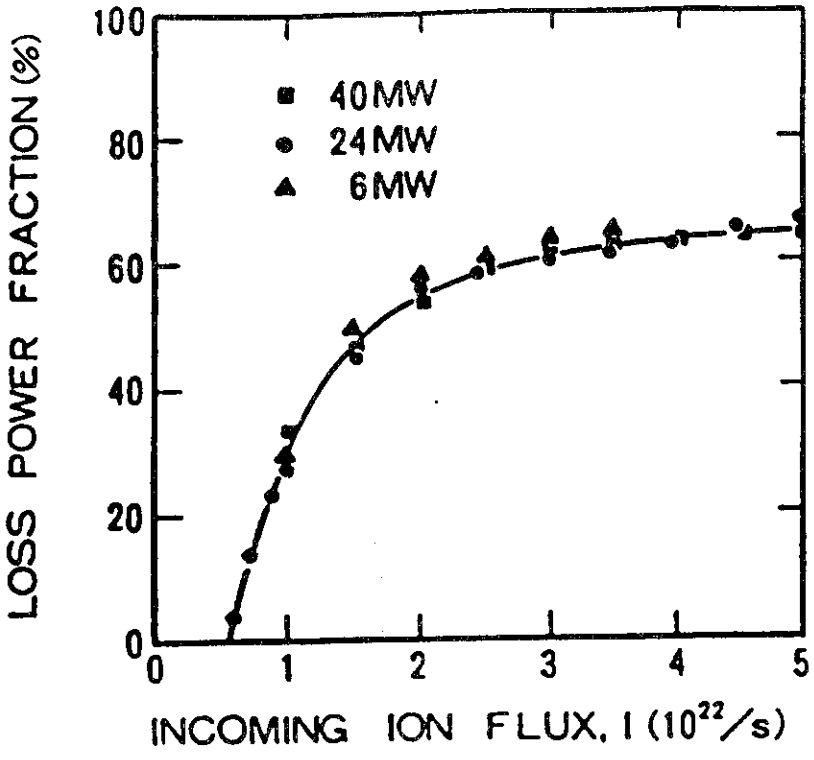

Fig. 1.2.3.7 Calculated fractions of the total loss power of the divertor plasma as a function of the incoming ion flux.

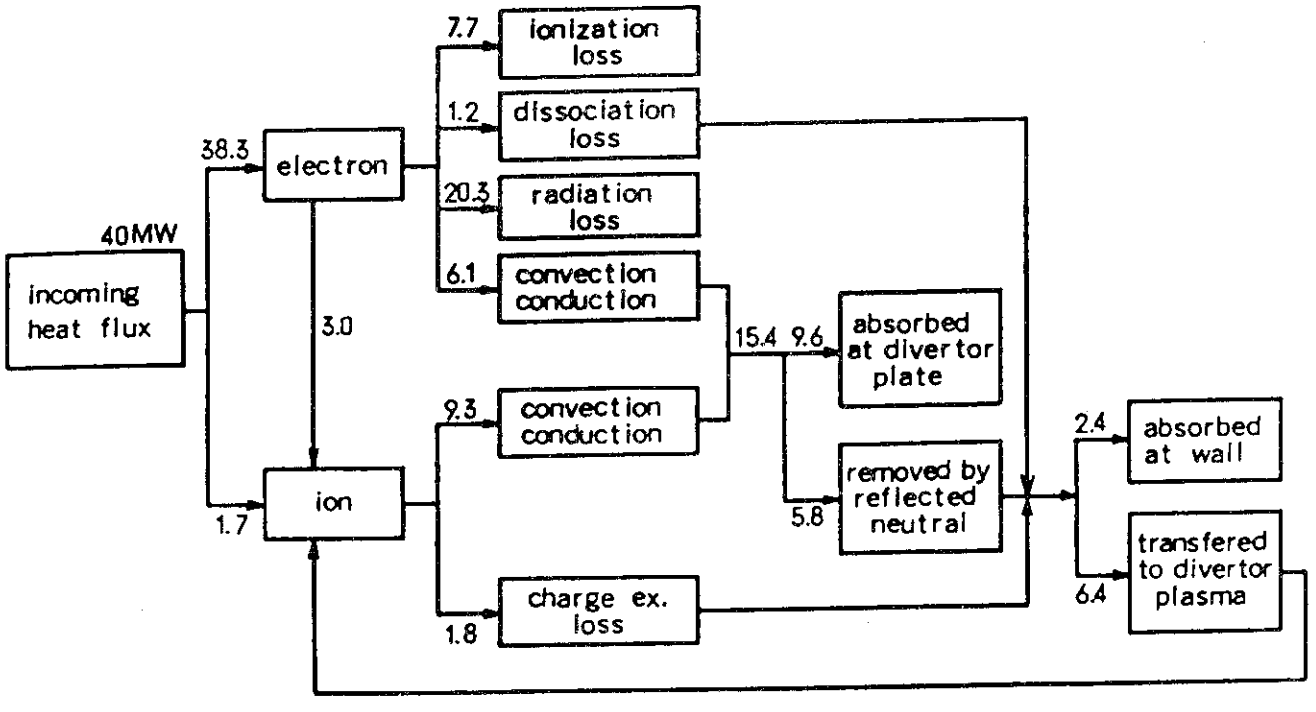

Fig. 1.2.3.8 Energy balance of the divertor plasma and neutral particles in the INTOR divertor. (Q=40 MW, I=3x10^{22}/s)

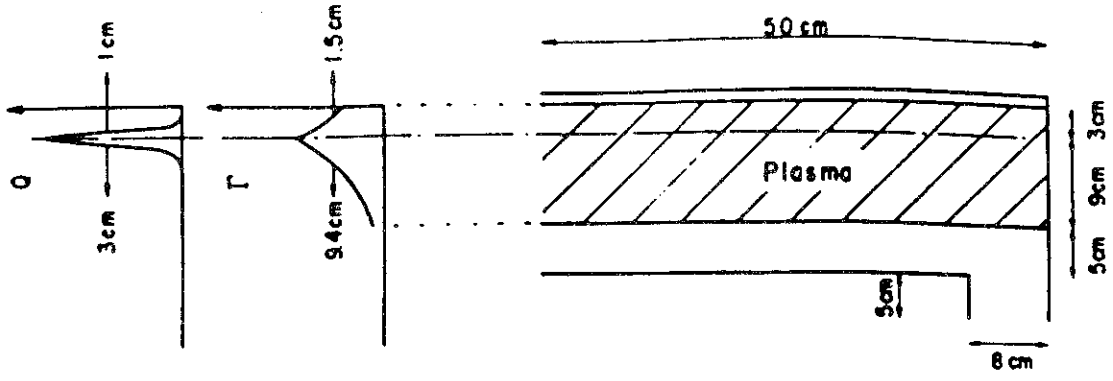

Fig. 1.2.3.9 Geometrical configuration and widths of particle and heat fluxes are shown.

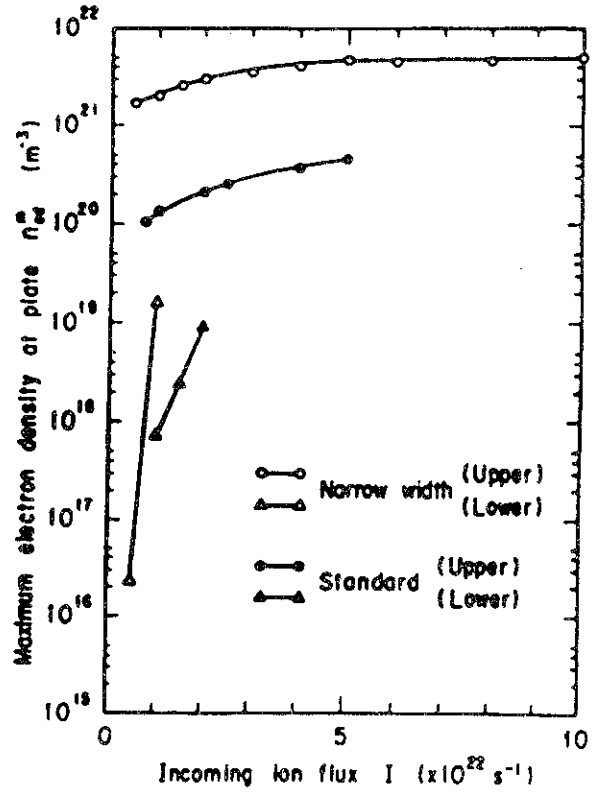

Fig. 1.2.3.10 Maximum electron densities at divertyor plate vs. incoming ion flux are shown. All the results are obtained by 2-D numerical code. Open circles and triangles show the results with heat flux Q=40 MW and no radiation for the configuration in Fig. 1.2.3.9. Closed circles and triangles with heat flux Q=24 MW and radiation loss for the standard configuration.

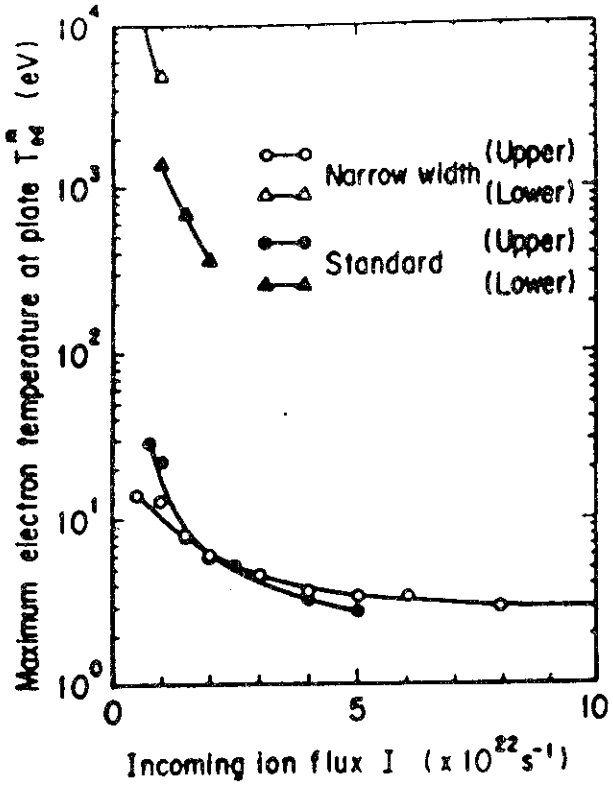

Fig. 1.2.3.11 Maximum electron temperatures at divertor plate vs. incoming ion flux are shown. All the results are obtained by 2-D numerical code. Open circles and triangles show the results with heat flux Q=40 MW for the configuration and no radiation in Fig. 1.2.3.9. Closed circles and triangles with heat flux Q=24 MW and radiation loss for the standardconfiguration.

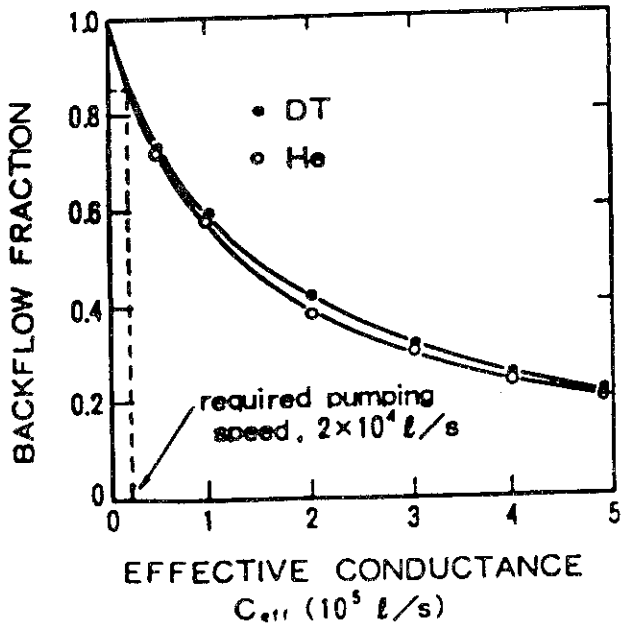

Fig. 1.2.3.12 Relation between the backflow fraction and the effective conductance of the exhausting system. (Q=40 MW, I=3x10^{22}/s)

1.2.4 Impact upon INTOR design concept

1.2.4.1 Height of divetor chamber

One of the major penalties of using a poloidal divertor instead of a pumped limiter is the greater volume inside the vacuum vessel required by the divertor chamber compared to a pump limiter. The current INTOR divertor design calls for a relatively short divertor like the Doublet III divertor, compared to a conventional divertor of the DIVA type. Nonetheless, the volume required is still large and it would be advantageous to further reduce the size of the divertor chamber.

The modelling results indicate that the high recycling region is localized very near (10-20 cm) the neutralizer plate. The density and temperature gradients are localized in the recycling region. The size of this region is determined by the meanfree path of neutral hydrogen formed at the neutralizer plate. For $T_e \sim 10$ eV, $n_e \sim 10^{20}$ m^{-3}, the meanfree path for ionization is less than 7 cm for 30 eV D°. Molecules have much shorter mean free paths. Furthermore, experiments on Doublet III show that the electron temperature drops from 35 eV to 8 eV along the separatrix within 13 cm of the plate (in the poloidal cross section). Probe measurements on Doublet III also indicate that relatively little plasma flows radially across the separatrix after the plasma flows by the X point. The measured scrape-off distances are much shorter on the inside of the separatrix than on the outside. Thus the region between the two separatrixes past the X point has little or no plasma, and does not play a large role in the recycling of plasma near the divertor plates. It should be feasible to reduce the distance between the separatrix and the divertor plates from the current design value of 1 meter to 50 centimeters or less and still retain the advantages of high recycling with a low temperature and high density near the plate. The advantages of a short divertor configuration would be

1) smaller divertor chamber,
2) reduced peak heat load on the plate since the flux surface expansion is greatest at the X point, and
3) divertor coil closer to X point.

The disadvantage would be a possible increase in the risks of impurity production and contamination.

If a significantly shorteded divertor is feasible, the divertor would become more competitive with the pumped limiter in cost, while offering better impurity and particle control capability than the pumped limiter. Here, the feasibility of shortening the divertor is assessed.

The dependence of formation of cold and dense divertor plasmas on divertor geomeyry is studied in the previous section 1.2.3, where a simple analytic model is used to perform a wide range of a parameter survey, although the region analyzed is limited to a divertor chamber. In the previous section, some results of the short divertor is also discussed by a more developed modelling, which can describe the main and divertor plasmas consistently. From those studies, some results are described here on the short divertor.

1) The divertor geometry has two key parameters, the length of a divertor chamber and the width of the void between the divertor plasma edge and the wall surface, as shown in Fig. 1.2.4.1-1. They influence the

characteristics of the divertor plasmas, featured by three equilibrium states, as discussed previously. Shortening the chamber and widening the void mean the more open geometry of the divertor.

2) In the open geometry, cold and dense divertor plasmas are observed to be produced in a wide range of the incoming ion flux to the divertor. Temperatures at the plate become below 10 eV.

3) Even in the significantly open geometry, its length 25 cm and its void width 25 cm, very cold and dense plasmas can be observed at the plate, as shown in Fig. 1.2.4.1-2.

4) The key problem of the open geometry is that the range of the incoming flux, where triple equilibrium states are observed, becomes wide.

5) If the width of the void is retained narrow, it can be predicted that the short divertor of 50 cm length could produce cold and dense plasmas at the divertor plate. Even if the width of the gap is not so narrow, the low temperature plasmas at the plate can be obtained with some appropriate controls.

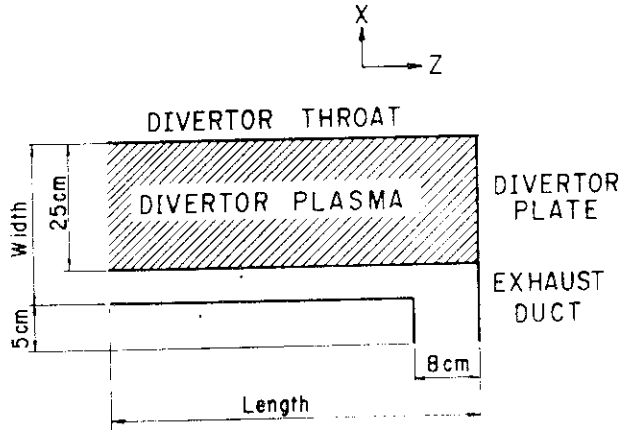

Case	Length (cm)	Width (cm)
A	50	25
B	75	30
S (standard)	50	30
C	50	50
D	25	30
E	25	50

closed ↑ ↓ open

Fig. 1.2.4.1-1 Various geometrical configurations to investigate the dependence of divertor performance on geometry.

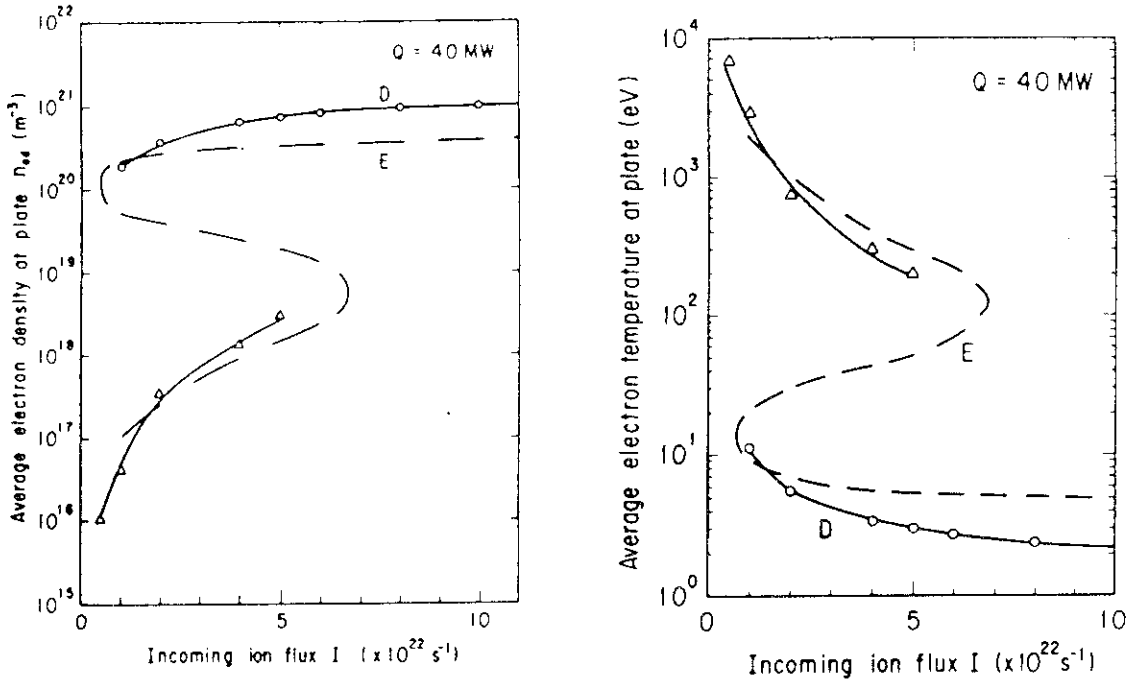

(a) (b)

Fig. 1.2.4.1-2 Average electron density(a) and temperature(b) at the divertor plate vs. incoming ion flux. Solid lines show the results by 2-D code and broken lines by simple analytic model for each case.

1.2.4.2 Comparison of single and double null divertor

Comparative studies on impurity control cncepts for Fusion Experimental Reactor (FER) at JAERI

1. Introduction

Fusion Experimental Reactor (FER) will succeed the large tokamak JT-60 to realize ignited DT plasma and to demonstrate engineering feasibility of fusion reactors. Synthetic comparative studies on impurity control concepts for FER were carried out to select a reference option. Four options evaluated are: (a) double null poloidal divertor (DND), (b) single null poloidal divertor (SND), (c) pumped limiter with medium edge temperatue (PLM), (d) pumped limiter with low edge temperature using a cold mantle (PLL). Plasma parameters of those four options are determined by keeping plasma confinement performance, i.e. confinement time and allowable beta value.

Four reactor concepts corresponding to tbose four impurity control options are assumed to have the following common features. The number of toroidal field (TF) coils is 14, which satisfies a field ripple limit of 0.75 % at a plasma edge. Both toroidal and poloidal field (PF) coils are superconducting coils with a pool boiling method. All PF coils are located outside of the TF coils. A tritium breeding blanket with Li_2O as breeding material with its breeding efficiency above unity is installed all around the plasma column. Plasmas are heated to ignition by a hybrid heating of radio frequency and neutral beam injection heatings, and seven heating ports are provided at every two TF coils.

Results of the comparative stidies are summaried in Table 1.2.4.2-1. It is recomended for the impurity control option for FER that the single null divertor should be a reference option and that the double null divertor and pumped limiter with the cold mantle should be retained as a back-up option. Those three options will be continued to be studied from both of engineering and physics viewpoints.

2. Comparative sutides of physics of features

2.1 Plasma parameters

The main plasma parameters for four options for impurity control are selected so that they have same plasma performance, and are listed in Table 1.2.4.2-2. The energy confinement time is evaluated with the INTOR scaling with some margins. The allowable beta limit is assumed to follow the theoretical beta maximum derived from ballooning instability, and to have some risk, i.e., the maximum beta value is assumed to exceed the theoretical one to some extent. All plasmas satisfy D-T ignition.

The plasma elongation and the safety factor are set 1.5 and 2.5, respectively. A burn time is 100 s and plasma current is inductively drived, which is supplied by hybrid PF coils with their maximum field, 8 T. The maximum experienced field of TF coils is 12 T. The width of a gap between a separatrix surface and a first wall is assumed to be 15 cm on a midplane of both of inboard and outboard sides for the DND option, and to be 15 cm at outboard and 30 cm at inboard for the SND and two limiter options. Plasma with a cold mantle are also assumed to have a layer with its width 20 cm inside a separatrix.

2.2 Physics data bases

Impurity control

A divertor configuration produced with the exterior PF coils to the TF coils is quite different from the conventional one. It is featured by a significantly wide divertor throat and no particular divertor chamber, so that it is called an open-type divertor. The divertor obtained in the Doublet III device is just an open-type one, and the results from it provide important data bases for a design of next tokamaks. The data bases of the open-type divertor are well assessed in the INTOR Workshop, Phase 2A (Part 2). The most remarkable feature, different from the conventional type, is a dense and cold plasmas fromed in front of the divertor plate. The dense and cold divertor plasma brings about several advantages to impurity control such as quite low sputtering erosion of a divertor plate which directly results in reduction of metal impurities in the main plasma, neutral gas compression near the plate which reduces the pumping requirement, coexistence with the so-called H-mode discharges, enhanced radiation in the divertor region which leads to reduction of heat load to the plate. Such a dense and cold divertor plasma is demonstrated to be reproduced in a FER divertor operation by an computational code, which can of course well explain the present divertor experiments.

A pumped limiter with medium temperature was studied in the INTOR workshop, Phase 2A (Part 1). It is found that limiter material is limited to low-Z and therefore its erosion becomes quite large. Then, behaviors of impurities have a key role in a physics aspect. At present impurity transport is uncertain and credible impurity control is an open question.

The pumped limiter with a cold mantle is an attractive option, which brings a lot of engineering advantages and could survive in future tokamak reactors. A present problem is, same as the pumped limiter without a cold mantle, uncertaity in impurity behaviors in plasma.

Beta limit

Theoretical studies on a beta limit due to ballooning instabilities show that a trianglar deformation of a plasma cross section is advantageous in increasing beta limit. In a elongated D-shaped plasma configuration, enhancement of the triangularity induces proximity of a magnetic null point to a plasma boundary. For limiter configurations and single null divertor, therefore, their triangularities must be moderate. On the other hand, the double null configuration can increase its deformation and attain slightly higher beta value than other three options, although the enhancement of triangularity needs larger currents of PF coils.

3. Comparative studies of engineering features

Comparative studies of engineering features for four impurity control options are conducted as qualitatively as possible to elucidate engineering gains and losses. The results are summarized in Table 1.2.4.2-3. Some details of engineering comparative studies are in a reference[13th SOFT (Sep., 1984, Italy) 5P03].

Table 1.2.4.2-1 Summary of comparative studies for four impurity control options

Items assessed	Summaries
1. Physics data bases	
Impurity Control	
Divertor	Impurities, particularly metal, are well controlled with an open-type divertor owing to a dense and cold divertor plasma.
Pumped limiter	
Medium temperature	Concerns on impurity control are large due to a large amount of sputtering and uncertainty of impurity transport.
Low temperature	Insufficient data base, but if a cold mantle coexists with a hot plasma, such a concept is attractive.
Beta limit	Double null divertor is somewhat superior to single null due to an available large triangularity.
2. Reactor structure	
Size	TF coil sizes of four options are almost same.
Maintainability	
Single	Plates, installed at botom, can be retracted with one straight radial motion through every window.

Items assessed	Summaries
Double	Plates, installed at top and bottom, are retracted with two straight (radial and oblique) motions through every two windows.
Earthquake-proff	
Single	Fairly good
Double	Somewhat difficult, when vacuum pumps are installed at top.
3. Collector plate	
Life	Limiter with a cold mantle is maximum (full life).
	Divertor is reasonable (1 ~ 2 years).
	Limiter without a cold mantle is low (less than one year).
4. TF Coil	
Stress due to out-of-plane	Limiters are almost half of divertors.
force	Single divertor is reduced by 20% from double divertor.
AC loss	Same as a case of stress mentioned above.
5. PF Coil	
Stored energy	Limiters are about half of divertors.
	Single divertor decrease by 20-30% from double divertor.

Items assessed	Summaries
MG peak power	Limiters are less than half of divertors. Single divertor is almost same as double divertor.
6. Vertical position control	Double divertor and limiter with a cold layer are somewhat unfavorable to single divertor and limiter with medium temperature
7. Tritium breeding	Double divertor is slightly disadvantageous compared with other three options.
8. Vacuum pumping	Double divertor needs approximately half of pumping speed of other three options.

* Synthetic judgement

1. Pumped limiter without a cold mantle should be excluded because of its uncertainty of impurity control and short life of cllector plates. (However, the latter difficulty is eased in a fairly low fluence reactor)
2. Pumped limiter with a cold mantle has a lot of engineering advantages, although physics uncertainties are large. Especially a long life of collector plate is preferable.
3. Double null divertor is not preferable in almost all items compared with single null divertor, especially, double is fairly more difficult in replacement of plates than single. The followings, however, should be kept in mind. 1) Allowable beta value of double null divertor is best, 2) No definite engineering items are found which reasonably exclude double divertor concept.
4. AC loss of TF coils and PF power supply are crucial items in a conventional tokamak reactor with inductive current drive, however their importance is significantly reduced when a scenario of PF current drive is used in a start-up phase.

Table 1.2.4.2-2 Main plasma parameters of Reference and Alternative design

	Double Null Divertor (DND)	Single Null Divertor (SND)	Pumped Limiter (PLM)	Pumped Limiter (PLL)
Plasma major radius (m)	5.5	5.72		6.01
Plasma minor radius (m)	1.1	1.17		1.46+
Aspect ratio	5.0	4.89		4.12
Plasma elongation	1.5	1.5		1.5
Plasma triangularity	$\gtrsim$ 0.2	$\gtrsim$ 0.2		$\gtrsim$ 0.2
First wall radius (m)	1.25	1.395		1.685
Average ion temperature(keV)	10	10	Same as single null divertor	10
Average ion density (m)	1.36	1.28		1.19
Toroidal fiels on plasma axis (T)	5.7	5.48		5.22
Peak thermonuclear power (MW)	440	458		480
Plasma current (MA)	5.3	5.54		5.8*
Safety factor	2.5	2.5		2.5*
Toroidal β (%)	4.0	4.1		4.1
Poloidal β	2.28	2.18		2.08

Note : Parameters are determined keeping equality of plasma confinement performance.

*) Plasma cold layer is excluded.
Current in cold layer is neglected.

+) Cold layer (0.2 m) is included.
Plasma confinement performance is evaluated for plasma minor radius of 1.26 m.

Table 1.2.4.2-3 Summary of engineering comparisons of four impurity control options

Items	DND	SND	PLM	PLL
Reactor structure				
TF coil perimeter (m)	29.2	29.1	27.5	29.5
TF coil bore (m × m)	6.3 × 9.4	6.6 × 8.9	6.6 × 8.2	7.2 × 8.8
Position of cryo-pump	Top and Bottom	Bottom	Bottom	Bottom
Earthquake-proof	Difficult	Easy	Easy	Easy
Segmentation of plate	3 sectors/2 TFC	2 sectors/TFC	2 sectors/TFC	2 sectors/TFC
Retraction motion	2 straight motion	1 straight motion	1 straight motion	1 straight motion
Collector plate				
Armor	Tungsten	Tungsten	Belyrium	Tungsten
Lifetime (Erosion)*1 (y)	1.4	1.4	0.45 (10 mm) 0.9 (20 mm)	20
Lifetime (Fatigue) (y)	1	1	Long	Long
TF coils				
Stress by out-of-plane forces (kg/mm^2)	45	37	17	18
AC losses (kW)	110	82	46	51
PF coils				
Maximum ampere-turn (MAT)	99	71	53	67
Stored energy (GJ)	6.0	4.9	2.7	3.5
MG peak power (MW)	1234	1208	462	637
Position control				
Growth time (ms)	36	54	71	32
Neutronics				
Tritium breeding ratio	1.10	1.14	1.14	1.14

* 1) Not include redepostion of sputtered material
Duty cycle = 50 %, Availability = 25 %
* 2) Plasma current induced inductively

1.3 Limiter

1.3.1 Experimental data base for limiters

1.3.1.1 Impurity control

Impurities in the tokamak plasma are classified into two groups, i.e. light and metal impurities. Light impurities can be reduced in the JFT-2 and -2M tokamaks by baking, low-power discharge cleaning (TDC) of the wall with hydrogen and titanium flashing. Dominant light impurity was oxygen and its level was 1-5 %.

In advanced tokamaks, the TDC will be confronted with the difficulties such as thermal stress of the first wall, a high operation cost and influences on superconductor coils. In order to overcome the difficulties of TDC, electron cycroton resonance discharge (ECR-DC) cleaning has been tested [1]. High power continuous wave magnetrons are available in the 2450 and 915 MHz band, and we demonstrated the possibility of a low operation cost. A microwave (2.45 GHz, 2 kW CW) was supplied from a magnetron oscillator. Comparison between the cleaning effect of the ECR-DC and TDC showed that both cleaning methods have similar cleaning effect. This shows that ECR-DC is applicable to advanced tokamaks.

The origin of metal impurities in tokamaks is generally considered to be due to three different types of wall interaction, i.e. arcing, evaporation and sputtering.

Arcing phenomena occur on the first wall in nonequiliblium phases such as the current rise and shut down phases as well as plasma disruption [2-7]. The most probable cause of unipolar arcing in tokamaks is that run away electrons increase the sheath potential between the wall surfaces and the non-equiliblium dense plasma in the scrape-off plasma, and produce the arcs. Unipolar arcing will hardly occur during the steady state even in future large tokamaks, if the first wall is well conditioned and the heat flux to the wall is kept below 500 W/cm^2 [6].

Evaporation due to the heat flux from the plasma does not constitute a mechanism of metal impurity production in normal discharges [8].

Sputtering is the dominant process in the stedy state of the JFT-2 tokamak. The energy E of the charged particle is given as,

$$E = T_{is} + 3T_{es}Z \ ,$$

where T_{es} and T_{is} are electron and ion temperatures of the scrape-off plasma, and Z is charge number of the ion. To reduce the amount of metal impurities released from the wall by sputtering, T_{es} and Z of the scrape-off plasma must be kept low. Metal impurity can be reduced by Ti gettering [9,10], gas puffing [10] and use of graphite limiter [11]. Metal impurity level was about (0.1-0.2) % even in neutral beam injection heating.

Light impurities (mainly oxygen) and their radiation loss were reduced by 1/3 - 1/10 with Ti gettering and simultaneously metal impurities were then reduced by about the same factor as shown in Tab. 1.3.1-1 [10]. It has to be noted that the T_{es} was almost the same in two cases; with and without Ti

gettering. Figure 1.3.1-1 shows the T_{es} was varied by adjusting the injection rate of working gas (H_2). At a higher injection rate, as the electron density rise up and the increase of the radiation loss was followed, the T_{es} was reduced to about half and the Mo density was also reduced. In contrast, at a lower injection rate the T_{es} increased a little and Mo density also increased. These results confirm that the reduction of T_{es} and Z results in the reduction of metal impurities.

Spatial behavior of emission from iron impurities with the different ionic charge is obtained in the JFT-2 discharges with neutral beam injection. Their concentration is in the range 10^{10} - 10^{11} atoms cm^{-3} and the impurity level is low. Figure 1.3.1-2 shows the Abel-inverted spatial distributions of the density of Fe^{17+}, Fe^{14+} and Fe^{9+} ions in the ground state at 100, 115, 120 and 130 ms (beam is injected at 100 ms) [12]. In co-injection, the population density of Fe^{17+} ion indicates a gradual increase with time (a factor of 1.7), and its profile is shallow-hollow during injection. The profile of Fe^{9+} ion becomes broad after injection, but the density at the peak changes slightly. The total number of this ion only indicates the increase of 33-37 %. In counter-injection, the population density of Fe^{17+} ion near the plasma center ($r < 5$ cm) at 120 ms increases to about 6 times that at 100 ms, although there are uncertainty of the Abel-inversion near the plasma center and the assumed profiles of the electron density and temperature. From 120 to 135 ms, the density is approximately constant. The time-variation of Fe^{9+} ion is similar to that in co-injection (the increase rate of the total number of this ion is about 40 %). The plasma density and population density of Fe^{17+} are $\sim 7 \times 10^{13}$ and $(5\text{-}10) \times 10^{10}$ cm^{-3}, respectively, and the impurity level is (0.1-0.2) %.

1.3.1.2 Pumping performance

No data base

1.3.1.3 Effect upon plasma confinement

It is important to reduce radiation loss in order to obtain stable high density plasma. In addition to the reduction of radiation loss, density profile control is a key factor to improve confinement characteristics in beam heated discharges. Good confinement and high density plasma has been obtained lately by using pellet injector in neutral beam injection heating [13].

The maximum attainable plasma density and plasma current in tokamaks are limited by the plasma disruption. The radiation loss and resulting current channel shrinkage are plausible for the cause of the plasma disruption [14]. The reduction of the radiation loss results in good confinement characteristics in the JFT-2 tokamak.

The electron thermal conductivity has been estimated from the measured radial profiles of the electron temperature and density, and diffusion coefficient was derived from the electrostatic density fluctuation [15]. The estimated electron thermal conductivity has weak dependence on effective Z of the plasma ($\chi_e \sim Z^{0.2}$).

A typical global energy confinement time τ_E in JFT-2 is around 10 ms in beam heated discharges with net input power P_{net} of (0.3-1.7) MW and around 20 ms in Joule heated discharges. No "H-mode" was obtained in the limiter experiment of the JFT-2 tokamak. The reason for "L-mode" is as follows [16].

Without the control of neutral gas flux, the boundary temperature significantly rises and density clamp occurs in the neutral beam injection heating. To overcome the density clamp intense gas puffing is necessary. Broader density profiles are inevitably obtained, because the low temperature neutral gases are mainly ionized at plasma boundary due to the higher boundary electron temperature compared with the case of ohmic discharge. The higher plasma density at the boundary region increases the deposition power near at the boundary and thus decreases that of the plasma center. Thus the density profile control is one of the key factor to improve τ_E in beam heated discharges.

By using a centrifuge pellet injectors as the principal D_2 fueling source, good confinement and high density plasmas have been obtained in the neutral beam injection heating of Doublet III tokamak [13]. Comparison of the dependence on the beam power between gas and pellet fueled discharges are shown in Fig. 1.3.1-3. The neutral pressure at the upper chamber and the particle recycling at the limiter surface, as infered from the D_2 emission level, for pellet fueled discharges are two to three times lower than those of gas fueled discharges (Fig. 1.3.1-3(a)). The global energy confinement time, τ_E, obtained by diamagnetic measurement degrades in beam heated gas fueled discharges as observed generally in present tokamaks. The confinement time is improved 1.7 times by central fueling (pellet fueling) compared peripheral fueling (gas fueling) discharges at 2.4 MW of beam power, however degrades with increasing the beam power corresponding to decreasing the pellet penetration (Fig. 1.3.1-3(b)).

1.3.1.4 Scrape-off plasma condition

Scrape-off plasma determines the energy flow of the charged particles to the limiter and wall in tokamak. The boundary characteristics are an important factor determining impurity generation. Particle and energy fluxes in the scrape-off layer behind the limiter have been studied in the JFT-2 tokamak. The diffusion coefficient of the scrape-off plasma is the order of the Bohm diffusion coefficient.

Table 1.3.1-2 summarizes the value of the e-folding length, the electron temperature T_{es}, the diffusion coefficient D, and the safety factor for six cases [17]. Where, suffix 1 and 2 correspond to the regions behind the rail (r=19.5 cm) and aparture (r=25 cm) limiters. The Bohm diffusion coefficient is also shown in addition to the diffusion coefficient determined by the e-folding length. From this we can say that $D_\perp$ is the order of, but a little larger than, the Bohm diffusion coefficient and $D_\perp$ has a dependence of T_{es}/B in the boundary region.

The total heat flux density q_t to the rail limiter (r=19.5 cm) during a discharge are compared between the electron and ion sides of the limiter in Fig. 1.3.1-4 [18]. They were estimated from the observations by the infrared camera and the probe, respectively. On the electron side of the limiter, q_t in the region $-8\ \text{cm} < x < 8\ \text{cm}$ in larger in case A ($\bar{n}_e = 1.3\times10^{13}\ \text{cm}^{-3}$) than in case B ($\bar{n}_e = 2.8\times10^{13}\ \text{cm}^{-3}$), at x = 0, q_t in case A is 2.6 times that in case B, whereas on the ion side of the limiter q_t is almost the same in cases A and B. There was good correlation between heat flux density on the limiter and X-ray emission from the limiter in cases A and B. This indicates the higher heat flux on the electron side is mainly due to accelerated electrons. In order to reduce the heat flux to the limiter, it is important to operate the higher density.

References for Section 1.3.1

[1] Y. Sakamoto, Y. Ishibe, K. Yano, H. Oyama, Y. Tanaka, et al., J. Nucl. Mater. 93 & 94 (1980) 333.
[2] Y. Gomay, N. Fujisawa and M. Maeno, J. Nucl. Mater. 85 & 86 (1979) 967.
[3] H. Ohtsuka, N. Ogiwara and M. Maeno, J. Nucl. Mater. 93 & 94 (1980) 161.
[4] M. Maeno, H. Ohtsuka, S. Yamamoto, T. Yamamoto, N. Suzuki, et al., Nucl. Fusion 20 (1980) 1415.
[5] H. Ohtsuka, M. Maeno, N. Suzuki, S. Konoshima, S. Yamamoto and N. Ogiwara, Nucl. Fusion 22 (1982) 823.
[6] N. Maeno, S. Yamamoto and H. Ohtsuka, Jpn. J. Appl. Phys. 22 (1983) 764.
[7] H. Ohtsuka, Vacuum 33 (1984) 155.
[8] M. Maeno, H. Kawamura, Y. Gomay, N. Fujisawa, N. Suzuki, et al., Jpn. J. Appl. Phys. 18 (1979) 1549.
[9] S. Konoshima, N. Fujisawa, M. Maeno, N. Suzuki, T. Yamamoto, et al., J. Nucl. Mater. 76 & 77 (1978) 581.
[10] N. Suzuki, N. Fujisawa, S. Konoshima, M. Maeno, T. Yamamoto et al., in Controlled Fusion and Plasma Physics (Proc. 9th Europ. Conf. Oxford, 1979) p. 90.
[11] T. Shoji, A. Funahashi, K. Hoshino, S. Kasai, T. Kawakami, et al., in Controlled Fusion and Plasma Physics (Proc. 11th Europ. Conf. Aachen, 1983) Vol. 1, p. 55.
[12] S. Kasai, T. Hirayama, T. Yamauchi, T. Sugie, S. Yamamoto, et al., Japan Atomic Energy Research Institute Rep. JAERI-M 82-164 (1982).
[13] S. Sengoku, M. Abe, K. Hoshino, K. Itoh, A. Kameari, et al., Proc. 10th Int., Conf. Plasma Physics and Controlled Nuclear Fusion, Research London, 1984 IAEA-CN-44/JI-1.
[14] M. Maeno, N. Suzuki, S. Konoshima, T. Yamamoto, M. Shimada and N. Fujisawa, J. Phys. Soc. Jpn. 48 (1980) 273.
[15] T. Shoji, T. Yamamoto, A. Funahashi, M. Shimada, N. Fujisawa, et al., Japan Atomic Energy Research Institute Rep. JAERI-M 9799, 1981.
[16] S. Yamamoto, M. Maeno, S. Sengoku, N. Suzuki, S. Kasai, et al., in Plasma Physics and Controlled Nuclear Fusion Research (Proc. 9th Int. Conf. Baltimore, 1982) Vol. 1, IAEA, Vienna, (1983) 73.
[17] K. Uehara, Y. Gomay, T. Yamamoto, N. Suzuki, M. Maeno, et al., Plasma Phys. 21 (1979) 89.
[18] Y. Gomay, N. Fujisawa, M. Maeno, N. Suzuki, K. Uehara, et al., 18 (1978) 849.

Table 1.3.1-1 Effect of Ti gettering on light and metal impurities [10].

	V_l (Volt)	OVI (cm^{-3})	OVIII (cm^{-3})	MoXIII (a.u.)	Tes (eV)	Zeff	P_R (kW)
without Ti-getter	2.7	3×10^{10}	1×10^{12}	28	30	5.5	60
with Ti-getter	1.5	3×10^{9}	2×10^{11}	2.6	30	2.0	20

Table 1.3.1-2 Summary of e-folding length, electron temperature T_{es}, diffusion coefficient, Bohm diffusion coefficient D_B, and safety factor q_a at the boundary region for each case, where the small suffixes 1 and 2 denote the rail and aperture limiter region, respectively [17].

	λ_1, cm	λ_2, cm	T_{e1}, eV	T_{e2}, eV	$D_{\perp1}$, cm^2s^{-1}	$D_{\perp2}$, cm^2s^{-1}	D_{B1}, cm^2s^{-1}	D_{B2}, cm^2s^{-1}	q_a
Case I	4.1	1.4	30	30	7.4×10^4	3.7×10^4	1.1×10^4	1.1×10^4	4.3
Case II	4.1	1.4	30	30	7.4×10^4	3.7×10^4	1.1×10^4	1.1×10^4	4.3
Case III	4.8	1.4	30	30	1.0×10^4	3.7×10^4	1.1×10^4	1.1×10^4	4.3
Case IV	4.8	1.4	30	30	1.0×10^4	3.7×10^4	1.1×10^4	1.1×10^4	4.3
Case V	5.2	1.8	20	16	4.8×10^4	4.5×10^4	7.3×10^4	5.9×10^3	8.6
Case VI	7.5	4.2	30	35	2.5×10^5	2.7×10^4	2.2×10^4	1.5×10^4	4.3

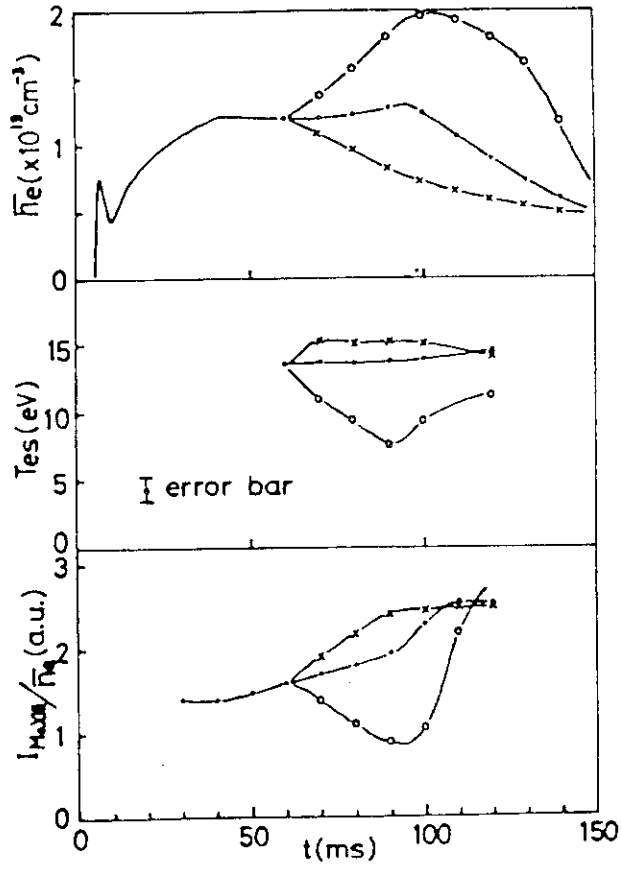

Fig. 1.3.1-1 T_{es} dependence of Mo line. T_e is varied by adjusting the injection rate of working gas (H_2) [10].

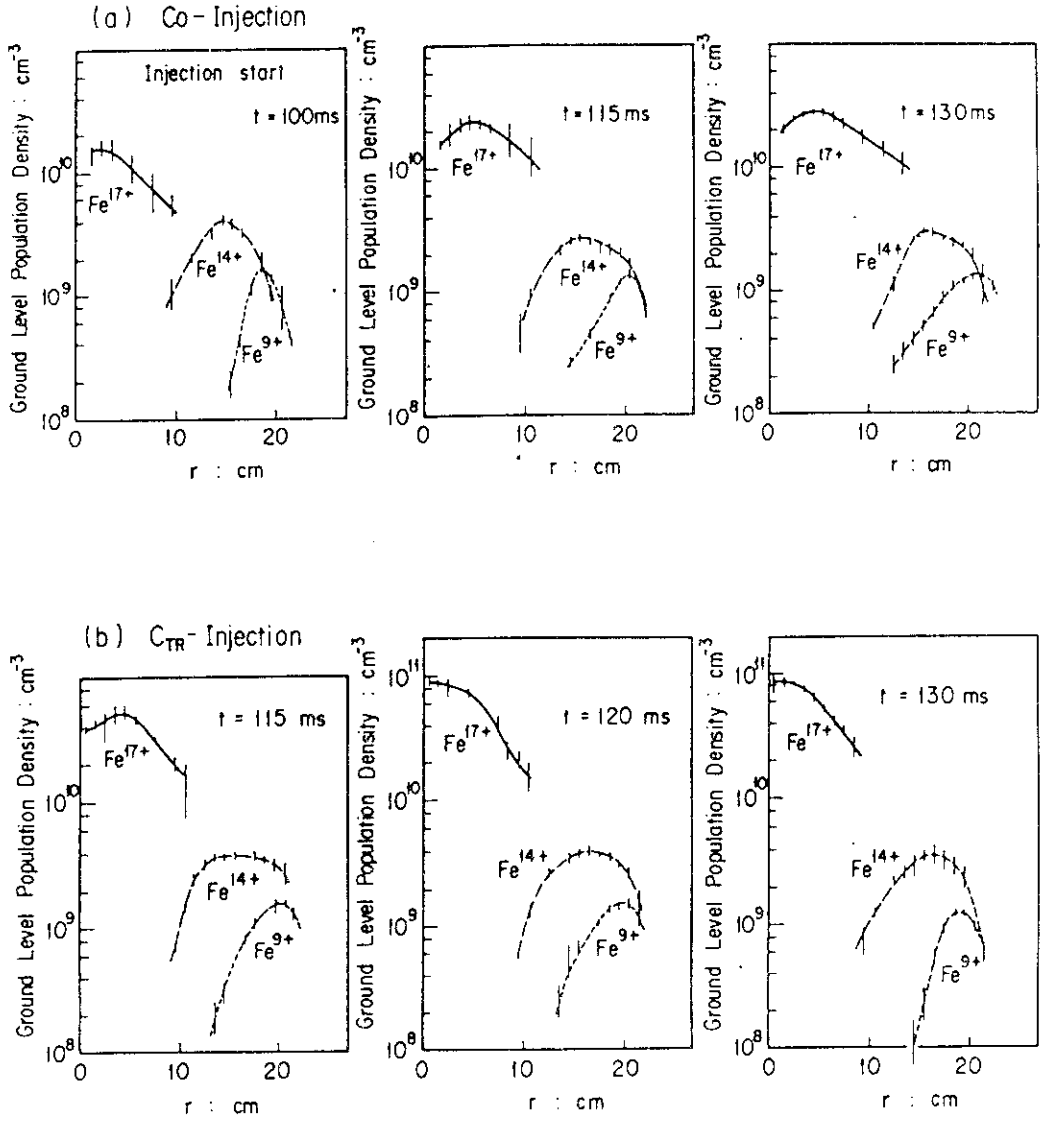

Fig. 1.3.1-2 Radial distribution of the population density of the Fe^{17+}, Fe^{14+} and Fe^{9+} ions in the ground state in (a) co- and (b) counter-injections [12].

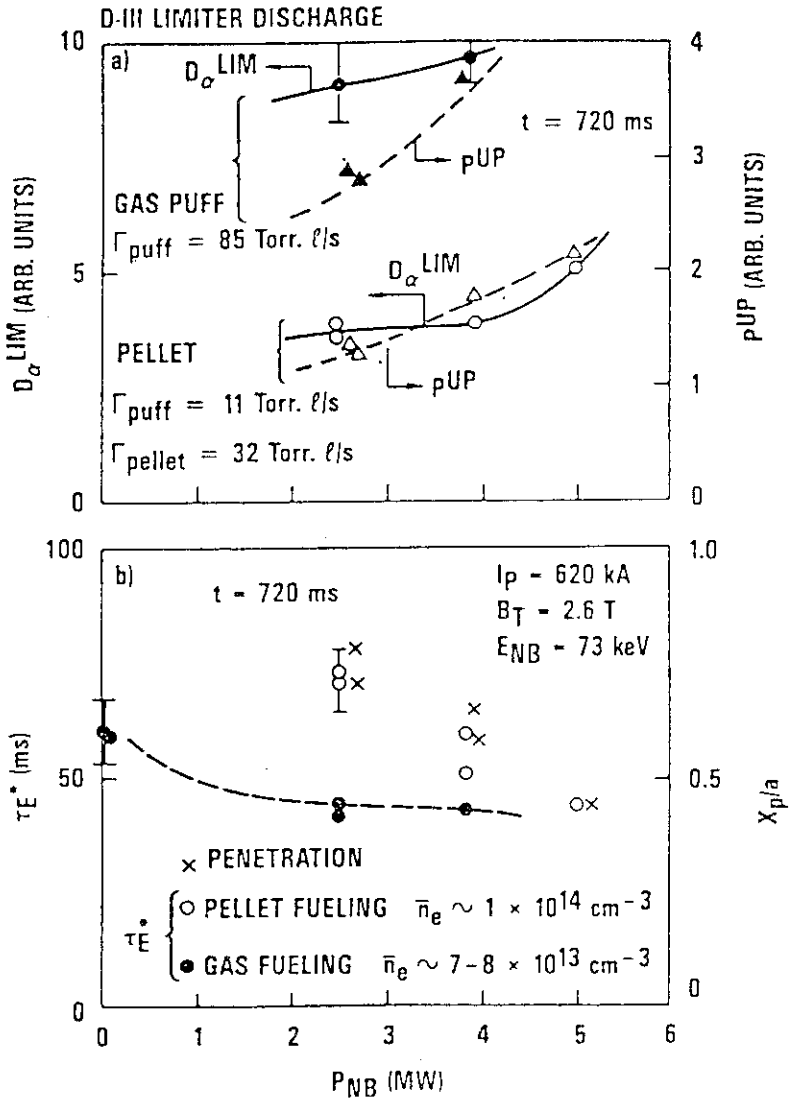

Fig. 1.3.1-3 Neutral beam power dependence of a) D_α signals at the limiter surface (D_α^{LIM}) as the peripheral recycling level and neutral pressure at the upper chamber (p^{UP}); b) global energy confinement time obtained by diamagnetic measurement and pellet penetration measured from the limiter surface and normalized by the minor radius, X_p/a, (X). Solid symbols correspond to gas fueled discharges ($\bar{n}_e \sim 7\text{-}8 \times 10^{13}$ cm^{-3}) and open symbols to pellet fueled discharges ($\bar{n}_e \sim 1 \times 10^{14}$ cm^{-3}) [13].

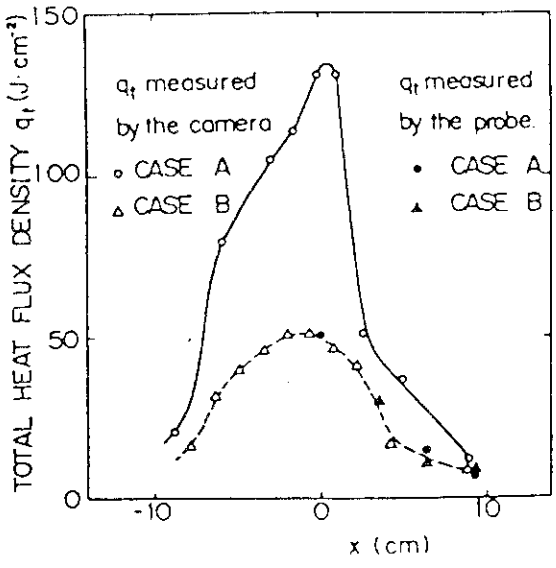

Fig. 1.3.1-4 Comparison of total heat flux density q_t between the electron and the ion sides of the limiter. The two sides were observed with the infrared camera and the probe, respectively [18].

1.3.2 Limiter modelling and validation

In the design studies [1,2], simple point model calculations have been done to roughly determine the necessary pumping speed and the limiter configuration. However, the performance of the helium ash exhaust crucially depends on the particle recycling in the peripheral region of the plasma, which cannot be treated by simple point model calculations. In addition, heat load and erosion of the limiter surface are very sensitive to the radial profiles of the particle flux and temperature in the scrape-off layer plasma. Thus, in order to assess correctly the necessary width of limiter opening and pumping speed for helium ash exhaust, heat load and erosion rate of the limiter surface, detailed power and particle balance both of fuels and heliums under the reactor plasma condition must be examined. The density and temperature profiles in the scrape-off layer plasma strongly depend on the detailed process of the particle recycling on the limiter surface, limiter opening and the first wall. In addition, the main plasma must also be solved to examine the helium ash accumulation and exhaust.

Therefore, we will perform detailed recycling calculations of neutral particles on the limiter surface and the first wall with the aid of one-dimensional tokamak transport code which calculates the transport process in the main plasma including the scrape-off layer plasma. In the pumped-limiter chamber, the behavior of the neutral particles is calculated beforehand by the two-dimensional Monte-Carlo code with fixed parameters of the scrape-off layer plasma. The average energy of the neutral particles flowing back to the main plasma from the limiter chamber calculated by the Monte-Carlo code is used in the transport code, and the equilibrium state both of main and scrape-off layer plasma is obtained.

A schematic drawing of the calculational model is shown in Fig. 1.3.2.1. We define the separatrix line as the tangent magnetic field line with the limiter (in contrast to the usual separatrix line in the case of divertor, any magnetic null point does not appear on it). We will assume a concentric magnetic flux surfaces with circular plasma cross section. Pumped-limiter is installed continuously in toroidal direction at the bottom of the plasma. We define the length l_L which is the distance between the leading edge and the separatrix line. We will hereafter call l_L limiter length, while l_L is actually the projected length of the limiter on the minor radius direction. The length l_L is most important parameter for the performance of the pumped-limiter, since the particle flux into the pumped-limiter chamber as well as the heat flux on the leading edge are predominantly determined by l_L.

Required functions and engineering requirements for pumped-limiter and possible control methods to meet them are summarized in Table 1.3.2.1.

References

[1] C.C. Baker, M.A. Abdou, R.M. Arons, P.A. Finn, B. Misra, A.E. Bolon, R.E. Fuji, J. Rest, C.D. Boley, Y. Gohar, H.L. Schreyer, J.N. Brooks, V.Z. Jankus, D.L. Smith, R.G. Clemmer, et al., ANL/FPP-80-1 (1980).

[2] S. Saito, N. Fujisawa, M. Sugihara, K. Ueda, H. Nakamura, Japan Atomic Energy Research Institute Report, JAERI-M 82-011 (1982).

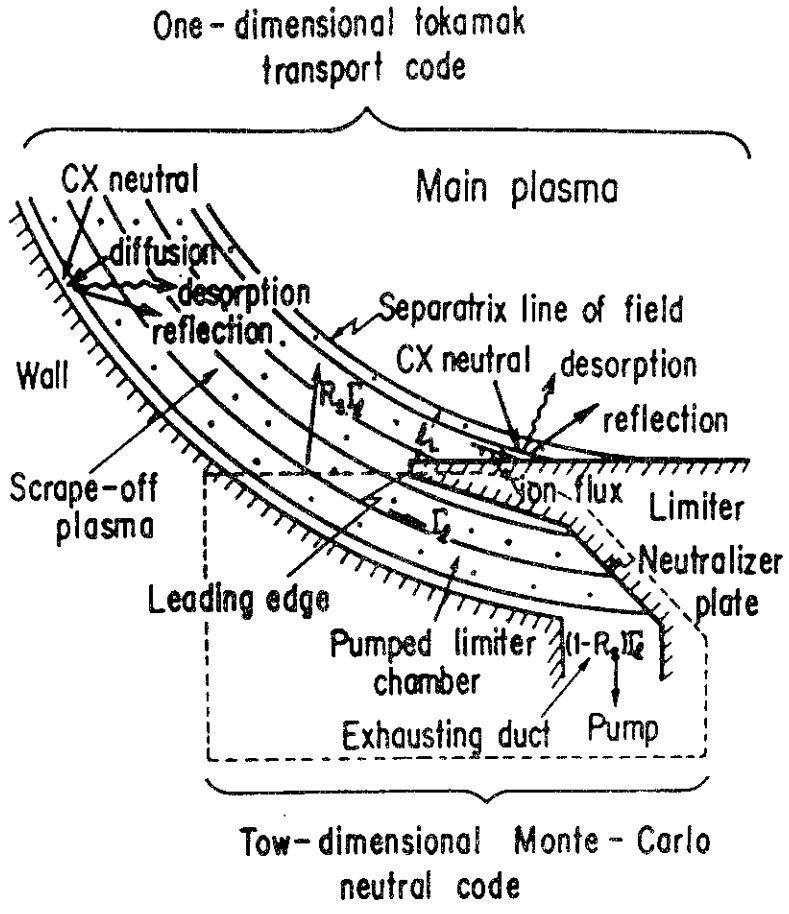

Fig. 1.3.2.1 Schematic drawing of calculational model. Main plasma including scrape-off layer plasma is calculated by one-dimensional tokamak transport code. In pumped-limiter chamber, neutral particle behavior is calculated by two-dimensional Monte-Carlo code.

Required function	Engineering requirements	Possible control method
1. Helium ash exhaust	minimizing pumping capacity and pumped out tritium	o adjusting width of limiter opening o adjusting pumping speed o employing suitable fueling method (pellet/gas-puff)
2. Heat removal and impurity control	minimizing heat flux and erosion of limiter surface	

Table 1.3.2.1 Various required functions and engineering requirements for pumped-limiter and possible control methods to meet them.

1.3.3 Predictive modelling

1.3.3.1 Modelling concepts

The main plasma including the scrape-off layer plasma is calculated by the one-dimensional tokamak transport code, in which four species of ions (D, T, He^+ and He^{++}) are treated separately. Particles flowing onto the limiter surface or diffusing onto the wall are also neutralized there. Some of them are reflected and others are adsorbed and desorbed with the energy of wall temperature. In the case of fuel particles, charge exchange reaction exists. Neutral fuel particles produced by charge exchange reaction collide with the wall or the limiter surface and are also reflected or adsorbed and desorbed. Helium ash accumulation is determined by the particle balance between the production rate in the central region of the main plasma and the exhausting rate in scrape-off layer region. The amount of pumped out fuel particle is also determined by the incoming particle flux to the limiter chamber and the exhausing rate. Heat load and erosion of the limiter surface and the leading edge are determined by the ion particle flux along the field line and their temperature. They strongly depend on the detailed particle recycling on the limiter and the wall.

We will employ the following recycling model of neutral particles on the limiter and the first wall in the one-dimensional tokamak transport code. Particles colliding with the limiter and the wall are assumed to be reflected at the rate R_N given by [1]

$$R_N(E_{in}, \theta) = 1 + (1 - \frac{\theta}{90°})(R_N^0(E_{in}) - 1) \quad ,$$

where E_{in} is the incident energy, θ is the incident angle measured from the normal to the surface and

$$R_N^0(E_{in}) = -0.24 \log_{10}(\frac{E_{in}}{E_L}) + 0.19 \quad ,$$

where E_L is the reduced energy factor having typical value[1] of

$$E_L = \begin{cases} 2990 \text{ eV} & \text{for D, T} \\ 6290 \text{ eV} & \text{for He} \end{cases} .$$

On the other hand, reflected particles may have energy E_{ref} given as

$$E_{ref} = \frac{R_E(E_{in}, \theta)}{R_N(E_{in}, \theta)} E_{in} \quad ,$$

where

$$R_E(E_{in}, \theta) = 1 + (1 - \frac{\theta}{90°})(R_E^0(E_{in}) - 1) \quad ,$$

and

$$R_E^0(E_{in}) = -0.22 \log_{10}\left(\frac{E_{in}}{E_L}\right) + 0.06 \quad .$$

Particles which are not reflected are adsorbed and then desorbed with the energy of wall temperature. The angle of reflected or desorbed particles is assumed to be isotropic. Deuterium and tritium particles desorbed from the limiter and the wall or gas-puffed are in molecular form. These molecules will soon be dessociated, so that we assume the energy of fuel particles desorbed or gas-puffed to be 5 eV (Frank-Condon neutral energy). Recycling rate at any point on the wall and the limiter is assumed to be unity, that is, the total number of neutrals reentering into the plasma from these points is equal to the sum of the ions and charge-exchange neutrals entering into those respective points.

The average energy of neutral particles, flowing back to the main plasma from the pumped-limiter chamber is calculated by the two-dimensional Monte-Carlo neutral code. The neutral particle motions initiated at the neutralizer plate are followed with fixed plasma parameters of the scrape-off layer in the limiter chamber. Neutral particles traversing the scrape-off plasma have chances for ionization and charge exchange reactions with plasmas.

Neutral particle density in the main plasma including the scrape-off layer is obtained by the solution of the Boltzmann equation for neutral particles in cylindrical geometry [2,3]. We divide the limiter surface into several meshes, and consider several velocity groups for recycling neutral particles at each mesh point according to the recycling model. For helium particles, the rate coefficients for charge exchange bettween helium-hydrogen and helium-helium are smaller than that of electron impact ionization by about two order of magnitude for the temperature range of $10\text{-}10^3$ eV [4,5].

The average energies of fuel and helium neutral particles flowing back to the main plasma through the opening of the limiter are calculated beforehand by two-dimensional Monte-Carlo neutral code over the wide range of plasma parameters of the scrape-off layer. We express the average energies for fuel and helium by linear functions of the average electron temperature $\bar{T}_e$ in the limiter chamber from Fig. 1.3.3.1. By using these energies, neutral particle transport calculation in the main plasma is recalculated in the one-dimensional transport code until the consistent solution between the plasma and neutral energy are obtained. We assume that the neutral particles flow back to the main plasma uniformly throughout the limiter opening.

We will introduce the backflow fraction R_s to denote the efficiency of the helium ash exhaust. This is defined as

$$R_s = \frac{\text{particle flux returning back to main plasma}}{\text{particle flux flowing into the limiter chamber } (= \Gamma_1)} .$$

In fact, $(1\text{-}R_S)$ denotes the efficiency of the exhaust and R_S corresponds to the recycling rate at the opening of the pumped-limiter in the one-dimensional transport code. R_S can also be calculated by this code as a function of the effective pumping speed C_d at the entrance of the evacuating

duct. The results are shown in Fig. 1.3.3.2 with the plasma density as a parameter. This value is very sensitive to the plasma density of the scrape-off, but is not very much to the temperature. The value of R_s for deuterium, tritium and helium differ slightly each other depending on the processes of the neutral-wall interaction adopted [6,7]. In the present paper, we will assume for simplicity that R_s takes the same value for D, T and He. This assumption becomes correct when the plasma density of the scrape-off becomes high [6,7]. The pumping speed for fuel particles at the very front of the pump, especially if cryogenic pumps were used, becomes fairly larger than that for helium. However, the conductances of the evacuating duct for fuel particles (D_2, DT, T_2) are smaller than that for helium by a factor of the square root of mass ratio, so that the former differences will strongly be compensated by the latter. Therefore, it will be reasonable to assume that C_d of fuels and helium take the same value for the same pumping capacity.

The basic equations of the one-dimensional transport code consist of continuity equations for the densities of deuterium, tritium and helium, n_D, n_T, n_{He+} and n_{He++}, electron and ion energy conservation equations and toroidal current diffusion equation. They are extended from the simple original one [8,9] to multi-species ions including fusion reaction and scrape-off layer. For heliums, ionization and recombination source from different state of ionization are included. We have assumed that four species of ions have the same temperature, since the ion-ion energy relaxation time is considerably short and the differences of the temperature between ion species are not essential in the present analysis. As for the alpha particle heating, we have assumed that alpha particles generated by fusion reaction deliver their energy to the field particles instantaneously, since the birth profile and heating profile is almost the same [10] and the slowing down time is not essential in the steady state.

We use the standard INTOR scaling for the transport coefficients in the main plasma. In the scrape-off layer transport coefficients in radial direction are assumed to be of Bohm type having a constant value throughout the layer.

We employ two methods for fueling; pellet injection and gas-puffing. We use the simplified penetration model for the pellet injection [11]. In gas-puffing case, neutral particles enter into the main plasma from the wall with Frank-Condon energy of 5 eV. We consider three fueling scenarios as typical references. They are tabulated in Table 1.3.3.1.

Recently, in ASDEX, radial profiles of electron density and temperature in the scrape-off layer for Ohmically heated limiter (toroidal carbon limiter in the midplane) discharges are measured by Thomson scattering [12]. We will simulate this experiment by our numerical model to determine the ambiguity factors in the transport process in the scrape-off layer. First, we show the case, in which the conventional transport assumption is employed [13], that is $\gamma_e=5.8$, $\gamma_i=2$, $v_f=0.3C_s$, $D=\chi_e=\chi_i=0.3D_{Bohm}$, in Fig. 1.3.3.3. Although the plasma current is not clearly indicated in Ref. [12], we have determined I_p (400 kA) to reproduce the measured average electron temperature ($T_e\sim 400$ eV) for the average electron density ($\bar{n}_e\sim 1.6\times10^{19}$ m^{-3}). Solid lines represent the numerical calculations for density n_e and temperature T_e. Closed circle and triangle represent the experimental data for n_e and T_e, respectively. They are apparently inconsistent. Based on the suggestion obtained in Fig. 1.3.3.3, we have made wide range of parameter survey in the transport

coefficients. Best fitting case is shown in Fig. 1.3.3.4, in which γ_e=15, γ_i=2, v_f=C_s, D= χ_e= χ_i=0.5D_{Bohm} are employed. We will use these values for the extrapolation to future tokamak reactor.

1.3.3.2 Control of impurities

No contribution.

1.3.3.3 Pumping of helium

Figures 1.3.3.5 and 1.3.3.6 show the electron temperature and density in the scrape-off layer. The abscissa is the distance from the separatrix line in radial direction. The arrows on the figures indicate the position of the leading edge of the limiter. The characteristic decay length of the temperature in radial direction in scrape-off layer is considerably short (~ 1cm), so that the heat flux to the limiter plate will be considerably large. On the other hand the decay length of density is longer than that of the temperature. This implies that the decay length of the perticle flux is not so short, so that the helium ash exhaust is rather easily achieved, since the particle flux flowing into the limiter chamber is rather large.

Figure 1.3.3.7 shows the helium ash accumulation in the main plasma as a function of R_s for l_L=3 and 5 cm. Fueling is performed by pellet injection (1). Considering that the saturated helium accumulation of 4% does not change for various l_L and over the wide range of R_s, this value should be determined by the balance between the particle confinement time in the central region of the plasma (we call it the bulk plasma later on) and the production rate of alpha particles. We now evaluate the pumping speed to realize the required backflow fractions. To do this, the average density of the limiter chamber (the average density of the scrape-off layer, which covers the opening of the limiter chamber) is shown in Fig. 1.3.3.8 for each l_L as R_s is varied. From this figure, we see that the requird C_d is 10^5 l/s to realize R_s=0.9 for l_L=3 cm.

Let us now evaluate the particle load to the pump. We will introduce the overall particle confinement time, which is defined by $\tau = N/\Gamma$, where Γ is the total particle flux to the limiter and the wall, and N is the total particle number in the plasma. Figure 1.3.3.9 shows the overall particle confinement times of D, T and He for l_L=3 cm. In the case of the helium particles, the overall particle confinement time τ_{He} becomes longer and approaches to that in the bulk plama, as the pumping speed becomes large. The absolute amount of tritium pumped out is more straightforward than the characteristics of overall particle confinement time for the particle load to the pump or the required amount of circulating tritium. The results are shown in Fig. 1.3.3.10. The amount of tritium pumped out becomes smaller when R_s is larger and/or l_L is longer. If, however, we intend to realize the same helium accumulation (5%) by different values of l_L, the absolute amount of tritium pumped out are almost the same for all l_L as shown by the arrows in the figure. When the allowable helium accumulation can be increased, the amount of tritium pumped out can be decreased.

1.3.3.4 Optimization of geometry

In considering the heat load and erosion of the limiter, the electron temperature and density of the scrape-off plasma and the total ion particle

flux to the limiter and chamber are important parameters. To avoid the maximum erosion rate, the plasma temperature T_{es} should be lowered or raised. Figure 1.3.3.11 shows T_{es} by various fueling methods for l_L=3 cm (pellet (1) and (2) and gas-puffing) and l_L=2 cm (pellet (2)) as R_s is varied. We now evaluate the heat load and erosion of the limiter for three cases as tabulated in Table 1.3.3.2. Since the heat load and erosion depend strongly on the practical position and configuration of the limiter and magnetic flux surface, they should be evaluated in the practical design. We use the equilibrium magnetic field configuration according to the INTOR design [14] and install the limiter at the bottom of the plasma. The heat and ion particle flux, ion and electron temperature on the midplane calculated so far by the one-dimensional transport code are reevaluated on the limiter surface.

Figure 1.3.3.12 shows the distributions of the heat and ion flux and erosion on the limiter surface for Case I. The abscissa of the figure is the position of the limiter surface in major radius direction. The position tangential to the separatrix line is 5.0 m, and the positions of the leading edge are shown by the arrows. The heat and ion flux and the erosion on the large major radius side limiter are larger than those on the small major radius side limiter due to the toroidal shift of the plasma. The heat and ion flux and the erosion both at the maximum point and the leading edge of the limiter are summarized in Table 1.3.3.3 for Case I $\sim$ III. The heat flux is almost the same for Case I $\sim$ III. In the case of Case II, however, the heat flux on the leading edge is rather large and the erosion is also very large. To lower these values, it is necessary to install the limiter with longer l_L. In the case of Case III, the heat flux and the erosion on the leading edge is decreased significantly. When the length of the limiter is further lengthened, the particle recycling on the limiter surface dominates the overall particle recycling, so that the difference by the pumping and fueling scheme between Case I and Case II, III almost vanishes.

In any cases, however, heat flux and erosion seem to be intolerably large. it will be impossible to realise low heat flux and low erosion by only adjusting the fueling, exhaust and limiter configuration. Redeposition of the sputtered materials could alleviate the erosion, while the characteristics of the redeposited materials are quite uncertain, so that it will be too risky to rely on the redeposition scenario. In addition, if the erosion is such high, the sputtered materials will greatly cool the boundary plasma by radiation down to the temperature, at which the sputtering does not increase the amount of impurities any more. Under this circumstance, the erosion and heat flux should be greatly reduced. Formation of such a cool boundary plasma seems to be the sole case, in which the pumped-limiter can be used in the reactor.

1.3.4 Impact upon the INTOR design concept

We performed a detailed recycling calculations of neutral particles on the limiter and the first wall with the aids of the one-dimensional tokamak transport code. The energy of neutral particles flowing back from the limiter chamber and the necessary pumping speed to realize the recycling rate used in the one-dimensional transport code are calculated by the two-dimensional Monte-Carlo neutral code independently. The feasibility of the pumped-limiter were analysed. The main conclusions obtained are summarized as follows.

(1) The electron temperature in the scrape-off layer decays in radial direction toward the wall very rapidly with the characteristic decay length of about 1 cm, while the density distribution is slightly broad.

(2) When a rather short limiter is installed (e.g. l_L=3 cm on the midplane), moderate pumping system is sufficient to keep the helium accumulation in the main plasma at the desired level (e.g. 1×10^5 l/s for 5% in INTOR). There is a certain pumping speed, above which the accumulation of the helium in the main plasma decreases only slightly even when the pumping speed is increased, while, under which, it increases very rapidly as the pumping speed is decreased.

(3) Overall particle confinement time for helium becomes much longer than that for fuel particles, when more particles are pumped out by larger pumping system.

(4) The minimum amount of tritium pumped out is almost uniquely determined by the allowable helium accumulation in the main plasma. This value does not depend on the length of the limiter, if the pumping speed is appropriately adjusted so as to keep the accumulation at the same level. It is smaller as the allowable accumulation level is higher.

(5) The electron temperature at the separatrix is about 400 eV when the realistic pellet injection by the present-day technology is employed. It will be difficult to further lower the temperature without increasing the helium accumulation level. Fueling by gas puffing gives almost the same results.

(6) The high temperature operation parameter ($700\sim900$ eV) could be realized by large pumping system and ideal pellet injection with short limiter length, and the maximum erosion of the limiter surface could be decreased by a factor of two or more. However, the heat flux and erosion of the limiter are still very large.

(7) To solve the high heat flux and erosion of the pumped limiter, cool boundary plasma may be indispensable. This cool boundary plasma must be restricted to the periphery and the hot core plasma must be unaffected by it to sustain the self-ignition state.

There may be several possibilities to realize cool boundary plasma. The first one is the cooling by impurity radiation [15]. By selecting the appropriate impurity, it may be possible to restrict the radiation energy loss only in the boundary plasma region. This possibility, however, crucially depends on the impurity transport.

The second possibility is the increase of the particle recycling on the limiter surface. This increase has been observed in divertor experiments [16], while not yet clearly observed in the limiter experiment. In the case of the limiter, the main plasma is very close to the limiter surface, so that the neutral particles emitted from the limiter can easily escape to the main plasma, resulting in little increase of the particle recycling. However, the particle recycling strongly depends on the heat and particle fluxes in the scrape-off layer and the geometrical configuration, so that there remains the possibility of cool boundary plasma by the particle recycling. Realization of any of these possibilities of cool boundary plasma will be the essential purpose of the theory and experiment for the pumped limiter in future.

References for 1.3.2

[1] G.M. McCracken, P.E. Stott, Nucl. Fusion 19 (1979) 889.
[2] T. Kobayashi, T. Tazima, K. Tani, S. Tamura, Japan Atomic Energy Research Institute Report, JAERI-M 7014 (1977).
[3] S. Tamor, J. Comp. Phys. 40 (1981) 104.
[4] R.L. Freeman, E.M. Jones, CLM-R137, Culham Laboratory (1974).
[5] D.E. Post, D.B. Heifetz, M. Petravic, J. Nucl. Mater. 111 & 112 (1982) 383.
[6] Y. Seki, Y. Shimomura, K. Maki, M. Azumi, T. Takizuka: Nucl. Fusion 20 (1980) 1213.
[7] J.D. Callen, G.A. Emmert, A.M. Bailey, M.E. Benchikh-Lehocine, J.N. Davidson, et al., in Plasma Physics and Controlled Nuclear Fusion Research (Proc. 8th Int. Conf. Brussels, 1980) Vol. 1, IAEA, Vienna (1981) 775.
[8] D.F. Duchs, D.E. Post, P.H. Rutherford, Nucl. Fusion 17 (1977) 565.
[9] J.P. Boujot, C. Mercier, Computer Physics Communications 4 (1972) 89.
[10] M. Ohnishi, N. Ao, J. Wakabayashi, Nucl. Fusion 18 (1978) 859.
[11] S.L. Mirola, C.A. Foster, ORNL/TM-5776 (1977).
[12] M. Keilhacker, K. Lackner, K. Behringer, H. Muramnn, H. Niedermeyer, Physica Scripta T2/2 (1982) 443.
[13] DIVA Group, Nucl. Fusion 18 (1978) 1619.
[14] INTOR Group, International Tokamak Reactor: Phase One (Rep. Int. Tokamak Reactor Wrokshop, Vienna, 1980-81), International Atomic Energy Agency, Vienna (1982).
[15] Y. Shimomura, Nucl. Fusion 17 (1977) 1377.
[16] M. Shimada, M. Nagami, K. Ioki, S. Izumi, M. Naeno, H. Yokomizo, K. Shinya, H. Yoshida, N.H. Brooks, C.L. Bsieh, R. Groebner, A. Kitsunezaki, Nucl. Fusion 20 (1982) 643.

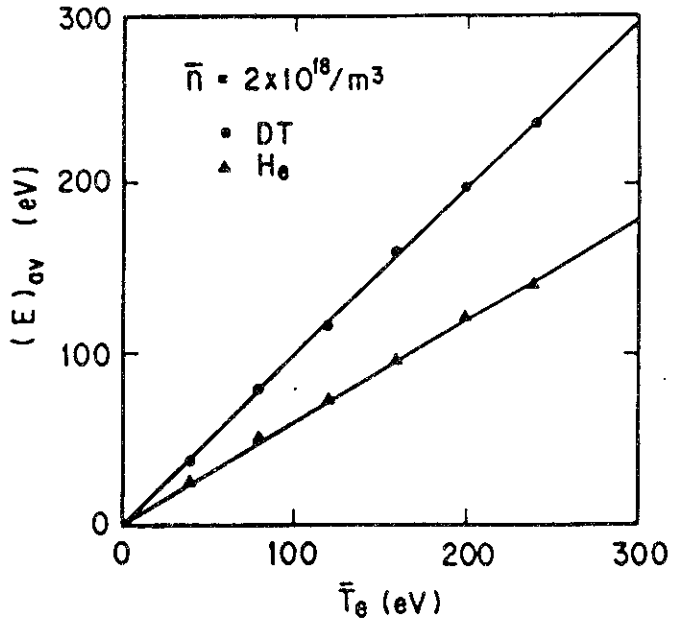

Fig. 1.3.3.1 Average energy of fuel and helium neutral particles, which flow back to the main plasma, calculated by two-dimensional Monte-Carlo neutral code as a function of temperature of scrape-off layer plasma. Density of the scrape-off layer plasma is 2×10^{18} m^{-3}.

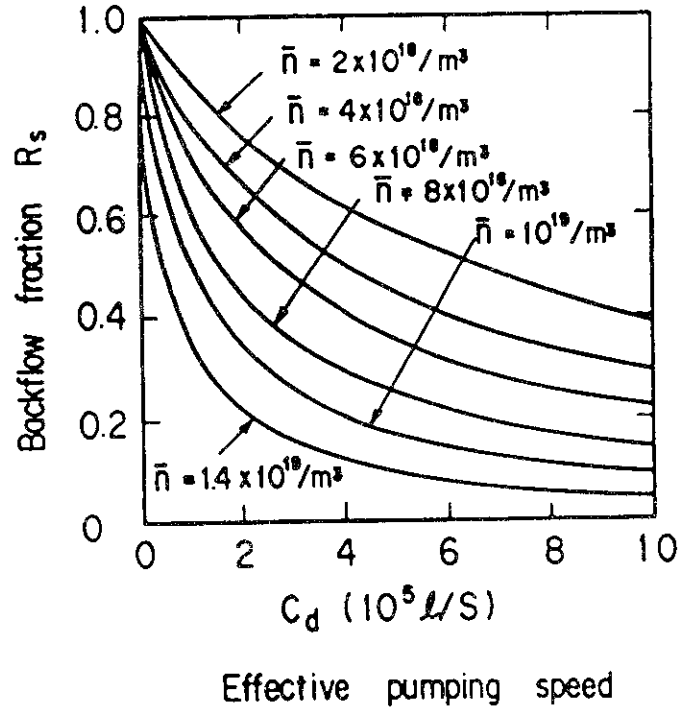

Fig. 1.3.3.2 Backflow fraction R_S vs. effective pumping speed C_d at the entrance of the evacuating duct with density of scrape-off layer plasma as parameters.

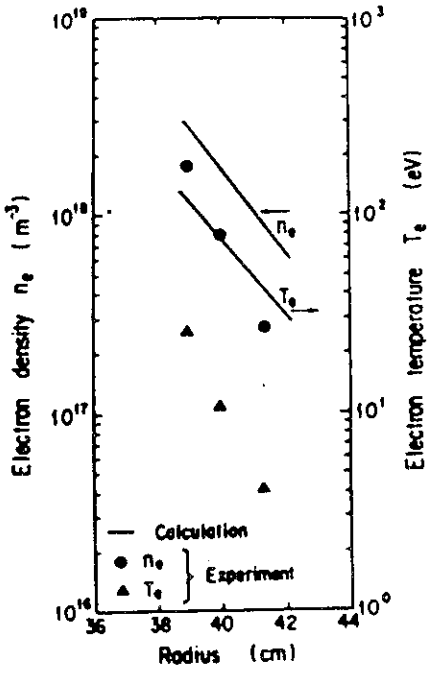

Fig. 1.3.3.3 Numerical calculation for the radial profiles of the electron density n_e and temperature T_e (solid lines) for the limiter operation in ASDEX. Closed circle and triangle show the experimental results. γ_e=5.8, γ_i=2.0, v_f=0.3C_s and D= χ_e= χ_i=0.3D_{Bohm} are employed.

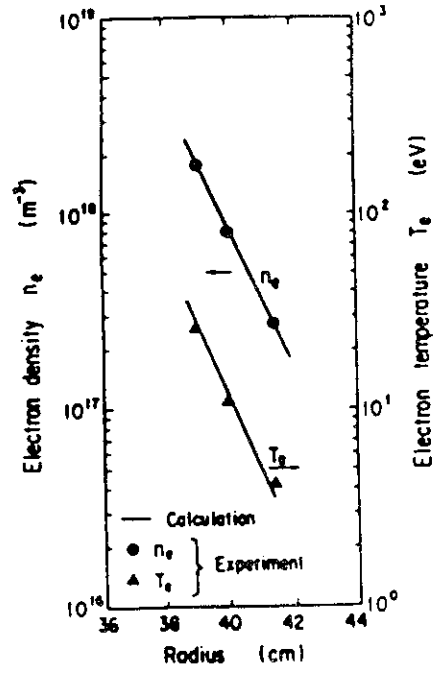

Fig.1.3.3.4 Best fitting of the numerical calculation for the radial profiles of the electron density n_e and temperature T_e (solid lines) for the limiter operation in ASDEX. Closed circle and triangle show the experimental results. γ_e=15.0, γ_i=2.0, v_f=C_s and D= χ_e= χ_i=0.5D_{Bohm} are employed.

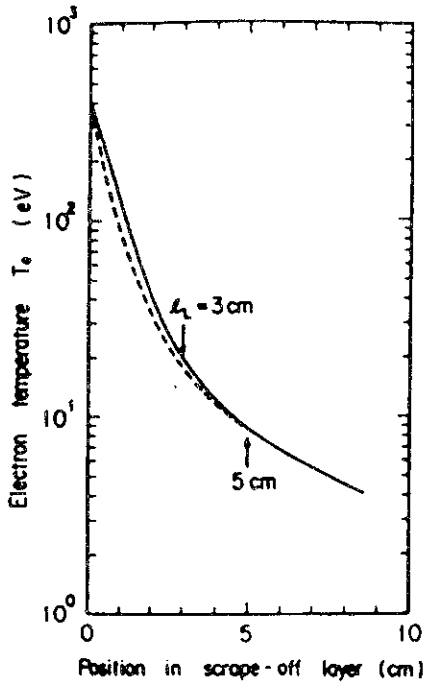

Fig.1.3.3.5 Profile of electron temperature in scrape-off layer. Pellet injection (1) and R_S=0.9 are employed. Arrows indicate the position of leading edge of limiter.

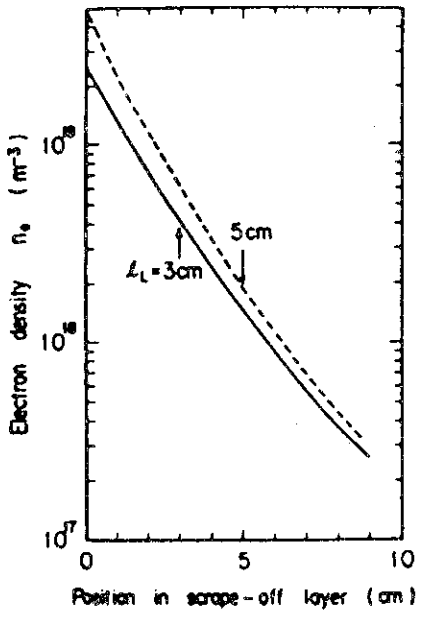

Fig.1.3.3.6 Profile of electron density in scrape-off layer. Pellet injection (1) and R_S=0.9 are employed. Arrows indicate the position of leading edge of limiter.

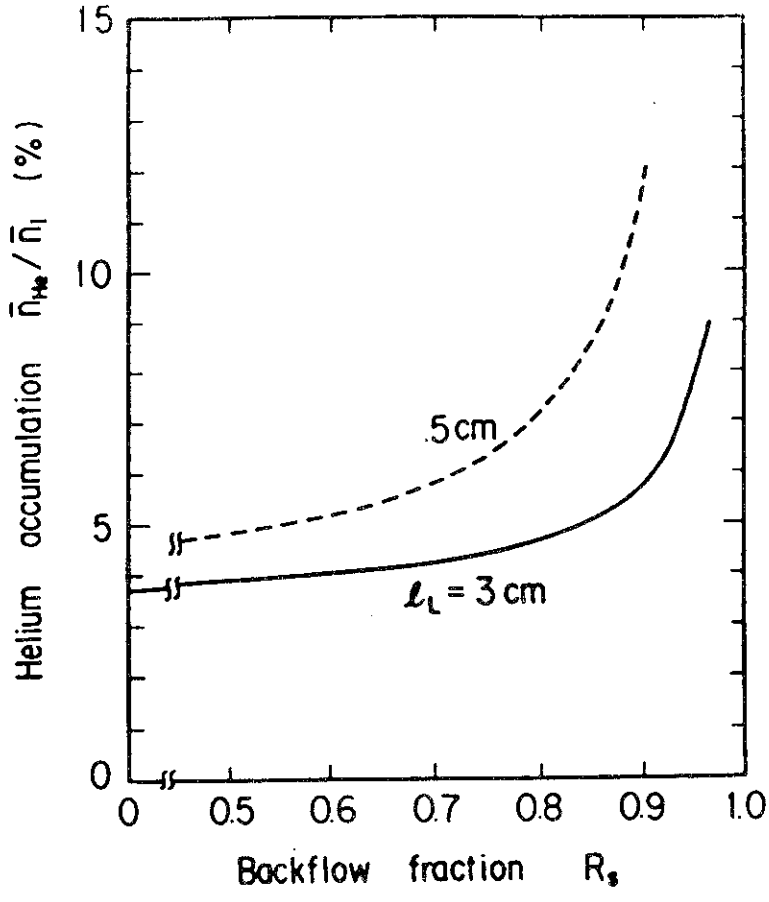

Fig. 1.3.3.7 Helium ash accumulation in main plasma as R_S is varied for l_L=3 and 5 cm. Fueling is performed by pellet injection (1).

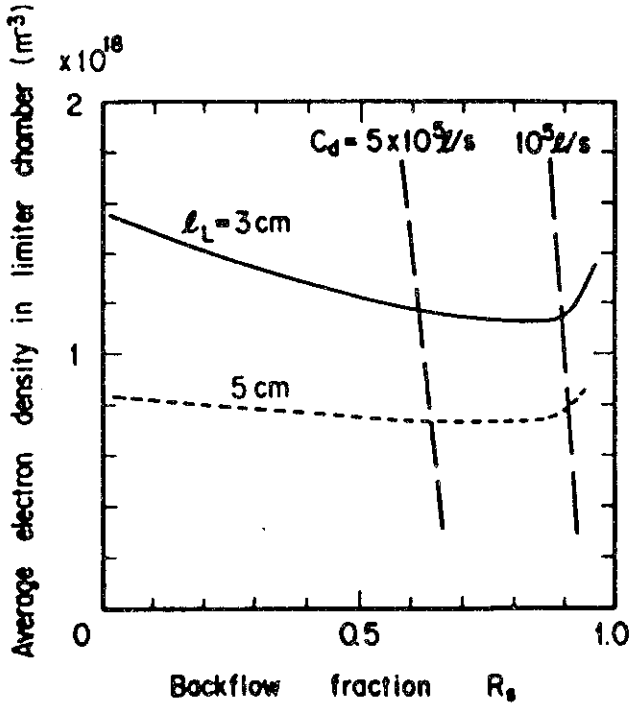

Fig. 1.3.3.8 Average densities in limiter chamber for each l_L as R_S is varied. Relations between plasma density and R_S of Fig. 4 with C_d being fixed are also shown by long broken lines.

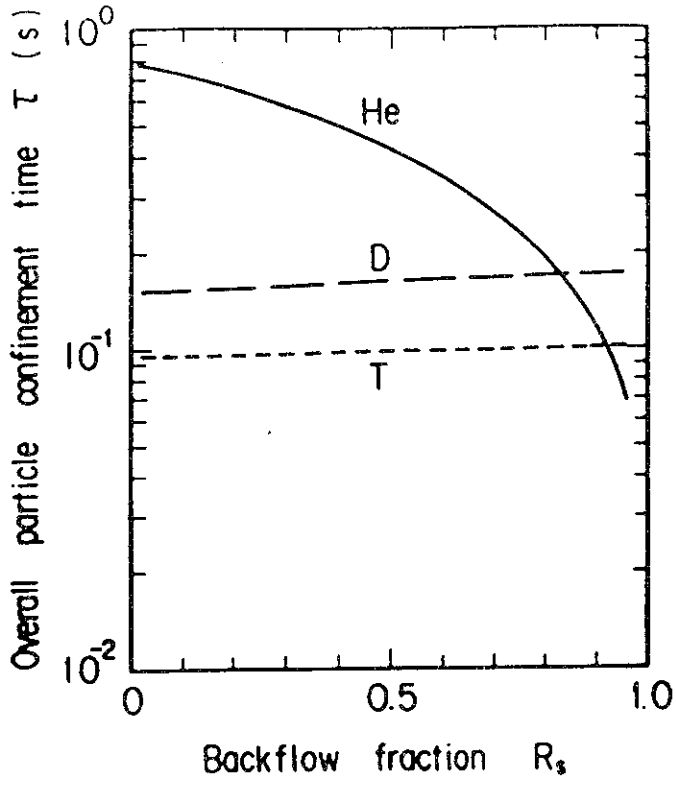

Fig. 1.3.3.9 Overall particle confinement times for deuterium (D), tritium (T) and helium (He) for l_L=3 cm. Fueling isperformed by pellet injection (1).

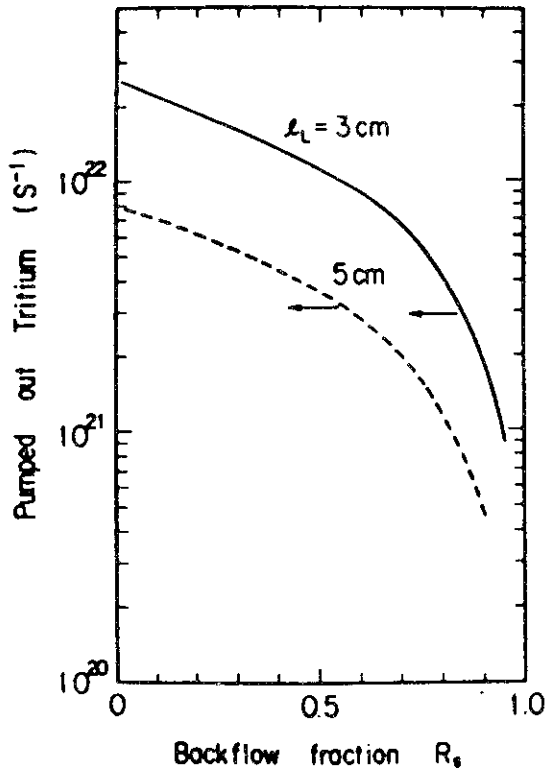

Fig. 1.3.3.10 Absolute amount of tritium pumped out as R_S is varied for various l_L. They are almost the same for all l_L as shown by arrows, if the accumulation is same (5%).

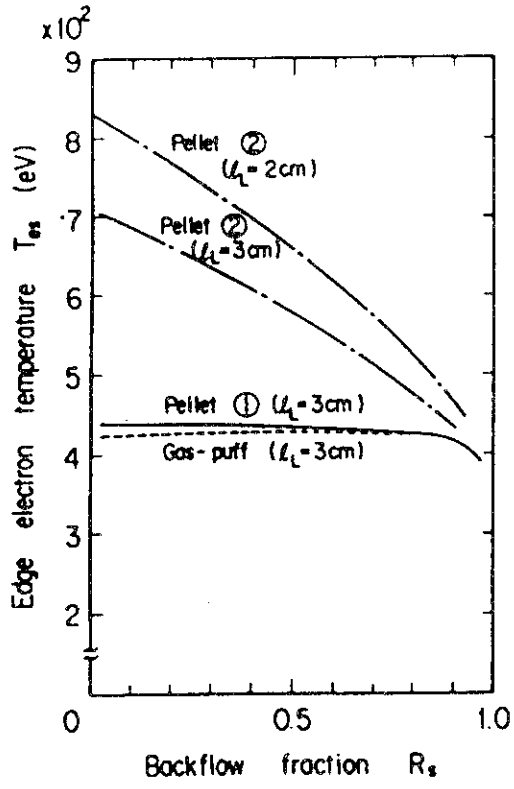

Fig. 1.3.3.11 Electron temperature at separatrix by various fueling method for l_L=3 cm(pellet (1) and (2) and gas-puffing) and l_L=2 cm (pellet (2)) as R_S is varied.

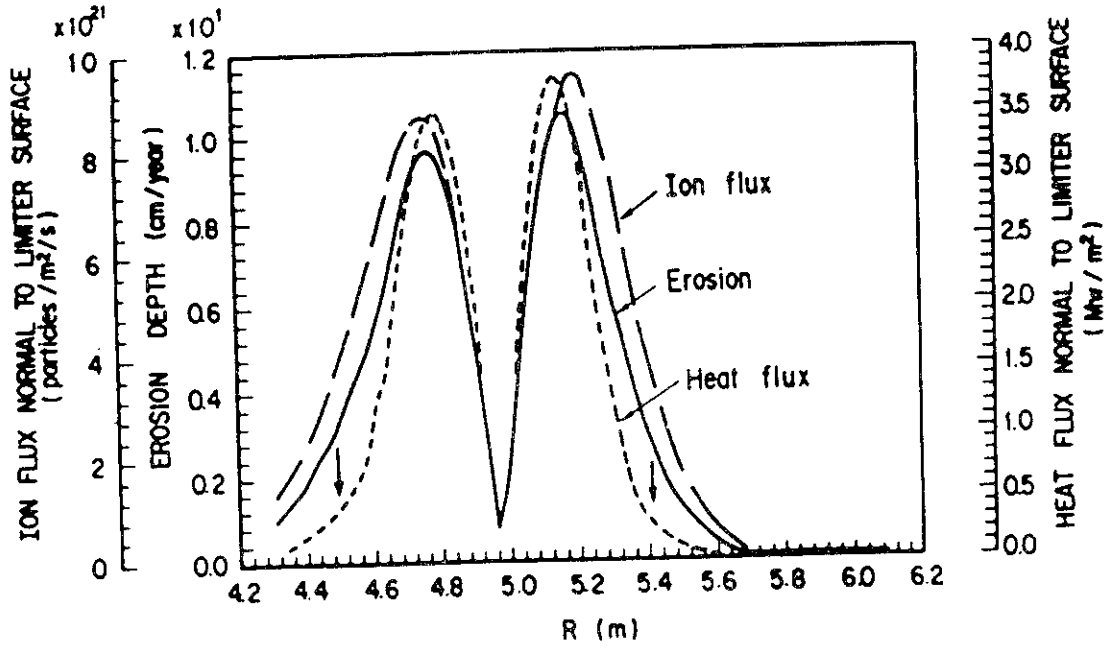

Fig. 1.3.3.12 Distributions of heat and ion particle flux and erosion on carbon limiter surface for Case I. Arrows indicate the positions of the leading edge.

1. pellet ①	r_p = 1 mm U = 2×10^3 m/s	(shallow penetration)
2. pellet ②	r_p = 3 mm U = 10^4 m/s	(moderate penetration)
3. gas-puffing	5 eV neutral energy	(surface fueling)

Table 1.3.3.1 Three typical fueling scenarios and their characteristic features used in the calculations.

Case I	pellet injection ① R_s = 0.9, ℓ_L = 3 cm	: medium T_{es}
Case II	pellet injection ② R_s = 0.5, ℓ_L = 2 cm	: high T_{es}
Case III	pellet injection ② R_s = 0.5, ℓ_L = 3 cm	: medium-high T_{es}

Table 1.3.3.2 Three typical cases used to calculate heat load and erosion of the limiter.

Case		Case I	Case II	Case III
		pellet ① ℓ_L = 3 cm R_s = 0.9	pellet ② ℓ_L = 2 cm R_s = 0.5	pellet ② ℓ_L = 3 cm R_s = 0.5
maximum on limiter surface	heat flux (MW/m^2)	3.8	4.0	4.0
	ion flux ($1/m^2S$)	9.6×10^{21}	5.0×10^{21}	6.2×10^{21}
	electron temp. (eV)	115	180	173
	ion temp. (eV)	255	360	314
	erosion (cm/y)			
	C (500 C)	10.6	6.1	7.7
	Fe	5.7	3.7	4.3
leading edge	heat flux (MW/m^2)	0.74	3.3	0.84
	ion flux ($1/m^2S$)	4.2×10^{21}	3.8×10^{21}	3.5×10^{21}
	electron temp. (eV)	14	73	23
	ion temp. (eV)	186	330	240
	erosion (cm/y)			
	C (500 C)	7.3	11.7	6.3
	Fe	2.7	5.1	2.5

Table 1.3.3.3 Heat and ion particle flux, electron and ion temperature and erosion both at a maximum point and leading edge of limiter for Case I, II and III. Erosion is calculated both for carbon and ion limiter.

1.4 Innovative schemes

1.4.1 Electric field effect

No data base

1.4.2 Ergodic limiters

Ergodic Magnetic Limiter and Wall Lapping Plasma by Subsidiary Helical Coils in a Tokamak

It has been suggested that the ergodic magnetic layer produced in the periphery of the tokamak plasma by subsidiary helical currents (Ergodic Magnetic Limiter) can be effective for equalizing the heat load on the first wall. And it is also proposed that the several sets of helical coils carrying the alternating currents should produce a wall lapping plasma rotating along the first wall and promote the uniform heat flux to the first wall. In order to examine the possibilities of these concepts we numerically analysed the formation and destruction of the magnetic islands produced by resonant helical currents, and confirmed the rotation of islands by sets of alternating currents. Tokamak parameters refered to the R-tokamak project in IPP-Nagoya ($R=2.1$ m, $a_p=0.6$ m, $B_t=5$ T, $I_p=1.5$ MA).

At first we calculated the case in which a single set of double $l=3$, $n=1$ helical coils with same constant current I_H in opposite directions was applied. The results show that the magnetic surfaces outsides the $q=3$ surface ($r \geq 0.6$ m) are effectively destructed, when the value of helical currents I_H is larger than a critical value (3 kA for R-tokamak) which is very small compared to the plasma current.

Next we considered the case of three $l=3$ double helical coil sets which were shifted by 20° in the poloidal direction with respect to each other and which carry time-dependent sinusoidal alternating currents with shifted phases. The results show that the alternating currents certainly produce the rotation of resonance islands and the wall-lapping plasma concept.

Finally we examined the effect of the local helical coils which were wound in the localized regions along the toroidal direction of the torus, because they are of greater practical use from the engineering viewpoints. We used a set of local helical coils in which two local coils cover two toroidal regions with an angular span of $\Delta_H=30°$, $I_H=15$ kA (I_H is the amplitudes of the alternating currents with shifted phases) show that the magnetic islands also rotate in this case, although about five times larger current are needed than the case of full windings.

References for Section 1.4.2

[1] Interim Report on the First Phase Design of R-tokamak (Inst. of Plasma Physics, Nagoya Univ., Oct. 1981)
[2] T. Tazima and M. Sugihara, JAERI-M 8390 (1979)
[3] T. Kawamura, Y. Abe and T. Tazima, J. of Nucl. Mater. 111 & 112 (1982) 268.

1.4.3 Bundle divertor

No data base.

1.4.4 RF pumpout

Active Control of Impurities by Radio-Frequency Divertor

A magnetic divertor has been recognized the most reliable method of impurity control in present-day tokamaks. Also much attention has been focussed on a mechanical divertor (pump limiter) from an engineering assessment point of view. Both magnetic and mechanical divertors are essentially passive since the impurities diffusing spontaneously out of a hot plasma core are removed at the plasma periphery. If the impurity transport itself is artificially controllable, then this active control will facilitate not only the impurity suppression in the hot plasma core but also the positive use of impurities (e.g., the first wall protection with radiative cooling by impurities).

The active control of impurities requires some additional input of momentum (energy) into a plasma. The external momentum injection by means of neutral beams has been investigated experimentally [1,2] and theoretically [3,4]. Instead of particle momentum, the use of radio-frequency (RF) wave momentum has recently been proposed [5-7]. This is called RF divertor where waves are launched into a plasma by external RF generator in the ion-cyclotron range of frequencies (ICRF). In prinicple, RF divertor uses wave-particle interactions in a plasma. Depending on the species of resonant particles, two schemes of RF divertor are considered, i.e., the direct method and the indirect method.

DIRECT METHOD

In this case, the resonant particles are impurity ions. An ion Bernstein wave or an ion cyclotron drift wave [8] is excited in the impurity-ion cyclotron range of frequencies, and the wave momentum (energy) is selectively deposited to the impurity ions. The resultant impurity-ion heating diminishes the Coulomb-collision diffusion, and enhances the neutral-collision diffusion and the ripple diffusion. Thus, the RF impurity heating is an effective means controlling the impurity transport. Recent model experiments in TFR [9] have demonstrated this divertor effect. Even if no heating takes place, the stationary cross-field impurity flux can be driven by the wave: the wave poloidal momentum G_{pol} is deposited to the impurity ions, and they are driven radially outward by $G_{pol} \times B_{tor}$ drift. This is an application of RFFC [10] to the impurity control.

INDIRECT METHOD

When the main ions are resonant with waves, the wave energy is given to the main ions which indirectly modify the impurity diffusion. In this case, the ICRF heating is adopted in a conventional way except for the uni-directional travelling wave. The main-ion heating asymmetric in the velocity space induces the toroidal rotation of the plasma. If the speed of the rotation driven by the wave exceeds the thermal speed of the impurity-ion, the impurity transport is reversed to the radially outward flow [4]. The estimation of the dissipated power supports the practicality of this scheme in a tokamak reactor.

References for Section 1.4.4

[1] R.C. Isler et al., Phys. Rev. Lett. 47 (1981) 649.
[2] D.R. Eames, Ph.D. Thesis, Princeton University (1980) unpublished.
[3] W.M. Stacy Jr. and D.J. Sigmar, Nucl. Fusion 19 (1979) 1665.
[4] K.H. Burrell, T. Ohkawa and S.K. Wong, Phys. Rev. Lett. 47 (1981) 511.
[5] H. Sugai, Phys. Lett. 91A (1982) 73.
[6] H. Sugai, Phys. Lett. 93A (1983) 483.
[7] H. Sugai, Proc. 11th Europ. Conf. Controlled Fusion and Plasma Physics (Aachen, 1983) Vol. II, p. 423.
[8] M. Kando, S. Ikezawa and H. Sugai, Phys. Lett. 101A (1984) 204.
[9] TFR Group, Nucl. Fusion 22 (1982) 956.
[10] K. Itoh and S. Inoue, Comments Plasma Phys. Cont. Fusion 5 (1980) 203.

1.4.5 Flow reversal

No data base.

1.4.6 Liquid and droplet limiters

No data base.

1.5 Fuelling

A data base for fueling is needed for INTOR to increase a plasma density during a start-up and to replenish a D-T fuel in a burn phase. Most of present tokamak experiments use a gas puffing to control plasma densities by adjusting an amount of gas feed. Fueling by a pellet injector has made remarkable progress in both of fueling physics and technology.

Recent experiments indicate that fueling physics is deeply correlated with plasma confinement property. Discharges without degradation of a confinement time during NBI heating, the so-called H-mode, are found to be strongly influenced by the fueling and recycling at a plasma edge. The fueling is expected to become more important for INTOR.

1.5.1 Data on gas fuelling

A gas puffing is a simple gas supply method and is widely used in tokamak experiments. It has a wide range of gas supply amount and the prescribed plasma density is successfully obtained by preprogram or feedback controls.

The recent tokamak experiments shows that a deep correlation is observed between the gas puffing and the plasma confinement time. In the Doublet III experiments, the so-called H-mode discharges are obtained by reducing a gas supply at a plasma edge with adjusting the gas puffing[1]. A large amount of gas puffing from the plasma edge makes discharges difficult to become a type of H-mode. The ASDEX experiments also show the abrupt appearance of H-mode discharges due to the self-controlled gas puffing in a range of certain plasma densities[2]. They indicate that the gas fueling is crucial for attainment of good confinement discharges and that high plasma densities with large gas puffing change discharges from the H-mode to L-mode of degraded confinement.

The physical machinary of H-mode discharges is not clear so far, the above experimental results however suggest that the gas fueling is a key factor for H-mode. INTOR discharges with high plasma densities will need strong gas fueling and are expected to need both of the gas puffing and the pellet injection to attain good confinement.

1.5.2 Data on pellet fuelling

Use of a pellet injection as a fueling is observed to improve confinement times of discharges with limiter and divertor in recent experiments[3]. It seems to be on the same line as the improvement of the H-mode with adjusting a gas puffing.

Discharges with a limiter has been appreciated to become L-type ones with increasing NBI heating. Remarkable improvement in a confinement time of limiter discharges are lately observed in Doublet III by using a pellet injection[3]. A pellet injection during NBI heating encountered some difficulties in its penetration into the plasma, i.e. some high energy ions resulted from the ionization of NBI beams at the outer plasma region impede the pellet from going into the central region of the plasma due to ablation at the plasma periphery. The difficulties are overcome in such a way that the neutral beams are intermittently operated and during the cessation of the beams the pellet is injected after fast ions in the edge plasma well slow down

(~8ms). This way, the confinement time of discharges with a limiter is significantly improved by the deep penetration of the pellet and reach the almost same value of the H-mode discharges with a divertor. The results indicate importance of the low recycling in the edge plasma and is consistent with the feature of the H-mode discharges.

The H-mode discharges with a divertor are observed to change from the H-mode to L-mode, increasing their densities, as mentioned previously. The amount of a gas feed to increase plasma densities may raise the recycling in the plasma edge and results in the degradation of the confinement. The difficulties are also surmounted by the pellet injection, which can reduce the edge recycling, retaining high density plasmas[3].

INTOR plasma will be heated with ICRF heating. Fast ions by the RF heating are expected to exist in the center region of the plasma, different from the NBI heating. The pellet will easily penetrate into the central region, if the pellet has enough speed, and plasmas may increase their densities, keeping good confinement property.

During a burn phase, a part of fast ions goes out without slowing down due to ripple of toroidal field, and they ablate the pellet in the plasma edge and discharges result in degradation of the confinement time. However, those ions appear in a limited region, i.e. the upper or lower half of the plasma cross section. The interaction between the fast ions and the pellet could therefore be avoided, when the pellet is injected into the region free of the fast ions.

References for subsection 1.5

[1] N.NAGAMI, et al., Nuclear Fusion, 49(1984)183.
[2] F.WAGNER, et al., Phy. Rev. Let., 49(1982)1408.
[3] S.SENGOKU, et al., 10th IAEA Conference (London, 1984), Post-deadline paper.

1.6 Basic science data

1.6.1 Atomic processes

1.6.1.1 Data center activities on atomic and molecular (A&M) data for fusion in JAERI

The major activities of JAERI A&M Data Center have been devoted to the compilation of 1) atomic collision data, 2) particle-material interaction data and 3) atomic structure data. A review on the recent activities and future programs is given.

1. Organization

Activities on atomic and molecular (A&M) data for fusion in JAERI are carried out by A&M Section of Nuclear Data Center, Department of Physics, in co-operation with the Research Committee on A&M Data of JAERI which consists of the members of in and outside of JAERI. In Figure is shown the organization for A&M activities in JAERI.

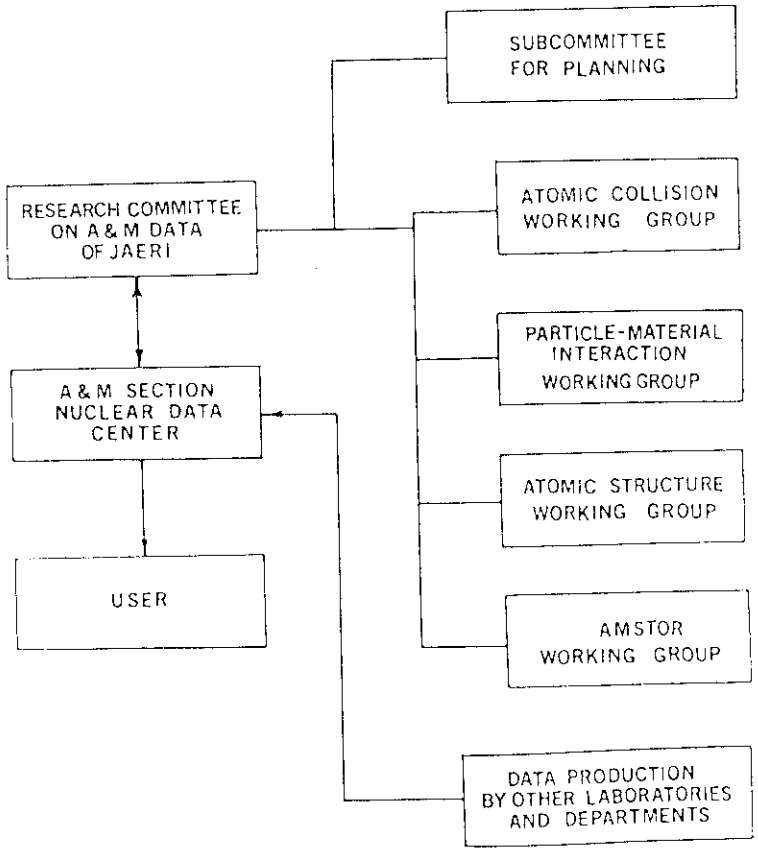

2. Data compilation and evaluation

Japanese Evaluated A&M Data Library, 1st Volume (JEAMDL-1) program is being in progress. This is systematic sets of compilations of evaluated A&M data on specific items relevant to controlled fusion research and technology such as designs of fusion devices, plasma modellings, diagnostics and particle recycling.

2.1 Atomic collision data

Following processes have been compiled and partially evaluated in the form of empirical formulas: (1) Total charge transfer cross sections in the energy range of 1 and 10^7 eV/amu for (a) H atoms and ions with conventional vacuum impurities such as H_2, N_2, O_2, H_2O and carbon containing molecules, and with inert gases, (b) He atoms and ions with above molecules and gases, and (c) multi-charged impurity ions with He. And (2) ionization cross sections for H^+, H_2^+, H_3^+, He^+, $He^{++}+H$, H_2, He systems. Several numerical data compilations are also now in progress as followings: (3) Total charge transfer cross sections for (a) H and He atoms and ions with metal vapors, and (b) multi-charged ions with other inert gases and molecules. (4) Cross section of electron capture into excited states for light and heavy ions with various target atoms and molecules. And (5) $(H^+, H) + (H^+, H)$ collision data.

2.2 Particle-material interaction data

They are composed of the following three items: (1) Data on elementary processes for hydrogen recycling in fusion devices, such as (a) trapping and detrapping process, (b) diffusion and (c) radiation effects and segregation for hydrogen isotopes and helium ions implanted on refractory and wall coating materials. (2) Surface effects on damaged profiling in fusion materials by ion beam bombardment. And (3) electron-materials data for the bremsstrahlung produced by 1 - 30 MeV electrons normally incident on thick targets such as C, Al, Fe, Cu, Mo and W.

2.3 Atomic structure data

Atomic energy level and transition probability data are necessary in the field of impurity diagnostics. Species of impurity are Ti, Fe, Ni, Mo and Nb constituting the first wall materials. As to Ti we have been published a data compilation in the forms of wave-length tables and Grotrian diagrams. At present we go on to compile the data of other atoms to make wave-length tables and Grotrian diagrams by using our computer programs.

3. Atomic and molecular data storage and retrieval system (AMSTOR) program

AMSTOR is a computerized data storage and retrieval system to represent the numerical data in the graphical and tabular forms. Database of this system consists of three subdivided databases because data descriptions in the three fields mentioned above are different from each other. (1) For atomic collision data, numerical data format is developed with reference to the exchange format (EXFOR) of IAEA. (2) For particle-material interaction data, at present a format for plotting numerical data is designed, and an appropriate format for data storage/retrieval is being planned. And (3) for atomic structure data, programs for making the wave-length tables and Grotrian diagramsare developed and are ready to use at present. The experimental data

compiled up to now have already been stored in this database, so that we can make use of this database in data evaluation.

All the compiled data of above three items of Sec. 2 are now stored in our computer system by our own formats. Some of them are available to interested user on magnetic tapes for their requests as well as other informations related to those data compilations, which are being published as JAERI-M Reports. (Ask to Y. Nakai, Nuclear Data Center, Department of Physics, JAERI)

We are also keeping to open our door to compile other A&M data which are urgently needed and requested by fusion cummunities.

APPENDIX Publication List

1. Y. Nakai, M. Sataka and T. Shirai: Data on Collisions of Helium Atoms and Ions with Atoms and Molecules I. (Cross Sections for Charge Transfer of He, He^+ and He^{++} with H, H_2, and He) (in Japanese), JAERI-M 8849 (1980)
2. M. Sataka, T. Shirai, A. Kikuchi and Y. Nakai: Ionization Cross Sections for Ion-Atom and Ion-Molecule Collisions I. (Ionization Cross Sections for H^+, H_2^+, H_3^+, He^+ and He^{++} incident on H, H_2, and He), JAERI-M 9310 (1981)
3. K. Mori: Grotrian Diagrams for Highly Ionized Titanium Ti V - Ti XXII, JAERI-M 82-078 (1982)
4. S. Yamaguchi, K. Ozawa, Y. Nakai and Y. Sugizaki: Data on Trapping and Re-emission of Energetic Hydrogen Isotopes and Helium in Materials, JAERI-M 82-118 (1982)
5. Y. Nakai, A. Kikuchi, T. Shirai and M. Sataka: Data on Collisions of Hydrogen Atoms and Ions with Atoms and Molecules (I) (Cross Sections for Charge Transfer of H, H^+ and H^- with H_2, N_2, O_2, H_2O, C and Carbon Containing Molecules), JAERI-M 83-013 (1983)
6. S. Tanaka, R. Tanaka, T. Tabata, R. Ito, Y. Nakai and K. Ozawa: Data on Thick Target Bremsstrahlung Produced by Electrons, JAERI-M 83-019 (1983)
7. K. Ishii: Atomic Structure Calculation of Enerkgy Levels and Oscillator Strength in Mo Ion, I ($3p^63d^8$-$3p^53d^9$, $3d^8$-$3d^74p$ and $3d^8$-$3d^74f$ Transitions in Mo XVII), JAERI-M 83-034 (1983)
8. Y. Nakai, A. Kikuchi, T. Shirai and M. Sataka: Data on Collisions of Hydrogen Atoms and Ions with Atoms and Molecules (II) (Cross Sections for Charge Transfer of H, H^+ and H^- with He, Ne, Ar, Kr and Xe), JAERI-M 83-143 (1983)
9. K. Ishii: Atomic Structure Calculation of Enerkgy Levels and Oscillator Strength in Ti Ion, I (3s-3p and 3p-3d Transitions in Ti IX), JAERI-M 83-155 (1983)
10. K. Ishii: Atomic Structure Calculation of Enerkgy Levels and Oscillator Strength in Ti Ion, II (3s-3p and 3p-3d Transitions in Ti X), JAERI-M 83-164 (1983)
11. K. Ishii: Atomic Structure Calculation of Enerkgy Levels and Oscillator Strength in Ti Ion, III (3s-3p and 3p-3d Transitions in Ti XI), JAERI-M 83-198 (1983)
12. M. Kitagawa: Stopping Power for Ions in Solids (in Japanese), JAERI-M 83-223 (1983)

13. Research Committee on A&M Data, JAERI: Report of Workshop on Computer Simulation of Atomic Collision Processes in Solids (in Japanese), JAERI-M 83-226 (1984)
14. Research Committee on A&M Data, JAERI: Report of The 2nd Workshop on Particle Material Interactions for Fusion Research (in Japanese), JAERI-M 83-235 (1984)
15. K. Ishii, H. Kubo and K. Ozawa: Atomic Structure Calculation of Energy Levels and Oscillator Strength in Fe Ion, I (3s-3p and 3p-3d Transitions in Fe XV), JAERI-M 83-240 (1984)
16. N. Oda and J. Urakawa: Data on Ionization, Excitation, Dissociation and Dissociative Ionization of Targets by Helium Ion Bombardments (I). (Target Ionization, Excitation, Dissociation and Dissociative Ionization induced by Several keV to 3.5 MeV Helium Ions incident on a Thin Gas Targets), JAERI-M 84-049 (1984)
17. Y. Nakai, A. Kikuchi, T. Shirai and M. Sataka: Data on Collisions of Helium Atoms and Ions with Atoms and Molecules (II) (Cross Sections for Charge Transfer of He^{2+}, He^{+}, He and He^{-} with He, Ne, Ar, Kr and Xe), JAERI-M 84-069 (1984)
18. K. Ozawa, K. Fukushima and K. Ebisawa: Data Compilation for Irradiation Effect on Hydrogen Rekcycle in Fusion Materials, JAERI-M 84-089 (1984)
19. M. Terasawa, S. Nakahigashi and K. Ozawa: Data Compilation of Ion-Induced Damage and Ion-Implanted Atoms, JAERI-M 84-092 (1984)
20. S. Yamaguchi, K. Ozawa, Y. Nakai and Y. Sugizaki: Data on Trapping and Re-emission of Energetic Hydrogen Isotopes and helium in Matyerials, Supplement 1., JAERI-M 84-093 (1984)
21. T. Oshiyama, S. Nagai, K. Ozawa, and F. Takeuchi: Data Compilation for Particle Impact Desorption, JAERI-M 84-094 (1984)

1.6.1.2 Data Compilation and Evaluation for Atomic and Molecular Processes and for Plasma-Surface Interactions at Institute of Plasma Physics, Nagoya University

1. Data compilation and evaluation

Well before establishing the Research Information Center at IPP, data compilation for A&M processes relevant to fusion plasma researches started [1,2]. Since then, such activities have been extended to those for plasma-surface interaction processes. These activities are generally supported by a number of volunteer scientists in these fields and the results are reported in Internal Reports IPPJ-AM series (see a list of reports). Some of them are further refined and published in International Journals (see list of publications). In the following is given a short description of these activities:

1) The atomic structure data of Fe ions, one of the most common impurities, were compiled and published. Similar works are now mainly being made at Japan Atomic Enerkgy Research Institute.

2) The charge transfer cross sections of ions in collisions with atomic and molecular hydrogens are compiled. These data are stored in our computer as a data base CHART (Charge Transfer) and can be retrieved. Also those for other target gases are compiled.

3) The compilation and evaluation of excitation cross sections and rate coefficients in electron impact for carbon and oxygen ions in various ionization stages have recently be completed and these data are stored as a database AMDIS (Atomic and Molecular Data Interactive System). Similar systematic works for H-like ions to O-like ions in iso-electronic sequence are under way.

4) The ionization cross sections of ions by electron impact are compiled and stored in AMDIS. Also a critical evaluation of empirical formulas describing the ionization cross sections in electron impact has been made.

5) Bibliographic data on atomic processes in hot, dense plasmas (stored as a database HIDENS, High Density) and on ion-ion collisions, which are important in the inertial confining fusion research, are compiled.

6) The importance of understanding behavior of low temperature plasmas near the edges, limiters and divertors urged us to compile data involving the ionization of neutral atoms and excitation, dissociation and recombination processes of atomic and molecular hydrogen atoms/ions. This compilation is now under way.

7) Compilation and evaluation of sputtering data by ion impact have been completed for monatomic solid targets. The incident energy dependence, angular distribution and incident angle dependence of total sputtering yields have been evaluated and some empirical formulas for sputtering yields have been found. These data are stored as a data base SPUTY (Sputtering Yield). Compilation of the sputtering yields for compound metals/alloys is under way.

8) Data for the particle- and energy-backscattering coefficients are compiled and evaluated and empirical formulas for these data in normal and oblique incidences have been found.

9) Data compilation of the important basic processes relevant to hydrogen recycling processes is under way. It has been found, however, that some data are significantly dependent on the surface and other environmental conditions and it seems to be difficult to evaluate consistent data.

2. Bibliographic and numerical databases

In order to make easy access to the bibliographic and numerical data, a computer-based data storage and retrieval system has been developed. The databases developed by ourselves as well as those commercial and exchanged with other Data Centers are available. These data can be retrieved through TSS at the Institute or telephone line linkage from other Institute. In Table is shown a list of our databases together with their record numbers.

References for subsection 1.6.1.2

[1] Cross Sections for Atomic Processes Vol. 1 (IPPJ-DT-48) (1975)
[2] Cross Sections for Atomic Processes Vol. 2 (IPPJ-DT-50) (1976)

LIST OF IPPJ-AM REPORTS

IPPJ-AM-1 "Cross Sections for Charge Transfer of Hydrogen Beams in Gases and Vapors in the Energy Range 10 eV–10 keV"
H. Tawara (1977) [Published in Atomic Data and Nuclear Data Tables 22, 491 (1978)]

IPPJ-AM-2 "Ionization and Excitation of Ions by Electron Impact –Review of Empirical Formulae–"
T. Kato (1977)

IPPJ-AM-3 "Grotrian Diagrams of Highly Ionized Iron FeVIII-FeXXVI"
K. Mori, M. Otsuka and T. Kato (1977) [Published in Atomic Data and Nuclear Data Tables 23, 196 (1979)]

IPPJ-AM-4 "Atomic Processes in Hot Plasmas and X-Ray Emission"
T. Kato (1978)

IPPJ-AM-5 "Charge Transfer between a Proton and a Heavy Metal Atom"
S.Hiraide, Y. Kigoshi and M. Matsuzawa (1978)

IPPJ-AM-6 "Free-Free Transition in a Plasma –Review of Cross Sections and Spectra–"
T. Kato and H. Narumi (1978)

IPPJ-AM-7 "Bibliography on Electron Collisions with Atomic Positive Ions: 1940 Through 1977"
K. Takayanagi and T. Iwai (1978)

IPPJ-AM-8 "Semi-Empirical Cross Sections and Rate Coefficients for Excitation and Ionization by Electron Collision and Photoionization of Helium"
T. Fujimoto (1978)

IPPJ-AM-9 "Charge Changing Cross Sections for Heavy-Particle Collisions in the Energy Range from 0.1 eV to 10 MeV I. Incidence of He, Li, Be, B and Their Ions"
Kazuhiko Okuno (1978)

IPPJ-AM-10 "Charge Changing Cross Sections for Heavy-Particle Collisions in the Energy Range from 0.1 eV to 10 MeV II. Incidence of C, N, O and Their Ions"
Kazuhiko Okuno (1978)

IPPJ-AM-11 "Charge Changing Cross Sections for Heavy-Particle Collisions in the Energy Range from 0.1 eV to 10 Mev III. Incidence of F, Ne, Na and Their Ions"
Kazuhiko Okuno (1978)

IPPJ-AM-12 "Electron Impact Excitation of Positive Ions Calculated in the Coulomb-Born Approximation –A Data List and Comparative Survey–"
S. Nakazaki and T. Hashino (1979)

IPPJ-AM-13 "Atomic Processes in Fusion Plasmas – Proceedings of the Nagoya Seminar on Atomic Processes in Fusion Plasmas Sept. 5-7, 1979"
Ed. by Y. Itikawa and T. Kato (1979)

IPPJ-AM-14 "Energy Dependence of Sputtering Yields of Monatomic Solids"
N. Matsunami, Y. Yamamura, Y. Itikawa, N. Itoh, Y. Kazumata, S. Miyagawa, K. Morita and R. Shimizu (1980)

IPPJ-AM-15 "Cross Sections for Charge Transfer Collisions Involving Hydrogen Atoms"
Y. Kaneko, T. Arikawa, Y. Itikawa, T. Iwai, T. Kato, M. Matsuzawa, Y. Nakai, K. Okuno, H. Ryufuku, H. Tawara and T. Watanabe (1980)

IPPJ-AM-16 "Two-Centre Coulomb Phaseshifts and Radial Functions"
H. Nakamura and H. Takagi (1980)

IPPJ-AM-17 "Empirical Formulas for Ionization Cross Section of Atomic Ions for Electron Collisions –Critical Review with Compilation of Experimental Data–"
Y. Itikawa and T. Kato (1981)

IPPJ-AM-18 "Data on the Backscattering Coefficients of Light Ions from Solids"
T. Tabata, R. Ito, Y. Itikawa, N. Itoh and K. Morita (1981)

IPPJ-AM-19 "Recommended Values of Transport Cross Sections for Elastic Collision and Total Collision Cross Section for Electrons in Atomic and Molecular Gases"
M. Hayashi (1981)

IPPJ-AM-20 "Electron Capture and Loss Cross Sections for Collisions between Heavy Ions and Hydrogen Molecules"
Y. Kaneko, Y. Itikawa, T. Iwai, T. Kato, Y. Nakai, K. Okuno and H. Tawara (1981)

IPPJ-AM-21 "Surface Data for Fusion Devices – Proceedings of the U.S–Japan Workshop on Surface Data Review Dec. 14-18, 1981"
Ed. by N. Itoh and E.W. Thomas (1982)

IPPJ-AM-22 "Desorption and Related Phenomena Relevant to Fusion Devices"
Ed. by A. Koma.(1982)

IPPJ-AM-23 "Dielectronic Recombination of Hydrogenic Ions"
T. Fujimoto, T. Kato and Y. Nakamura (1982)

IPPJ-AM-24 "Bibliography on Electron Collisions with Atomic Positive Ions: 1978 Through 1982 (Supplement to IPPJ-AM-7)"
Y. Itikawa (1982)

IPPJ-AM-25 "Bibliography on Ionization and Charge Transfer Processes in Ion-Ion Collision"
H. Tawara (1983)

IPPJ-AM-26 "Angular Dependence of Sputtering Yields of Monatomic Solids"
Y. Yamamura, Y. Itikawa and N. Itoh (1983)

IPPJ-AM-27 "Recommended Data on Excitation of Carbon and Oxygen Ions by Electron Collisions"
Y. Itikawa, S. Hara, T. Kato, S. Nakazaki, M.S. Pindzola and D.H. Crandall (1983)

IPPJ-AM-28 "Electron Capture and Loss Cross Sections for Collisions Between Heavy Ions and Hydrogen Molecules (Up-dated version of IPPJ-AM-20)
H. Tawara, T. Kato and Y. Nakai (1983)

IPPJ-AM-29 "Bibliography on Atomic Processes in Hot Dense Plasmas"
T. Kato, J. Hama, T. Kagawa, S. Karashima, N. Miyanaga, H. Tawara, N. Yamaguchi, K. Yamamoto and K. Yonei (1983)

IPPJ-AM-30 "Cross Sections for Charge Transfers of Highly Ionized Ions in Hydrogen Atoms (Up-dated version of IPPJ-AM-15)"
H. Tawara, T. Kato and Y. Nakai (1983)

IPPJ-AM-31 "Atomic Processes in Hot Dense Plasmas"
T. Kagawa, T. Kato, T. Watanabe and S. Karashima (1983)

IPPJ-AM-32 "Energy Dependence of the Yields of Ion-Induced Sputtering of Monatomic Solids"
N. Matsunami, Y. Yamamura, Y. Itikawa, N. Itoh, Y. Kazumata, S. Miyagawa, K. Morita, R. Shimizu and H. Tawara (1983)

IPPJ-AM-33 "Proceedings on Symposium on Atomic Collision Data for Diagnostics and Modelling of Fusion Plasmas, Aug. 29 – 30, 1983"
Ed. by H. Tawara (1983)

IPPJ-AM-34 "Dependence of the Backscattering Coefficients of Light Ions upon Angle of Incidence"
T. Tabata, R. Ito , Y. Itikawa, N. Itoh, K. Morita and H. Tawara (1984)

List of publications in international journals

1. H. Tawara, Atomic Data and Nuclear Data Tables 22 (1978) 491; Cross Sections for Charge Transfer of Hydrogen Beams in Gases and Vapors in the Energy Range 10 eV - 10 keV
2. K. Mori, M. Otsuka and T. Kato, Atomic Data and Nuclear Data Tables 23 (1979) 196; Grotrian Diagrams of Highly Ionized Iron Fe VIII - Fe XXVI
3. N. Matsunami, Y. Yamamura, Y. Itikawa, N. Itoh, Y. Kazumata, S. Miyagawa, K. Morita and R. Shimizu, Rad. Eff. Lett. 57 (1980) 15; A Semiempirical Formula for the Energy Dependence of the Sputtering Yield
4. T. Kato, Y. Itikawa, Y. Kanada and R. Watanabe, Physica Scripta 23 (1981) 198; Database and Retrieval-Display System of Atomic Data for Fusion
5. T. Tabata, R. Ito, K. Morita and Y. Itikawa, Japanese J. Appl. Phys. 20 (1981) 1929; Empirical Formulas for the Backscattering of Light Ions from Solids
6. E.W. Thomas, N. Itoh and R.A. Langley, J. Nucl. Mater. 111 & 112 (1982) 809; Surface Data for Fusion Devices, Progress Report on Data Compilation and Assessment by the U.S., Japanese and IAEA Data Centers
7. Y. Yamamura, N. Matsunami and N. Itoh, Rad. Eff. Lett. 68 (1982) 83; A New Empirical Formula for the Sputtering Yield
8. T. Tabata, R. Ito, Y. Itikawa, N. Itoh and K. Morita, Atomic Data and Nuclear Data Tables 28 (1983) 493; Backscattering Coefficients of H, D and He Ions from Solids
9. K. Morita, Japanese J. Appl. Phys. 22 (1983) 1112; Analytical Calculation of Energy Spectra of keV Light Particles Reflected from Solid Surface
10. K. Morita, J. Appl. Phys. 53 (1984) 776; Reflection of keV Light Ions from Compound Targets
11. N. Matsunami, Y. Yamamura, Y. Itikawa, N. Itoh, Y. Kazumata, S. Miyagawa, K. Morita, R. Shimizu and H. Tawara, Atomic Data and Nuclear Data Tables, 120 (1984) 36; Energy Dependence of the Yields of Ion-Induced Sputtering of Monatomic Solids
12. Y. Yamamura, Rad. Eff. 80 (1984) 193; A Simple Analysis on Angular Dependence of Light-Ion Sputtering yield
13. N. Itoh, R. Ito, Y. Itikawa, Y. Kazumata, N. Matsunami, S. Miyagawa, K. Morita, R. Shimizu, T. Tabata, H. Tawara and Y. Yamamura, J. Nucl. Mater. 122 & 123 (1984) 1613; Data Center Activities on Plasma-Wall Interaction at Institute of Plasma Physics, Nagoya University
14. T. Kato, H. Tawara, N. Matsunami, K. Morita, Y. Yamamura, R. Shimizu and N. Itoh, J. Nucl. Mater. (1984); Database and Retrieval-Display System for Compiled Sputtering Data
15. K. Morita, T. Tabata and R. Ito, J. Nucl. Mater. (1984); Universal Relations for Reflection of keV Light Ions from Solid Targets
16. H. Tawara, T. Kato and Y. Nakai, Atomic Data and Nucl. Data Tables (accepted); Cross Section for Electron Capture and Loss by Positive Ions in Collisions with Atomic and Molecular Hydrogen
17. T. Tabata, R. Ito, K. Morita and H. Tawara, Radiation Effects (accepted); Empirical Formulas for the Backscattering Coefficients of Light Ions Obliquely Incident in Solids
18. Y. Itikawa, S. Hara, T. Kato, S. Nakazaki, M.S. Pindzola and D.H. Crandall, Atomic Data and Nucl. Data Tables (accepted); Electron-Impact Cross Sections and Rate-Coefficients for Excitations of Carbon and Oxygen Ions

19. T. Tabata, R. Ito, K. Morita and H. Tawara, Nucl. Instr. Meth. (submitted); Universal Semiempirical Formulas for the Backscattering Coefficients of Light Ions

1.6.2 Surface interaction

1.6.2.1 Surface effects related to impurity production

For the last five years, the data base on sputtering has been extensively produced and compiled both experimentally and theoretically, which is summarized as follows.

1) Hydrogen chemical sputtering yields of low-Z materials such as C, SiC and TiC have been measured in the energy range between 0.1 and 6 keV in connection with R&D for JT-60 on screening the best low-Z material [1-3]. Among them TiC has the lowest value of chemical sputtering of carbon atoms in the form of CH_4 molecules, 3×10^{-3} atoms/H^+. That is, this value is approximately one-third and one-tenth as much as those of SiC and C, respectively.

2) Along with the measurements of chemical sputtering yield of carbides mentioned above, surface compositional changes by bombardment with energetic hydrogens have been measured [2,4-6].

3) Concerning the energy dependence of the hydrogen chemical sputtering of carbon materials, a theoretical model has been proposed to explain the maximum around 1 keV [7,8].

4) Chemical erosion of graphite by atomic hydrogen exposure has been measured [9,10]. After conditioning the surface by the exposure, the erosion yield is reduced by one order of magnitude [9]. The yield has been measured also in the case of simultaneous bombardment with energetic protons [10], indicating that it would be enhanced by the simultaneous bombardment [11].

5) A detailed measurement has been made on chemical erosion by oxygen ion bombardment of refractory metals such as W and Mo, which are candidate materials for divertor plates of INTOR [12].

6) Energy dependence of self sputtering yields of W and Mo has been measured at room temperature in the energy range between 0.1 and 10 keV [13].

7) An empirical formula for the energy dependence of physical sputtering yield of monatomic solids has been proposed, which takes into account the threshold effect in the original Sigmund's theory [14,15].

1.6.2.2 Surface effects related to particle recycling

1) A hydrogen recycling model at wall surfaces in tokamaks has been proposed in connection with recycling rate control in JT-60 [16]. Hydrogen diffusivity in TiC necessary for the calculation have been estimated from measurement of the decay of the deuterium re-emission from a deuteron saturated TiC sample [17].

2) Hydrogen diffusivity data on Ni and Mo have been estimated from measurement on energetic hydrogen beam re-emission and permeation during bombardment of the beam [18]. It shows that hydrogen diffusivity estimated from the re-emission measurement is approximately two orders

of magnitude lower than that of bulk material.

3) An effect of radiation damage on deuteron re-emission and trapping has been measured in carbon showing that the effect is marked in the energy above 250 eV [19].

4) Deuterium re-emission measurement during energetic deuteron bombardment has been made in Mo, Inconel 625 and TiC [17]. The result indicates that a considerable fraction of incident deuterium atoms are trapped in TiC at relatively low temperatures around 100 °C compared to that in Mo and Inconel 625.

5) Ion-induced release of deuterium from Mo by low energy proton bombardment at room temperature has been investigated in the energy range between 0.5 and 6 keV for both deuterons and protons [20]. The release curves of deuterium atoms pre-implanted at 1 keV consist of two exponential decay curves due to bombardments with protons from 1 to 6 keV, but only one exponential decay curve was observed at 0.5 keV H^+. The desorption cross section decreases with increasing deuteron fluence.

6) Empirical formulas of light ion backscattering coefficient for both particle and energy as a function of incident energy have been proposed by fitting the compiled experimental data [21]. Empirical formula of particle backscattering coefficient as a function of energy and angle of incidence has been also proposed [22].

References for subsection 1.6.2

[1] R. Yamada, K. Nakamura, K. Sone and M. Saidoh, J. Nucl. Mater., 95 (1980) 278.
[2] K. Sone, M. Saidoh, K. Nakamura, R. Yamada, Y. Murakami, T. Shikama, M. Fukutomi, M. Kitajima and M. Okada, J. Nucl. Mater., 98 (1981) 270.
[3] R. Yamada, K. Nakamura and M. Saidoh, J. Nucl. Mater., 111 & 112 (1982) 744.
[4] H. Tanaka, K. Saiki, S. Otani, A. Koma and S. Tanaka, J. Nucl. Mater., 116 (1983) 317.
[5] S. Fukuda, M. Mohri and T. Yamashina, J. Vac. Sci. Technol., in press.
[6] S. Fukuda, M. Mohri and T. Yamashina, to be published in Nucl. Technol./Fusion.
[7] K. Sone, Culham Laboratory Research Report CLM-R236 (1982).
[8] R. Yamada and K. Sone, J. Nucl. Mater., 116 (1983) 200.
[9] T. Abe, K. Obara and Y. Murakami, J. Nucl. Mater., 91 (1980) 223.
[10] R. Yamada, K. Nakamura and M. Saidoh, J. Nucl. Mater., 98 (1981) 167.
[11] R. Yamada and K. Sone, J. Nucl. Mater., 120 (1984) 119.
[12] M. Saidoh, Int. Conf. Plasma-Surface Interactions in Controlled Thermonuclear Fusion Devices, May 1984, Nagoya (to be published in J. Nucl. Mater.)
[13] M. Saidoh and K. Sone, Japan. J. Appl. Phys., 22 (1983) 1361.
[14] N. Matsunami, Y. Yamamura, Y. Itikawa, N. Itoh, Y. Kazumata, S. Miyagawa, K. Morita and R. Shimizu, Radiat. Eff. Lett., 50 (1980) 39.
[15] Y. Yamamura, N. Matsunami and N. Itoh, Radiat. Eff., 71 (1983) 65.
[16] K. Sone and Y. Murakami, J. Nucl. Mater., 123 (1984), in press.

[17] Fusion Research Center, Annual Report April 1, 1982 - March 31, 1983, Japan Atomic Enerkgy Research Institute Report JAERI-M 83-182 (1983) p.68.
[18] T. Tanabe, N. Saito, Y. Etoh and S. Imoto, J. Nucl. Mater., 103 & 104 (1981) 483.
[19] K. Sone and G.M. McCracken, J. Nucl. Mater., 111 & 112 (1982) 606.
[20] R. Yamada, K. Nakamura, K. Sone and M. Saidoh, J. Nucl. Mater., 101 (1981) 100.
[21] T. Tabata, R. Ito, K. Morita and Y. Itikawa, Japan. J. Appl. Phys., 20 (1981) 1929.
[22] T. Tabata, R. Ito, Y. Itikawa, N. Itoh, K. Morita and H. Tawara, Institute of Plasma Physics/Nagoya Univ. Report IPPJ-AM-34 (1984).

1.6.3 Plasma edge transport

No contribution

1.7 Data on vacuum vessel preparation

New Japanese data developed since the previous assessment studies can be seen in the following technical papers. The outline of and some comments on each paper are given under the title.

1) Y. Sakamoto (IPCR), "ECR discharge cleaning of toroidal machines", Proc. 9th Intern. Vac. Congr. & 5th Intern. Conf. on Solid Surfaces, Madrid, 1983, p.716;
S. Ishii, K. Okazaki, Y. Sakamoto and K. Yano, "ECR discharge cleaning for liner-containing tokamaks", Jap. J. Appl. Phys. 22 (1983) L403.

Experiments on electron-cyclotron-resonance (ECR) discharge cleaning have been performed on JFT-2 (JAERI), JIPP T-II (IPP, Nagoya University) and TEXTOR. In this method, a cleaning plasma is produced by the ionization of hydrogen molecules and atoms by electrons which absorb microwave energy under cyclotron resonance conditions. The discharge does not need electrodes in the vacuum vessel. The operating pressure is in the range 10^{-3} - 10^{-2} Pa. Typical plasma parameters are $n_e = 10^{16}$ m^{-3} and $T_e = 10$ eV. It has been proved that the vacuum components between the liner and vacuum vessel can be cleaned by this method.

In order to select (a) discharge cleaning method(s) appropriate to the INTOR vacuum vessel, comparison should be made among pulse discharge cleaning, glow discharge cleaning and ECR discharge cleaning.

2) S. Sengoku, et al (JAERI), "Carbon wall experiment in DIVA", J. Nucl. Mater. 93&94 (1980) 178.

The sticking coefficient and saturation density of oxygen and CO on carbon surface are extremely low. These may retard the accumulation of oxygen-containing gases on clean surface of the vacuum vessel wall. A carbon wall experiment on DIVA supported the idea, in which once clean surface was obtained by discharge cleaning very low q plasmas with a good confinement characteristic were maintained for several hundreds shots without any additional cleaning procedure.

3) K. Yoshihara and K. Nii (NRIM), "Development of self-healing coating method for vacuum vessel materials", Proc. 7th Intern. Conf. on Vacuum Matallurgy, Tokyo, 1982, p.492.

When a special stainless steel doped with boron (0.01 %) and nitrogen (0.16 %) is heated to about 800 °C in vacuum, a very thin layer of hexagonal boron nitride is formed on the surface. The adsorption characteristic of this material is very similar to that of carbon or graphite.

Although the precipitation temperature is too high to apply this method directly to large vacuum vessels, it is worth while to develop the idea as a potential method of surface preparation.

4) S. Komiya, N. Umezu and C. Hayashi (ULVAC), "Titanium nitride film as a protective coating for a vacuum deposition chamber", Thin Solid Films 63 (1979) 341.

A hard and anti-corrosive titanium nitride coating is proposed for use as a protective coating for the inside of vacuum vessels, components and other fixtures. The titanium nitride coating can be formed by activated reactive evaporation. The outgassing rate of the TiN-coated surface is about one-fifth of the corresponding value of a bare stainless steel surface at room temperature.

5) Y. Murakami, T. Abe and H. Nakamura (JAERI), "Development of low-Z surface coatings for JT-60 first wall", J. Nucl. Mater. 111 & 112 (1982) 861;
Y. Murakami, "The vacuum and surface technological aspects of the JT-60 tokamak", Proc. 9th Intern. Vac. Congr. & 5th Intern. Conf. on Solid Surfaces, Madrid, 1983, p.532.

In JAERI, development of surface coatings of low-Z materials were started in 1980. Work in this area includes evaluation of candidate coatings as well as development of coating techniques. From the results of several performance tests including thermal shock test, thermal fatigue test and sputtering yield measurement, titanium carbide was chosen as the coating material for the first stage use in JT-60 since CVD-TiC on molybdenum produced a favourable result in both refractory character and coating-substrate adhesion. In the improvement of deposition technique from 1982, the temperature of TiC deposition could be successfully reduced to about 900 °C where the recrystallization of molybdenum was found to be inconsiderable. The outgassing rate of the TiC-coated molybdenum is comparable to those of bare molybdenum and stainless steel.

6) G. Tominaga, K. Nakamura and Y. Murakami (JAERI), "Materials and methods for attaining to low outgassing rates without high temperature bakeout", JAERI-M Report 83-112 (1983).

Since the necessity for high temperature bakeout of fusion vacuum vessels imposes many restrictions on the machine design and consequently will raise the cost, the investigation and testing of materials and methods for attaining to low outgassing rates without bakeout is one of the major R&D items of fusion reactors. From recent investigations by Japanese scientists, the authors considered a hypothesis that the formation of dense oxide films crystallized on stainless steels and aluminum alloys is conducive to reduction of outgassing rate at room temperature. For the further development of this problem, they pointed out the importance of a full understanding of the mechanism of gas desorption from oxide films and of similar investigations on the films of nitride and carbide.

1.8 Physics conclusions and R and D

Divertor plasmas, observed in the Doublet III experiments, significantly enhance the credibility of dense and cool divertor plasmas. They provide precious data bases for impurity control studies on INTOR. The divertor shape of the Doublet III is an open single-null type, which is almost same as the INTOR divertor. The Duublet III divertor plasmas near plates have temperatures of less than 10 eV and densities of more than 10^{20} m^{-3}. The high fuel gas pressure is observed to increase up to 10^{-3} Torr in the divertor region. The divertor operation demonstrates clean plasmas with a small amount of metal impurities. The strong radiation is also observed from the divertor region. Such a dense and cool divertor plasma is compatible with good confinement time. The above favorable results indicate that the dense and cool divertor concept is more credible than the other impurity control concepts.

The numerical analyses with a divertor simulation code have made great progress, along with the divertor experiments. The dense and cool divertor plasmas of the Doublet III are well reproduced with the divertor code, which however does not include impurity effects. The divertor code extrapolates to the INTOR conditions and elucidates what conditions should be satisfied in INTOR to realize the dense and cool divertor plasmas.

The limiter experiments have also made progress and the low-Z limiters provide clean plasmas under the intense additional heating of a MW level. The simple analyses on the INTOR limiter plasmas show that the limiter is limited to the low-Z materials, and that the temperature of the plasmas in contact with the limiter does not decrease below 100 eV. Then the erosion is the serious problems for the limiter concept.

Parametric studies on the divertor shape, with the divertor numerical code, indicate that even a fairly short divertor can provide a dense and cool plasmas near the divertor plate. The short divertor, having short distance between the null-point and the divertor plate, has some advantages on simplification of the reactor configuration. Comparison studies on single- and double-null divertor have also revisited and results from physics and engineering viewpoints show that the single-null concept is slightly more favorable than the double-null one.

Ergodic magnetic limiter and radio-frequency divertor concepts have been assessed as innovative schemes for impurity control. Further studies, especially experimental ones, are necessary to develop those concepts.

Data on fuelling are assessed. The fuelling is important for achieving the H-mode discharges. The pellet fuelling is observed to expand the operation regime with good confinement.

Data compilation and evaluation both for atomic and molecular processes and for plasma-surface interaction have made progress systematically. A computer-based data storage and retrieval system has also been significantly developed to make easy access to the bibliographic and numerical data.

Present programs

JT-60

The schedule of JT-60 operation is shown in the following table. The first plasma of the JT-60 is scheduled in spring, 1985, and Joule experiments will be conducted for a half year. After an installation of heating apparatus (NBI:20MW, RF:10MW), full-scale experiments, which mean to attain densities and temperatures of hydrogen plasmas equivalent to D-T plasmas with Q=1, will be in 1987-1988.

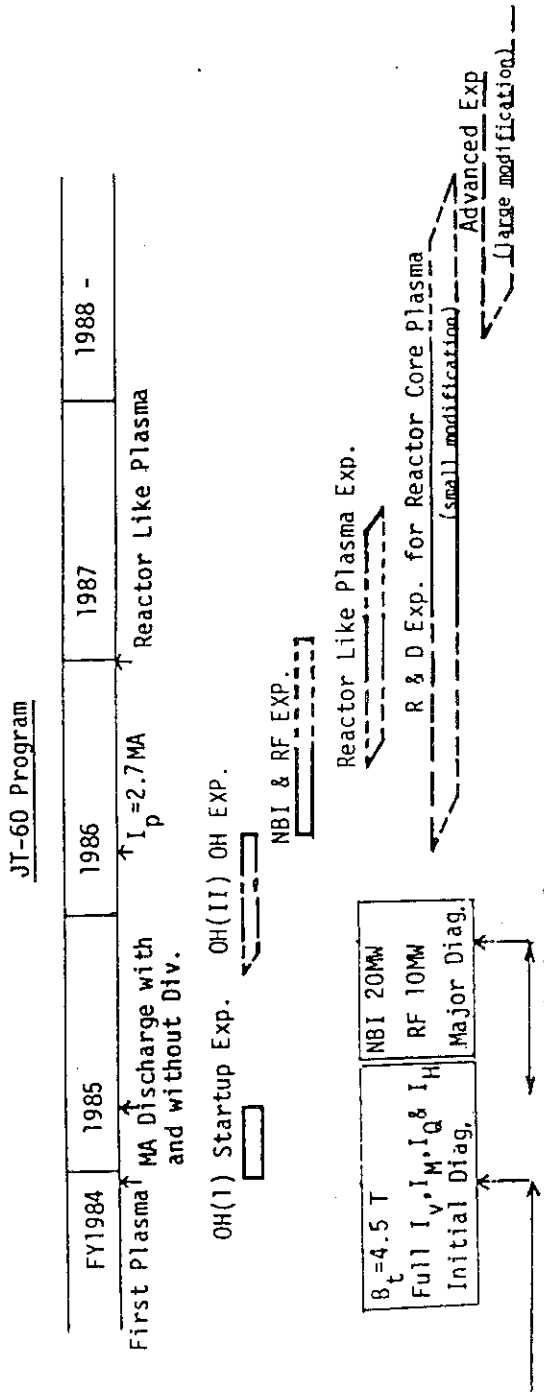

JT-60 experiments are featured with hydrogen plasmas and a long pulse of 10s. Capability in a divertor operation in JT-60 is outstandingly differnt from the other large tokamaks, TFTR, JET, and T-15. Then, the JT-60 operation will certainly enhance research and development of impurity control including a divertor concept, and it could provide very useful data base for INTOR impurity control.

Doublet III (Big D)

The Doublet III experiments are performing under a cooperative agreement between Japan and US. Lately, the contract was agreed to extend to 1988 to continue cooperative experiments of a Big-D project. In addition to the present NBI heating (around 10MW), an RF(ICRF, ECRF) heating is scheduled to be augmented. The Big-D experiment is expected to start at the beginning of 1986. Non-circular high beta plasmas with a divertor or limiter will be produced within a big chamber. Experimental results on impurity control, particularly in an open-type divertor, are expected surely reinforce the data base for INTOR.

JFT-2M

TFT-2M was modernized in 1983. Its major objectives are focussed on RF experiments. A heating power (NBI and RF) will reach about 10 MW. Impurity control experiments are planned to be performed with a pumped limiter and a divertor with non-circular plasmas. JFT-2M is not so big, but is able to make small adjustments as its objectives. Useful data, especially impurity control control under RF heating, are expected.

JIPP-T 2U

JIPP-T 2U was upgraded in 1983, and it has a circular cross section with a considerable heating power of NBI and RF (ICRF, LHRF, and ECRF). Regarding to impurity control, experiments on an ergodic limiter are sheduled in near future.

Recommended new programs

JT-60 is a large tokamak with a considerable heating power and with a copability of a divertor operation. Doublet-III and JFT-2M are non-circular tokamaks heated by a level of heating power of more than 10MW, and can be operated with an open-type divertor. Those machines could supply a lot of information deeply related to impurity control by a limiter and a divertor, if detail measurements were adequately performed, in particular about scrape-off plasma parameters and impuity behaviors. To establish a sufficient data base for INTOR, then, it is important to obtain detailed data from tokamaks mentioned above. It may be recommended that tokamak programs are almost enough for research and development for divertor and limiter concepts, and that detailed measurements should be performed to obtain adequate understandings for a reliable extrapolation to INTOR.

The problem of impurity control in tokamaks does not seem to be completely resolved by an INTOR operation, even though INTOR would work well, because demonstration and commercial reactors will increase their power up to about 1GW. Therefore, it is indeed necessary to develop other schemes for impurity control in parallel, which might not be adopted for INTOR, e.g. a cooling boundary layer, a bundle divertor, and so forth. There are not so many programs at present. These requirements are not so urgent, but they should be performed steadily.